Republic of Iraq
Ministry of Higher Education
and Scientific Research
Al-Nahrain University
College of Science
Department of Physics

Surface Modification of Titanium and Titanium Alloy Using Ceramic Biomaterials by RF Sputtering

A Dissertation

Submitted to the College of Science / Al-Nahrain University as a Partial Fulfillment of the Requirements for the Degree of Doctorate of Philosophy in Physics

By

Dunya Abdulsahib Hashim Hamdi

B.Sc. Physics/College of Science / Al-Nahrain University (1997)

M.Sc. Physics/College of Science / Al-Nahrain University (2003)

Supervised by

Dr. Thamir A. Jabbar Jumah	**Dr. Thair Latif Al-Zubaydi**
(Assistant Professor)	(Senior Scientific Researcher)

March 2016 A.D   Jamadi Al- Akhira 1437A.H

بسم الله الرحمن الرحيم

قَالُوا۟ سُبْحَٰنَكَ لَا عِلْمَ لَنَآ إِلَّا مَا عَلَّمْتَنَآ إِنَّكَ أَنتَ ٱلْعَلِيمُ ٱلْحَكِيمُ ﴿٣٢﴾

صدق الله العظيم

سورة البقرة

Supervisors' Certification

We, certify that this thesis entitled *"Surface Modification Of Titanium and Titanium Alloy Using Ceramic Biomaterials By RF Sputtering"*Was prepared by *"Dunya Abdulsahib Hashim Hamdi* "under our supervision at the College of Science/Al-Nahrain University as a partial fulfilment of the requirements for the Degree of Doctor of Philosophy in Physics.

Signature:

Name: Dr .Thamir A.Jabbar

Scientific Degree :Asst.prof

Date: 1 /11/2016

Signature:

Name: Dr. Thair Latif Al-Zubaydi

Scientific Degree: Senior Scientific Researcher

Date: 1 /11/2016

In view of the available recommendations, I forward this thesis for debate by the examining committee.

Signature:

Name: Alaa Jabbar Ghazai

Scientific Degree: Asst. Prof.

Title: Head of physics Department

Date: 1 /11/2016

Committee Certification

We, examination committee certify that we have read this dissertation entitled " *Surface Modification Of Titanium and Titanium Alloy Using Ceramic Biomaterials By RF Sputtering* "and examined the student" *Dunya Abdulsahib Hashim Hamdi* "in its contents and that in our opinion, it is accepted for the Degree of Doctorate of philosophy in Physics .

Signature:
Name: **Dr. Fadhil Attiya Chyad**
Scientific Degree:Professor
Data:2 /3/2016
(Chairman)

Signature:
Name: **Dr. Talib Saloom Hamdi**
Scientific Degree:Assistant Professor
Data: 11 /3/2016
(Member)

Signature:
Name: **Dr. Abdul Rahman Najeem Abed**
Scientific Degree:Assistant Professor
Data: 16 /3/2016
(Member)

Signature:
Name: **Dr. Ghazi Kamal Saeed**
Scientific Degree:Assistant Professor
Data: 16 /3 /2016
(Member)

Signature:
Name: **Dr. Ahmed Qasim Abdullah**
Scientific Degree:Assistant Professor
Data: 17 /3 /2016
(Member)

Signature:
Name: **Dr. Thamir A.Jabbar**
Scientific Degree:Assistant Professor
Data:17 /3/2016
(Member/supervisor)

Signature:
Name: **Dr. Thair Latif Al-Zubaydi**
Scientific Degree:Assistant Professor
Data: /7/3 /2016
(Member/supervisor)

I, here by certify upon the decision of the examining committee

Signature:
Name: **Dr. Hadi M.A.Abood**
Scientific Degree:Assistant Professor
Title: Dean of the Science College
Data:9 /3 /2016

Office of the Deputy Vice Chancellor (Research)
Professor David Morrison

90 South Street, Murdoch
Western Australia 6150
Telephone: +61 8 9360 6788
Facsimile: +61 8 9360 2931
david.morrison@murdoch.edu.au

5 February 2014

Ms Dunya Abdulsahib Hashim Hamdi
Al-Nahrain University
College of Science

Email: dunia_sh_7@yahoo.com

Dear Ms Hamdi

Visiting Occupational Trainee

I am writing to invite you to accept an appointment as a Visiting Occupational Trainee in Physics and Energy within in the School of Engineering and Information Technology at Murdoch University. Your time with Murdoch University will be for a period of six months commencing 5 May 2014 or as soon as practicable thereafter.

It is understood that during this period you will develop practical skills in the project "Surface Modification of Titanium and Titanium Alloys by Plasma Coating Using Nano Particles" under the supervision of Dr Zhong-Tao Jiang.

It is also understood that your visit will be funded by a scholarship from the Iraqi Ministry of Higher Education and Scientific Research, which will cover your airfare, living expenses, and bench fee which are expected to total $22,000 USD.

Please ensure that you obtain adequate travel/health insurance for the duration of your visit.

Murdoch University will nominate you for a Training and Research (Subclass 402) – Occupational Trainee Stream visa and if our nomination application is approved, you will be required to submit your visa application. Please access the following Department of Immigration and Citizenship (DIAC) web link for further information on how to apply for your visa:
http://www.immi.gov.au/visas/temporary-visa/402/occupational-trainee/

As confirmation you will accept this invitation, please sign the attached Visitor Agreement and return via email to the Human Resources Office. In anticipation of your acceptance, I would like to congratulate you and wish you well. I hope that your links with Murdoch University will be professionally beneficial and personally enjoyable.

Yours sincerely

Professor David Morrison
Deputy Vice Chancellor (Research)

Att: *Code of Ethics and Code of Conduct for Honorary Appointees*
Code of Conduct for Research
Visitor Agreement

South Street, Murdoch
Western Australia 6150
Australia
Telephone: (08) 9360 2867
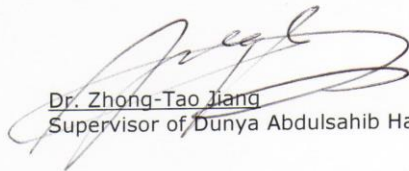Facsimile: (08) 9360 6346

Murdoch, 26th July 2015

Dr. Zhong-Tao Jiang
Physics and Nanotechnology Chair
School of Engineering & Information Technology
Murdoch University

Email: Z.Jiang@Murdoch.edu.au

To Whom It May Concern

I would like to verify that Ms. Dunya Abdulsahib Hashim Hamdi has taken training courses on XRD, FTIR, EDS, corrosion test, and SEM analyses of the thin films in my laboratory to then worked on it by herself for her PhD thesis research. Also worked in the staff of university and gave lectures to students.

Sincerely Yours

Dr. Zhong-Tao Jiang
Supervisor of Dunya Abdulsahib Hashim Hamdi at Murdoch University, Australia

KAIST

Prof. Kwangsoo No

Materials for Sustainable Technology Laboratory
Department of Materials Science and Engineering
KAIST, Daejon, Korea
+82-42-350-4116
ksno@kaist.ac.kr

November 13, 2014

Zhong-Tao Jiang, PhD
Surface Analysis and Materials Engineering Research Group
Physics and Nanotechnology (BSc and BSc(Hons)) Academic Chair
School of Engineering and Information Technology, Murdoch University
Engineering and Energy Building Room: 2.003B,
South Street, MURDOCH WA 6150, Australia
Tel +618 9360 2867   Fax +618 9360 6346
Z.Jiang@murdoch.edu.au

Invitation Letter for Ms. Dunya Abdulsahib Hashim Hamdi.

Dear Dr. Zhong-Tao Jiang:

I would like to invite Ms. Hamdi to work on a research project entitled surface modification of titaniun and titanium alloy by plasma coating using nano particles. The project would be supervised by Prof. Kwangsoo No.

Ms. Hamdi will be working on the preparation of deposition of multi-layer thin films structure of TiO_2, Al_2O_3 and HAp (hydroxyapatite) and stabilization of multi-layer thin films by annealing. She will be working with Prof. Kwangsoo No and interacting with a graduate student, Jaegyu Kim.

The proposed duration of the project is about from February 10, 2015 to April 15 , 2015 (2 month). Ms. Hamdi will be staying at the guest house of KAIST during the project.

We believe this will be mutually beneficial for both KAIST and Murdoch University (Surface Analysis and Materials Engineering Research Group). Should you have any inquiries about the project, please do not hesitate to contact me for further information.

With best regards,

Kwangsoo No.
Professor, KAIST.

Department of Materials Science and Engineering, KAIST

KAIST

To Whom It May Concern:

I would like to verify that Ms. Dunya Abdulsahib Hashim Hamdi has taken a training course on the RF sputtering in my laboratory to deposit thin films and then worked on it on her by herself to study her PhD thesis research. She also studied on XRD, optical microscope, and SEM analyses of the thin films.

Thank you, Sincerely.

July 19, 2015

Professor No, Kwangsoo
Materials for Sustainable Technology Laboratory
Dept. of Materials Science and Technology
KAIST
082-42-350-4116, 5116, 4156; 010-2422-2731;
(H) 043-732-4166 (Fax) 042-350-3310
kaistksno@gmail.com; http://mastlab.kaist.ac.kr
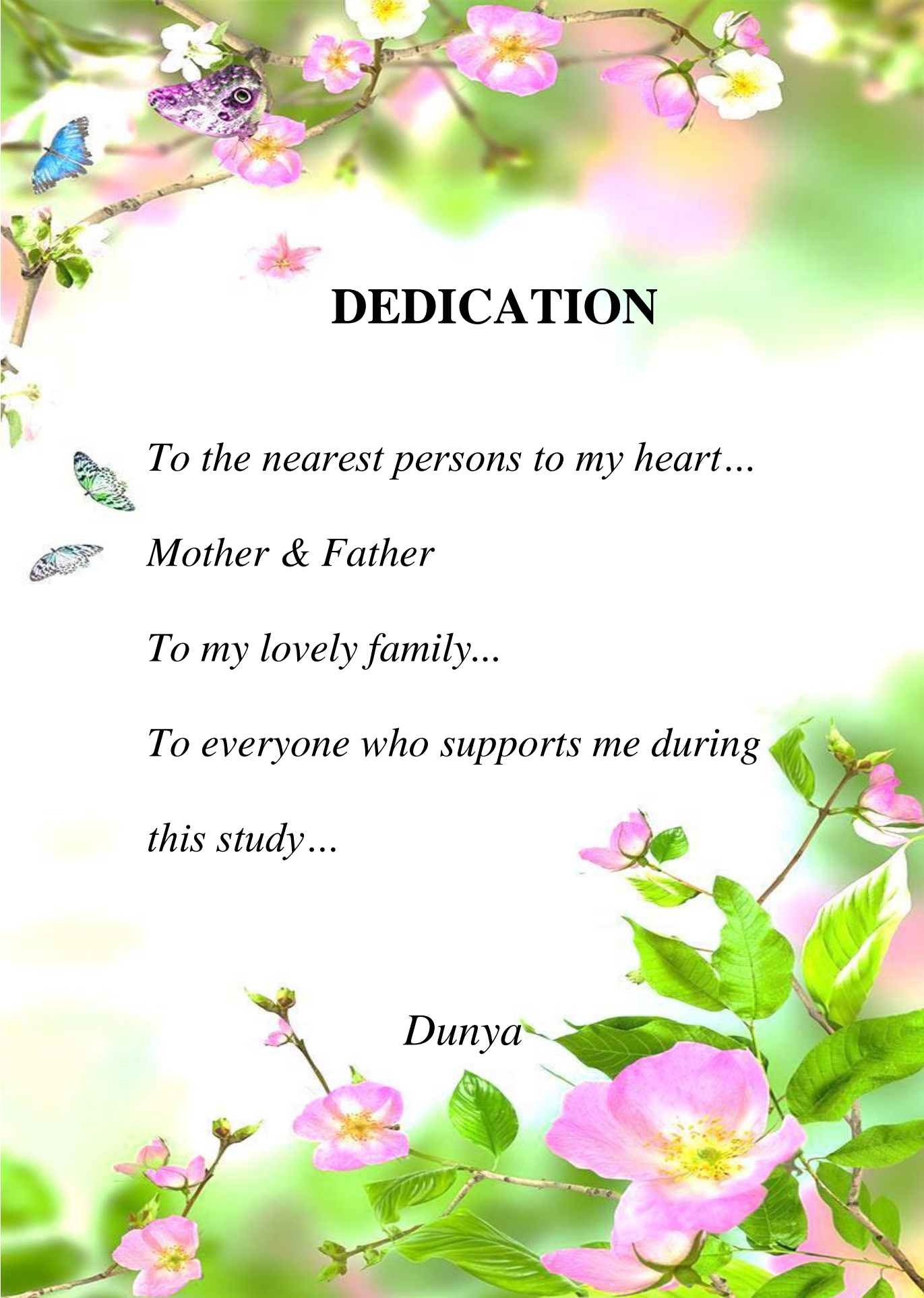
DEDICATION

To the nearest persons to my heart…

Mother & Father

To my lovely family…

To everyone who supports me during

this study…

Dunya

Acknowledgement

First of all I want to thank **God Almighty** for providing me with willingness and strength to accomplish this work and I pray that his blessings upon me may continuous throughout my life.

Great thanks and deepest gratitude to my supervisors **Dr. Thamir A.Jabbar** and **Dr.Thair Latif Al-Zubaydi** for their valuable scientific guidance, inspiring discussions, continuous support and great efforts in supervision this study.

I am gratefully thankful to **Dr. Ayad Murad**, Administrative Assistant to the President of the University, for his continuous help, guidance and support throughout the all research period.

Many thanks go to **Dr. Hadi Mohemmed Ali**, Dean of College of Science, University of Al Nahrain for his support to the higher studies program.

I am gratefully thankful to **Dr. Alaa Jabbar Ghazai**, Head of physics Department, for his constant care, valuable advice and continuous support throughout the course of the study.

My sincere thanks to my supervisors **Dr. Zhong Tao** , Murdoch University Australia and **Dr. No** , KAIST University Korea for her interest work of this study and their never-ending support and help whenever needed throughout my mission scholastic.

Deep appreciation to **Mr Akeel F. Hassan** and **Mr. Jammal F. Hamodi** for their great help that I will never forget

Dunya

Summary

The current in this thesis research deals with the plasma sputtering which was used to deposit single and triple layers ceramics on (cpTi) and (Ti-6Al-4V) alloy. Also ,in this work the *in vitro* electrochemical tests , formation of HAp by biomimetic process on the coated layers by the immersion in Simulated Body Fluid(SBF) at PH equal to 7.4 and room temperature was done . The single layer TiO_2 and HAp , multi-layer consist of TiO_2 and Al_2O_3 were deposited on cpTi and Ti-6Al-4Valloy, followed by the deposition of third layer of HAp. The deposition conditions in the RF sputtering system such as vacuum pressure, substrate temperature, power, gas type, gas flow and deposition time were fixed for the sputtering system where as the distance between the target and the substrate was varied (9 and 7 cm). Structural analysis was carried out , on the deposited layers(single and triple) using X-ray Diffraction (XRD), Scanning Electron Microscopy (SEM), Furrier Transformation Infra-Red (FTIR), Raman Spectroscopy and X-ray Photoelectron Spectroscopy (XPS). Elemental analysis for HAp deposited in the single and triple layer was done using Energy Dispersive X-ray Spectroscopy (EDS).

To investigate the biocompatibility of coatings the formed layers, were immersed in (SBF) for one month. After one month the samples were taken and anlyezed using the same structural analysis techniques used before immersion. Electrochemical investigation was carried out on the deposited layers used Open Circuit Potential (OCP),Linear Sweep Voltage(LSV) and Electrochemical Impedance Spectroscopy(EIS) in SBF. The XRD structural results show that the formation of HAp which was dominated on the phase formation on the surface of the single and triple layers. Also another Calcium –Phosphorus compound phases are found such as Tri Calcium Phosphate(TCP), Octa Calcium Phosphate(OCP) and Calcium Phosphate(CP) along with small fraction

of the Titanium phase belong the substrate .For TiO_2 single layer, XRD pat reins shows the formation of the rutile TiO_2which covered the substrate surface.

Elemental analysis by using EDS for the single and triple layer deposited in cpTi and Ti-6Al-4Valloy shows the energy transitions belong to the dominated elements, Ca and P, which contained in the HAp layer that already showed by XRD. Surface analysis by XPS for immersed samples in SBF for one month show the bonding type and the compound that formed. The XPS results confirmed the SEM observation, the FTIR and Raman results. It was found from the XPS analysis that most of the compound covers the surface are belongs to the Ca-P companies to the carboxyl groups (C-O, C-H) and this was confirmed by the XRD investigation which show the domination of (HAp) in the highest intensity (211) reflection at $2\theta^o$ of 31.7 for the single and triple layer coating. The XRD results also show the disappearance of the other CaP compounds after one month of immersion in SBF like TCP and CP .The increase in the HAp concentration after immersion indicates the occurrence of the biomimetic process that increases the precipitation of Ca^+ and P^- from the SBF and the two roots combined together to form CaP compound that increases the HAp concentration. The electrochemical parameters predicted from corrosion test show the improvement in the corrosion resistance of both cpTi and Ti-6Al-4Valloy after coated by shifting the OCP toward the nobel direction which was the same behaviour for the corrosion potential E_{corr}, and decreases in the corrosion current I_{corr} and the corrosion rate C_R comparing to the uncoated specimens. The (EIS) measurements conformed the improvement in the corrosion parameters result of from OCP and LSV by the very low capacitance for the coated specimens compared to that for the uncoated one which means that the single layer and triple layer protect the surface by increasing the equivalent circuit impedance blocking the path way for the active ions like Cl^- and O^+ to attack the base metal.

List of Contents

List of Figures

List of Abbreviations

Symbol	Description
ASTM	American Standard for Testing and Materials
Al_2O_3	Alumina
CP	Calcium Phosphate
α-CP	Alpha-Calcium Phosphate
cp	Commercially pure
D9	Distance between target and substrate 9 cm
D7	Distance between target and substrate 7 cm
EDS	Energy Dispersive X-ray Spectroscopy
EIS	Electrochemical Impedance Spectroscopy
FTIR	Furrier Transformation Infra-Red
HAp	Hydroxyapatite
ICDD	Introduction Center for Diffraction Data.
LSV	Linear Sweep Voltammetry
NASE	National American Corrosion Engineering
OCP	Octa Calcium Phosphate
Raman	Raman Spectroscopy
SBF	Simulated Body Fluid
SEM	Scanning Electron Microscopy
t_D	Time of deposition
TCP	Tri Calcium Phosphate
TiO_2	Titania or oxide titanium
XRD	X-ray Diffraction
XPS	X-ray Photoelectron Spectroscopy

List of Publications

No.	Title	Journal
1	Surface Modification of Titanium alloys by RF Magnetron Sputtering at Different Thin film TiO$_2$ Nano Thickness	IOSR Journal of Engendering (IOSRJENG). Vol4, issue 11, 2014
2	Investigation The Hydroxyapatite Coatings On Titanium Alloys Using Magnetron - Sputtered Process And Differentiate Between Single And Triple Layers.	Journal of Multidisciplinary Engineering Science and Technology (JMEST) ISSN: 3159-0040 Vol. 2 Issue 9, September - 2015

CHAPTER ONE

INTRODUCTION
AND
LITERATURE REVIEW

CHAPTER ONE

Introduction and Literature Review

1.1 Introduction

The natural synovial joints (hip, shoulder, knee or dental) are performing well under a wide variety of conditions. Unfortunately, these joints are also susceptible to inflammation and degenerative diseases that may result in pain and stiffness. Modern history of the world has huge military treatments including progress in old as well as wars that produce a large number of people's need replacing failed bones.

The typical cause of the degeneration is degradation in the joint's mechanical properties that results from a failure of the normal biological repair processes, or excessive loading conditions; and hence, the natural joints can no longer function, they can be replaced by artificial biomaterials in a procedure known as a total joint replacement (TJR) arthroplasty [1].

The studies in the biomaterial field are focused on Two areas:

- The development of the new metallic materials with mechanical properties close to the human bone and

- The surface modification techniques enabling optimum biocompatibility (which is closely related to their corrosion behavior in biological environments) and Osseo integration of medical alloy implants[2]. Osseointegration is defined as "the apparent direct attachment or connection of osseous tissue to an inert, alloplastic material without intervening connective tissue"[3].

The properties of alloys that used as orthopedic biomaterials are high specific strength and corrosion resistance protected from accelerated corrosion rate by natural passivation oxide layer created on the surface and

acts like an electrical resistor to retard the anodic dissolution of metal cations. Therefore, all implant alloys have a finite, albeit slow, uniform corrosion rate in *vivo*. The damage occurs to this passivation layer, such as by fretting or wear, maybe produce conditions conducive to accelerated focal corrosion and failure[4].

Today, many different metal alloys are used in implant materials, including titanium alloys such as commercially pure titanium CPTi, Ti-6Al-4V, stainless steels, Co-Cr-Mo alloys,…*etc*. The use of these materials dates back to the middle of the 20th century and use of titanium alloys for surgical implants dates are back to the 1940s[5].

The modulus elasticity for the cobalt-based alloys are higher than that of other materials such as stainless steels, while Ti-alloys have a modulus(96 GPa for cp Ti and 117 GPa for Ti-6Al-4V)and density about half that of the Co-alloys. The commercially pure titanium (cpTi) used in implants because it has an excellent tissue compatibility and better corrosion resistance than stainless steel, however, limited strength and very poor wear resistance hindered the material[6].

In the late 1970s, the Ti-6Al-4V alloy was used in prostheses grew because of its high excellent corrosion resistance due to an oxide film grows spontaneously on the surface upon exposure to air (repassivation ability) and good mechanical properties. Biocompatibility studies indicated that the chemical constitution of Ti-6Al-4Valloy is not perfect due to the presence elements of Al and V, undergoes rapid corrosion and ion that could be released in the human body, causing toxic effects environment leads to oxygen depletion and high concentrations of the element in the surrounding tissues. The vanadium generates cytotoxic reactions and aluminum results in the bones softening and neuron damage. The surface modification techniques were used to prevent the ion exchange in the body environment

and enhance the properties of the alloys surface, corrosion resistance and passivation ability [7,8].

Hydroxyapatite, HAp, Ca_{10} $(PO4)_6(OH)_2$, as a naturally occurring mineral found in the inorganic component of human bone' is ahighly bio-affinity that can make or form the bio-ceramic coatings and is bonded directly with bones and that are required for Osseo integration of the implant[9].

The structure, thickness and number of a HAp layers on surfaces effect on the quality of implants, coating with a single HAp layer, have poor mechanical, but much better bio-medical properties. Double and triple layers introduce a large number of interfaces, parallel to the substrate surface and may deflect micro cracks and wide different atomic intermixed between the substrate and the top-bio coating which improves of the adhesion strength.

HAp nanopaticles are one of the highest values in the biomedical field, are the major and most abundant material in human bones and teeth. As a result, synthetic HAp nanoparticles that mimic natural HAp are extensively synthesized to repair and substitute human bones [10].

Biocompatibility carried out by immersion test was performed on coated sample by immersed it in Simulated Body Fluid (SBF) for one month.

Using this solution, it is possible to form biomimetic apatite on bioactive surfaces[11].

In vitro carried out by corrosion test, the resout of corrosion behavior implantspacimen when coated surface with different thickness in SBF solution, compared tothe corrosion behavior of uncoated implant specimen. The corrosion resistance can be evaluated by electrochemical techniques, namely:

1-OCP -Open Circuit Potential consists in a period during which no current can flow and no potential can be applied to the working electrode

2-LSV-Linear Sweep Voltammetry measurements in hydrodynamic steady-state conditions and

3-EIS-Electrochemical Impedance Spectroscopy.

Corrosion is a natural process related to the nature of the passive film and it is surface phenomenon, that converts refined metal to their more stable oxide formed on the material in the intended environment [7].

1.2 Literature Review

Ceramic have played an important vital role to improve Osseo integration properties of the implant. It can be divided into two main types, oxides ceramic   (like ZrO_2, Al_2O_3, ,TiO_2,MgO ..*etc.*) and non-oxide ceramics (HAp, SiC, ZnS, Si_3N_4.. etc.)[12] .

A-Coating with Titanium Oxide TiO_2

Previous studies indicated the growth of apatite on TiO_2 coated specimens after imation in SBF. It is possible to increase the range of biomaterial applications and reduce from the release ion surface by depositing thin biocompatibility layer of TiO_2 ceramics on titanium alloys.

A.Dakka *et al* **(1999)**[13] Have been studied the optical response (as a function of oxygen partial pressure, target state and sputtering power) of TiO_2 layers prepared by RF sputtering used substrate mature SiO_2, Si and NaCl. They found that "TiO_2 layers deposited from a used target exhibit a high absorptance" which decreases highly when introducing oxygen partial pressure, whereas increasing the sputtering power will lead to an absorbent TiO_2 matrix.

L. Pawlowski (1999) [14] has studied the effect of ceramic Thick coatings TiO2, Al2O3 ceramics were deposited on NiTi alloys with high power lasers type CO2 by use powder injection to the melt pool using laser

deposition technique. The effect of mechanical interaction between a typical coating material with laser beam types and principal characteristics were reviewed. It was suggested that a better control of the process and better understanding of the physical phenomena occurring in laser treatment, such as injection of solid particles in a melt pool or solidification of the coating.

H.C.Yao *et al*(2000)[15] studied the deposited TiO_2 thin film on Si and glass substrates using RF magntron sputtering with the mixing of two gas types Ar and O_2. They found that crystallinity and microstructure of thin film depend upon the depostion time and $O_2/(Ar+O_2)$ mixing ratio. The crystalline phase occurs at high $O_2/(Ar+O_2)$ ratio and long deposition time; while low mixing ratio amorphous phase occurred. The thickness of thin films increases with depostion time.

Wenjie *et al*(2002)[16] Found that it anatase, rutile or amorphous TiO_2 films can be produced using RF magnetron sputtering deposited on the glass substrate with virus crystalline structures by varying charectrize sputtering such as gases, substrate temperature and annealing process.

Lei Miao *et at*(2002)[17] Studied the polycrystalline and epitaxial TiO_2 film formed on silicon and pyrex substrates using RF magntron sputtering with TiO_2 target in Ar and O_2 gas. They conformed that formation of the single phase TiO_2 can be achieved by changing the deposition parameters. A single phase rutil appears at fixed Ar pressure of 0.1Pa and 600°C heat substrate, also appears at 325°C while changed pressure from 0.1 to 1 Pa. Whereas anataes phase appears at 1Pa, with Oxygen flow ratio 0.1 to 0.7 sccm.

Janos Takacs *et al*(2005)[18] Have prepared coating on Ti and Ti-6Al-4V alloys substrate by Al_2O_3, HAp and TiO_2 Powder using plasma spraying

method. The results shows that "on the surface", the large particles compose increases porosity at increasing thickness of thin film coated.

Xiaobing Zhao(2006)[19] Studied the TiO$_2$ Powders coating on Ti-6Al-4V substrate using plasma spraying method. A chemical treatment method was used to increase surface bioactivity, the immersed sprayed TiO$_2$ coating in 10M of NaOH solution at 60C^o for 24h, then soaked in SBF to create bioactivity. A containing hydroxyapatite can be induced to form on the surface during the immersion in SBF *in vitro* test.

Maria C. Advincula *et al*(2006)[20] investigated the properties of surface titanium alloy properties by surface sol-gel processing (SSP) or by passivation with nitric acid to enhance the bio reactivity of Ti-6Al-4V substrate. Surface analysis of sol–gel–create oxide on Ti-6Al-4V substrates showed a prevalent titanium dioxide (TiO$_2$) composition with abundant hydroxyl groups. The surface was highly wet table, rougher, more porous and cells adhered to the sol–gel-coated surface compared to that of the passivated substrate.

Tuli Dey *et al*(2011)[21] Coated the surface of Ti by a robust (lum thick) mesoporous titania layer (MTL), and they found that the surfaces can very efficiently. These coatings are produced by anodization of Ti at elevated temperature in a glycerol/K$_2$HPO$_4$ electrolyte, followed by an appropriate etching process. Immersion tests in two types of simulated body fluids (Kokubo SBF and Bohner and Lemaitre SBF) are combined to examine these layers with regard to their ability to form hydroxyapatite. The MTL layers lead to a significant enhancement of HAp formation and anchoring in the structure compared with non-coated.

Chaing-Hua Wei *et al*(2011)[22] studied the effect of surface roughness on the crysralline strucur of TiO$_2$ by deposited polycrystalline TiO$_2$ thin films on various unheated glass and ITO rough substrates using RF magnetron

sputtering. The XRD results show that the polycrysralline structure was formed on the unheated glass while nano crystalline structure easily formed on the rough surface.

Krishna *et al* (2011)[23] studied the effect of titanium oxide under layer formed by DC sputtering on the crystalline phase of the TiO_2 thin films formed on 316L stainless steel by non-reactive RF magnetron sputtering of TiO_2 target. They used Ar gas of 0.5 psi and substrate temperature of 300°C, as deposition condtions. The resulting underlayer TiO_2 films have tribological properties, wear and corrosion resistance of the stainless steel in terms of of the reduced of friction coefficient and enhancement in the surface hardness.

V. Khalili *et al*(2013)[24] develop a bioactive and corrosion resistant by converting the bio inert surface of NiTi to bioactive and biocompatible surface by depositing TiO_2 particles on the NiTi surface using electrophoretic deposition process. TiO_2 particles were prepared using a mixture of acetone and n-butanol (0%, 30%, 60%, 80% and 100% acetone) without using any dispersant.Surface morphology of coatings shows deposition within 0% acetone cause to crack-free and dense coating with relatively coarse grains and high corrosion resistance.

B-Coating with hydroxyapatite HAp

Coating with HAp which can reinforce rapid bonding to natural bone, there are different techniques that commonly uses HAp to coat implant material include: immersion-coating, dip-coating, electrophoretic deposition, hot isotactic pressing, solution deposition, flame-spraying and sputter-coating. The biological, chemical and mechanical properties of the coating depend on the method used. The immersion coating and dip-coating methods disadvantage may degrade compromise the purity of the hydroxyapatite and they require high temperature for the post-sintering of

the ceramic layer. Electrophoresis results in non-uniform thickness, large agglomerates& poor biological fixation to the metal substrate. Hot isostatic pressing is two-stage technique which is difficult to seal borders on implants and cumbersome with complex shapes. Plasma spraying process with high velocity and temperature technique produce high degree of melting to ceramic powder. Limitations associated with the plasma-spraying process included; high porosity, poor adherence and cost[25].

Most sputter-coating techniques are slow and have an inadequate rate of deposit on a substrate that has been placed in a vacuum chamber, leading to overcome the contaminationencounter with other technigues.

Sputtering processes are common method to deposited thin film properties in ways not viable through other deposition techniques. This flexibility comes from many possible combinations and permutations of deposition process parameters, gas, target and sputtering equipment[26].

RF sputtering can be performed on all types of materials. One primary benefit of RF is the ability to deposit high melting point oxides at relatively low substrate temperature. RF sputtering is widely used in a variety of applications ranging from semiconductor industries to aerospace [27].

H.M.Kim *et al* **(1996)**[28] have prepared a sodium titanate layer on commercially pure titanium and different titanium alloys substrate using simple chemical method.This method includes the socking of cpTi, Ti-6Al-4V, Ti-6Al-2Nb-Ta, and Ti-15Mo-5Zr-3Al alloys substrates in 10M NaOH aqueous solution and then heat-treated at 600°C. The treatment resulted in the formation of a dense and uniform bone like apatite layer on surfaces after immersion in Simulated Body Fluid(SBF) with ion concentrations nearly equal to those of human blood plasma. The alkali (in NaOH) - and heat-treated (at 600°C) metals bond to living bone through the bonelike apatite layer formed on their surfaces in the body.

Karlis A. Gross *et al*(1998)[29] used atmospheric plasma spraying to creat a mixture of crystalline and amorphous phase of HAp on implants to enhance adhesion and fixation of the implant to the surrounding bone. Inthier study,heat treatment was used to convert the amorphous phase to crystalline followed by the diffusion of hydroxyl ions, the amorphous phase contracts, because of hydroxylation and crystallization, which produce cracks in the coating. They suggested that "the increasing in crystallanityof the coatings on the implant is not recommended"

J.G.C.Wolke *et al*(1998)[30] coated a cpTi substrate with Ca-P by using RF magnetron sputtering.A copper disc provided with plasma sprayed HA was used as target material. The substrate was coated with a film of different thicknesses (0.1, 1 and 4μm) and annealed at 500°C for 2h .The analysis results show that an amorphous film with low thickness 0.1 μm changed in crystalline apatite, while amorphous film with high film thickness(1 and 4 μm)sputter coating into amorphous–crstallinie structure shows some cracks. All the heat treated films showed stability when immersed in SBF. The authors concluded than the *In vitro* test of amorphous surface with low thickness dissolved after 4 weeks in SBF while high thickness only shows sign of surface dissolution.

Masayuki KON *et al*(2002)[31] investigated a HAp ceramic surface modification of the compositional gradient layer containing α-TCP using two-step treatment incloudes the immersion in5.0 mol/L H₃PO₄ solution and buffered solution (pH equile 4.0) consisting of phosphate and then heated at 1250°C for 1h. XPS analysis shows that HAp ceramic increases with increasing depth from the surface. The α -TCP transforms to HAp in water, *in vitro* or *in vivo*. Hence the surfaces of specimens can be modified with a compound such as α -TCP. However, the surface modified layer or compositional gradient layer is remarkably thin, with maximal thickness of

approximately 2μm. It appears that the compositional gradient layer containing α -TCP on the surface of HAp has more effective bioactivity than the non-treated HAP ceramic.

Takayoshi Nakano *et al*(2002)[32] studied the effect of heat treatment on improvement of the microstructure and solubility of HAp (*in vivo* test). The change in phase layer of surface and control grain size of the HAp were exaimend to improve the the solubility of HAp .They found that high solubility and boundary layer composed of (TCP,αTCP,CaO) was formed by annealing HAp at high temperature 1350°C in vacuum.

Ricardo M. Souto *et al*(2003)[33] investigated the degradation characteristics of hydroxyapatite (HA) coated on orthopaedic Ti–6Al–4V alloy using plasma spray .They studied the degradation by immersed in Ringer's salt solution and using electrochemical impedance spectroscopy(EIS). "The characteristic feature that describes the electrochemical behavior of the coated material by plasma spray is the coexistence of large areas of the coating itself with pores where the substrate is exposed to the aggressive media that is, the corrosion resistance of the biomaterial is not greatly affected by the presence of the ceramic coating, but rather depends on the passivation ability of the metallic substrate and, to a minor extent, on the porosity of the ceramic coating".

Shuyan Xu *et al*(2005)[34] studied the effect of time deposition t_D on thickness of thin film HA-coated on Ti-6Al-4Vorthopedic alloy using RF sputtering . The XRD intensity amplitude of HA crystalline content increases with increasing t_D and becomes more pronounced.

Chun-Cheng Chen *et al*(2006)[35] Studied the effect of heat treatment at range of 500–700°C on the improvement of bioactive hydroxyapatite (HAp)-coated Ti-6Al-4V alloy implants using plasma spray. Hanks' balanced salt solution was used *in vitro* corrosion test for samples plasma

spraed with heated and non-heated. They concluded that "the heat treatment at 600°C for 1h in air, endowing with increased recrystallization of amorphous calcium phosphate of as-sprayed HA coatings and reduced the defects without significantly reduced bond strength, provided a better corrosion protection than the other two treatment temperatures 500 and 700°C".

V.F.Pichugin *el at*(**2007**)[36] studied CaP thin film(0.09-2.7μm) deposited on pure titanium, 316L stainless steeland Ti-6Al-4V alloy by using RF sputtering. Ca-P coating prepared by RF-magnetron deposition has high values of adhesion strength, morphology increasing in roughness with increasing thickness of thin film without pores and micro cracks. Also at increasing thickness, the Ca concentration increases more than P concentration probable that during the sputtering the atoms of calcium Ca, which have a little more mass, displace the atoms of less mass, in particular phosphorus P. The cracks and damage of coated accure at thickness more than 1.6 μm.

Jidong Long *et al*(**2007**)[37] worked on graded Ca-P bioceramic on a Ti-6Al-4V orthopedic alloy by RF sputtering. They conclode that chemical composition and presence HAp, $CaTiO_3$, and CaO mineral phases can be effectively controlled by the process parameters. For the film synthesized at 700 W RF power, under 12 torr working gas pressure giving a Ca/P ratio of 1.64.Optical emission spectroscopy suggests that CaO^+ is the dominant species that responds to negative DC bias and controls calcium content. Biocompatibility tests in SBF at 36.5°C and a pH value of 7.4 confirm a positive biomimetic response evidenced by soaking for 24h, some small apatite particles were formed indicating the apatite nucleation onset and for 48h, it was observed that apatite had covered completely the surface.

Paulo G. Coelho *el at*(2009)[38] investigated the physico/chemically characterize of (Ca–P) thin film of 400–700nm thickness coated by a sputtering process on (Ti-6Al-4V) alloy. The corrosion resistance for coated and uncoated samples were determined and tested in Phosphate Buffered Saline (PBS). They found that by RF sputtered can produce thin bioactive ceramic with higher corrosion resistance compared to uncoated surfaces.

Christopher Jeremy Tredwin(2009)[25] used the sol-gel method to coat implant cpTi alloy by Hydroxyapatite (HAp), fluorhydroxyapatite (FHA) and fluorapatite (FHAp). Calcium nitrate and triethyl phosphite were used as precursors under an ethanol-water based solution. Increasing the coating speed decreases the porosity and thickness of the coatings, dissolution (Ca_2^+ and PO_4^{3-} rates) rates for ball rates could be decreased by increasing the sintering temperature.

V.A. Mamaeva *et al*(2009)[39] used the pulsed high power action on electrode electrolyte interface with microplasma discharges method for obtaining Hydroxyapatite (HAp) and HAp/yttria-stabilized zirconium (YSZ) nanostructural bioceramic coatings on titanium and titanium based alloys for stomatology and orthopedy. Such coatings can be uniformly and smooth.

Jayachandran Venkatesan *et al*(2010)[40] evaluated the effect of temperature on the charastristic and isolation of HAp from tuna bone at different temperatures ranging from 200 – 1200°C. Based on their analysis, the formation of nanostructured HAp (80–300 nm) with beast result characterization at 600 °C and crystal agglomeration was observed with an increase in temperature due to the appearance of tricalcium phosphate, the isolation temperature between 600–900°C has tremendous impact on the production of HAp. Low temperature needed to formation HAp.

Carl lindahl (2012)[41] investigate the nature of apatite coatings on implant Ti alloy prepared by the biomimetic method. The method is based on the soaking of solution PBS based process where the compositions of the soaking medium and thus the formed coatings can be controlled. The ions of solution exchange with ions of oxide layer; biologically active ions were substituted into the apatite coatings. The *in vivo* effects showed that the ion substituted apatite coatings have good biocompatibility and can promote early bone formation.

Rajan Anand (2012)[42] studied the improved properties of HAp of sintered (900° for 2h) and non-sintered hydroxyapatite layer coated on Ti6Al4V alloy by using electrophoretic deposition carried out at a constant voltage of 30V for 5, 10 and 15 minute duration at different pH values of 1.5, 2.5 and 3.5 respectively. SEM images show that at constant voltage of 30V and low pH of 1.5, coated surface shows no cracks. XRD analysis showed that "before sintering, few other compounds were present in HAp powder while after sintering they were not oxidized.The more coating layers, leads to a wide different atomic intermixed between the substrate and the top-bio coating which improves the adhesion strength.

C-Coated with Different doublelayer

Yong Liu *et al*(1998)[43] studied the behaviour of Ca/P enhanced by $MgAl_2O_4$ in (SBF) with PH value 11-12. The results show that at low concentration of $MgAl_2O_4$, the formation of apatite increases on the surface of Ca/P. The formation composite ceramic in SBF depends on dissolation of the surface Ca/P and amorphous material produces from reaction of HA with Mg Al_2O_4.

Shinn-Jyh Ding (2003)[44] worked on the development of biocompatiblity and improved the interface properties between the coating and the substrate coating by multi-layered concept. Ti and HAp layers deposited on Ti-6Al-

4V substrate by using RF magnetron sputtering, an underlying Ti bond coat, the alternating layer, and an HA top-layer. For corrosion test, itpresented multi-layered coatings exhibited a better immersion in SBF than single layer HA coatings and high adhesion on substrate.

Yu-PengLu *et al*(**2003**)[45]   used two layer hydroxyapatite (HAp)/HAp+TiO$_2$ to coat titanium . Three kinds of specimens,pure HA coating, 50 vol% HA+50 vol% TiO$_2$ composite coating and two-layer HA top coating/ bond coat composite coating on titanium were produced by plasma spraying followed by heat treatment at 650°C for 120 min which resulted in transfer calcium phosphates into HA. From EDS, there exists inter diffusion of the elements but from XRD no chemical product between HA and TiO$_2$, such as CaTiO$_3$ was formed. The positive effect of the composite coating is the decrease of residual stress in HA top coating. The Ti substrate bonds well via its TiO$_2$ hobnobbing with the Ti oxides formed on Ti substrate.

R.Tomaszek *et al*(**2004**) [46] investigated the effect of changing the mixing ratio of theTiO$_2$ and Al$_2$O$_3$ on microstructure of coated layer. The results showed that the mixing Al$_2$O$_3$ with 13%TiO$_2$ give the best ratio microstructure for coating titnium alloys by using plasma spraying.

Zuqiang Qi (2004)[47] reviwed the importance multilayer coatings such as Al/Al$_2$O$_3$,Ti/TiN have high potential for nourmas applications . These can exhibit enhanced properties due the effects on mechanical behavior of the multilayer. The Al in the multilayer has finer grains and   the interface between Al and Al$_2$O$_3$ layers is continuous without any major defects than those when deposited as single layer, Ti layer grows in coarse columns when deposited on TiN with sharp intephase between metal and ceramic.

Hae-Won Kim *et al*(**2004**)[48]   developed (HAp/TiO$_2$) coated on to Ti substrate by a sol–gel method with thicknesses of approximately 800 and

200nm. The HA coated up layer to enhance the bioactivity and osteoconductivity of the Ti substrate and, TiO_2 layer was inserted mid to improve the bonding strength between the HA layer and Ti substrate as well as to increasing corrosion resistance of the Ti substrate, With heat treatment thin film at 500° C. *In vitro* test, osteoblast-like HOS cells grew on HA/TiO_2 in a similar fashion but a little more actively compared to those on the bare Ti and TiO_2 coated Ti. *In vivo* corrosion test, with a physiological saline solution at 37°C, the TiO_2 coated improved corrosion resistance of the Ti substrate.

Chun-Cheng Chen *et al* **(2005)**[49] worked on deposit HAp as outer layer and TiO_2 under layer on Ti-6Al-4V substrate using plasma spraying to improve the coating–substrate interface properties. The results show that graded (HA/TiO_2) had better mechanical properties than single HA coatings, surface chemistry and morphology of the graded coatings were similar to those of single layer HA coatings. The *in vitro* electrochemical measurement results after immersion in HBSS for 1h,also indicated that the graded coatings seem to possess a better corrosion-resistant ability behavior than single HA coatings.

Zhou-Cheng Wang *et al***(2008)**[50]   carried out electrophoretic co-deposition of HAp and Al powder to form HAp/Al_2O_3 composite coating on cpTi alloy. The composite coating sintered at 850℃ ,and due to the thermal decomposition, the HAp phase appeared with no cracks and the bonding strength to the substrate was significantly improved compared to the single HAp coating.

Wisanu Boonrawd *et al***(2010)**[51] deposited composite of HAp/Ti target on silicon wafer and Ti-6Al-4V alloy substrates by using RF magnetron sputtering. The composite of HAp/Ti films annealed at 600°C and 700°C. The results showed that the filme exhibited high adhesion strength as

compared to monolithic HAp coatings on Ti-base substrates and the XRD analysis revealed peaks of HAp and calcium titanate ($CaTiO_3$).

I. Mercionu *et al*(**2012**)[52]   obtained new $HA/Y_2O_3:\alpha Al_2O_3$ system by deposition of a hydroxyapatite thin layer with thickness of (~150 nm), using RF magnetron sputtering, onto sintered substrates of low yttria (150 ppm) doped alumina. The morphology of the layers was homogeneous, while at the $HA/Y_2O_3:\alpha Al_2O_3$ showed a strong structural interdependence between the sintered substrate interface and covering layer with no loosening phenomena were evidenced. The grain size showed a linear increase with the annealing time.

L. Mohan *et al*(**2012**)[53]   studied the corrosion and scratch behavior of TiO_2 + 50%HAp nano ceramic coated on Ti–13Nb–13Zr orthopedic implant alloy using (EPD) sintering at 850 °C. The corrosion behavior of the coatings was evaluated using SBF-Hank's solution. The sintered coating exhibited higher density, adhesion and lower porosity compared to unsintered samples, and higher corrosion resistance compared to the substrate.

Conclusion Remark of Literature Review

1-Heat treatment was use to convert the amorphous phase to crystalline followed by the diffusion of hydroxylions .By increasing time of heat treatment wich lead to produce crack also formed layer composed (TCP,CaO).The cracks and damage of coated CaP accuer at thickness more than 1.6um .

2-The composite (HA/Ti) films annealed at 600°C ,the film exhibited high adhesion strength with composit ($CaTiO_3$).The $HA/YeO_3:\alpha Al_2O_3$ system deposited by using RFsputtering ,showed a strong structural

interdependence between the substrate interface and covering with biocompatibility layer.

3-Immersion tests for coated samples in (SBF)are combined to examine the coated layers with regard to their ability to form HAp.

4-Any change in RF sputtering conditions working effected on the characterize of thin film.

Present work will

Deposite TiO_2 and HAp as single layers ,TiO_2+ Al_2O_3 as multilayer and TiO_2+ Al_2O_3+HAp as three layer on cpTi and Ti6Al4V alloy using RFmagntron sputtering .Structure analysis and corrosion tests will be used to evaluate the properties of single and multilayers also the coating will be achieve biomimetic test to see the efficiency of the compatibility.

1.3 Thesis Aims

The main aims to:

1-Develop biocompatibility coating on the surface of cpTi and Ti6Al4V alloy using ceramic nanoparticle TiO_2,HAp and Al_2O_3 by using RFmagntron sputtering processing .

2- Enhance the interface properties between the coating and the substrate by using multilayer of different bioceramics .

3-Evaluation the corrosion resistance.

CHAPTER TWO

Theoretical Aspects

2.1 Introduction

This chapter provides a review of selected biomaterial alloy, methods of modification surface, coating by ceramic using modern technique and basic corrosion process. It starts with an introduction to the most impotent properties of titanium alloy as implant material, important of modification surface using ceramic as HAp, Al_2O_3, TiO_2 with general properties as biocompatibility coating, the advantage of using plasma RF sputtering technique for enhance the properties of surface and corrosion resistance followed by basic corrosion process and corrosion kinetics, descriptions of some major electrochemical techniques for corrosion rate evaluations such as(OCP, LSV, and EIS).

2.2 Biocompatibility Requirements for Joint Replacement Materials

Biomaterial is defined by the interaction between the body and the material; the effect of the material on the body and the effect of the body environment on the material [54]. The advent of an aseptic surgical technique developed by Dr. J.Lister in the 1860s mad the biomaterials become practical. The Consensus Conference of the European Society for Biomaterials (1986) defined biomaterials as (non-living) materials used in a medical device, intended to interact with biological systems; they have many characteristics including mechanical, physical, chemical and biological properties that make it suitable for safe, effective, and reliable use within a physiologic environment, an environment that is both extremely feudal and yet sensitive to unforgiving irritating foreign bodies also, the materials must be able to perform their functions within the body

environment for a long period of time (over 25 years) without decay. Bone is a living anisotropic and viscoelastic material that adjust to the loads placed on it, the elastic modulus of the material is the one of the most critical mechanical properties in implant applications with a low value that approaches that of natural bone which is critical in order to provide good load transfer between the implant and surrounding bone to spur new growth. Metal ions from metal implants are entry into the solution of body through an open wound and its follow corrosion by interaction with the surrounding tissues through reduction-oxidation (redox) reactions. The products of these reactions and the kinetics are determining factors that called the biocompatibility of an element. The titanium alloys are highly desirable for implant applications, high biocompatibility and inertness of titanium is due to the characteristics of its oxide layer. The oxide layer in titanium alloys represent in TiO_2 layer is an excellent insulator, and prevent transmit electrons from elements alloy to body tissues and fluids. Also, because the oxide layer forms by oxygen diffusing inward towards the metal interface instead of metal ions diffusing outward and combining with oxygen there is limited accumulation of ions into the surrounding tissue. Ni, Cu, Au, Mo, Ti, Nb, Ta, Zr, and Pt have the capacity to be used as alloying elements for improved biomedical titanium alloys, Fig. 2.1 describing the biocompatibility of some of the various elements [5]. Polarization resistance is the ratio of the applied potential and the resulting current response. This "resistance" is inversely related to the uniform corrosion rate, the higher the polarization resistance, the lower the corrosion rate [55].
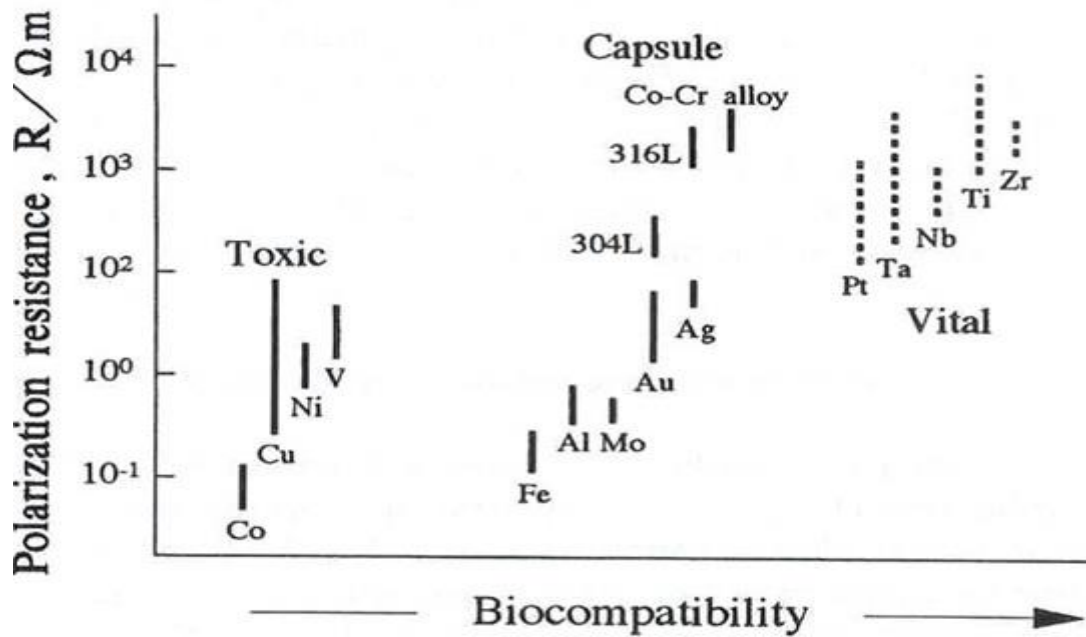
Figure 2.1: The relationship between polarization/corrosion resistance and biocompatibility of various metals [3].

2.3 The Basic Properties of Titanium

Titanium is one of the transition elements in group IV and period 4 of Mendeleef's periodic table. It has an atomic weight of 47.9 and atomic number of 22. Being a transition element, titanium has an incompletely filled d shell in its electronic structure. The incomplete shell enables titanium to form solid solutions with most substitution elements having a size factor within ±20% and in the element form, melting point (1668℃).The properties of titanium alloys are principally by two factors: the chemical composition and microstructure. The chemical composition of the titanium alloys primarily determines the properties and volume fraction of the phases, α hexagonal closely packed crystal structure (hcp) and β body centered cubic structure (bcc). Titanium alloys falls into three classes: α-alloys, α+β alloys and β-alloys. Up to a temperature of 882.5℃, titanium transforms from α to β. Titanium alloys may be classified as neutral, α

and β depending up on the room temperature microstructure. The main properties that make titanium attractive for a variety of applications:

1-Mechanical properties: Titanium is used in orthopedics due to high specific strength and low elastic modulus, wear, density and abrasion resistance because of its low hardness, this problem solved by surface modification to enhance the abrasive wear corrosion resistance.

2-Biological properties: it is generally regarded to have good biocompatibility, relatively inert and have good corrosion resistance because of thin surface oxide when compared to more conventional stainless steel and cobalt-based alloys [5, 56].

2.3.1 Commercial Pure Titanium cpTi

F67 cpTi alloy have grades from 1to 4 are based on the low temperature, α phase (hcp) the four different grades of cp Ti differ with respect to their oxygen content of cpTi affects its yield and fatigue strength. The type of grade is 2 the chemical composition (Ti, Fe, N, C and O), 98.9-99.6% titanium concentration, 0.25 oxygen concentration and the yield strength is about 550MPa as shown in Appendix A.

cpTi has excellent corrosion resistance, fabric ability but poor in mechanical properties, especially strength. There are growing numbers of applications such as pressure vessels and dental implant. The mechanical properties are an equally important criterion for materials selection [56].

2.3.2 Titanium Aluminum Vanadium Ti-6Al-4V alloy

F 136 Ti-6Al-4V for orthopedic load –bearing implants alloying, addition of 6% aluminum with α phase and 4% vanadium with β phase to cpTi as shown in Appendix B, results in any alloy having good mechanical

properties yield strength is about 880MPa (increasing the yield and tensile strength, acceptable elongations) and chemical inertness. From Fig.2.2 it is clear that for this aluminum level of about 6% the α / β, transformation temperature of 882°C for pure titanium is increase to about 1000°C for the two phase region α + β. Since vanadium is a β -stabilizer, this means that the higher temperature β more readily transforms to α during cooling after processing, and also during any subsequent heat treatment at relatively low temperatures, annealing at 700–750ºC.

The most popular titanium alloy, more than 50% of alloys in use today are of this composition [7,65].Ti- 6Al-4V alloy has been in clinical use since the 1950 there are reasons: good balance of its properties, ultimate strength, corrosion resistance, ductile behavior for loads exceeding the yield stress (thus reducing the risk of catastrophic brittle failure), fabric ability, available and cheap.
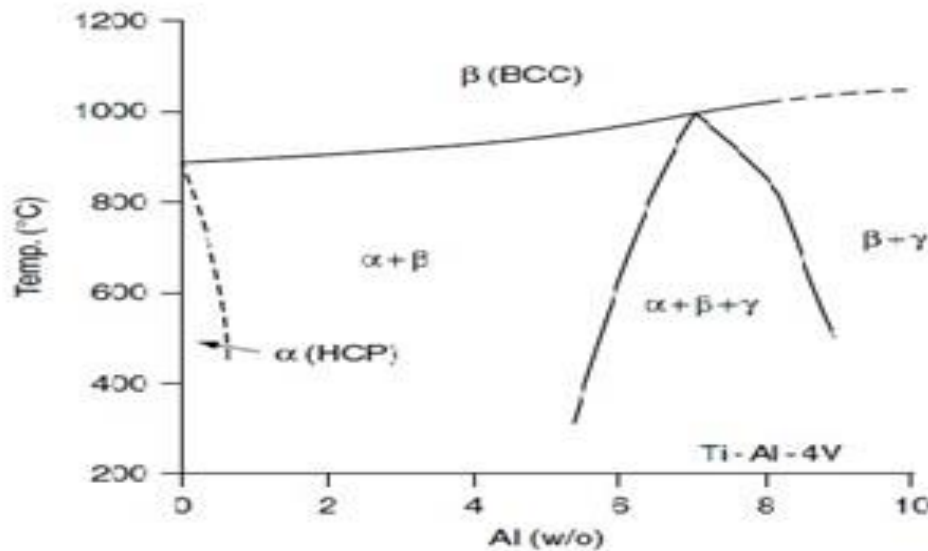
Figure 2.2: Phase diagram of Ti-Al-V alloy [57]

The passive film consists of TiO_2 as the major component and Aluminum oxide (Al_2O_3), vanadium oxide (VO_2) respectively on the metal surface. In return to VO_2 is thermodynamically unstable and performs into solution body. An inert fibrous capsule formation around the implant to prevent

damage to surrounding tissues and eliminated by body within 24 hours, this is presumably why implants made of Ti-6Al-4V alloy have not shown any serious disadvantages so far [7] . In general, there is a problem in using Ti-6Al-4V alloy for implant applications belong to the large modulus mismatch between the Ti-6Al-4V alloy (~110GPa) and the bone (~10-50GPa), which could cause insufficient loading of the bone adjacent to the implant. Development of new alloy materials and modification of the surface of the currently used Ti alloys have been widely explored to overcome these problems. Either the development of Ti6Al7Nb and Ti5Al2.5Fe, where Nb and Fe were substituted for Vin Ti-6Al-4Valloy as less toxic alternatives or numerous bioactive surface modifications of titanium alloys for biomedical applications are very important for achieving further developed biocompatibility [58, 7] .

2.4 Surface Modification

The bulk properties of biomaterials, such as non-toxicity, corrosion resistance or controlled degradability, modulus of elasticity, and fatigue strength have long been to recognize to be highly relevant in terms of the selection of the right biomaterials for specific biomedical application. The events after implantation include the interactions between the biological environment and artificial material surface, onset of biological reactions, as well as the particular response paths chosen by the body.

In implants made of titanium, the various surface modification techniques required because:

1. In implants made of titanium, the normal manufacturing steps usually lead to an   oxidized, contaminated surface layer that is surfaces are clearly not appropriate for biomedical applications and some surface treatment must be performed.

2. The specific surface properties that are different from those in bulk are often required. The difference between the modulus of elasticity of the metallic implant of Ti and the modulus of elasticity of bone tissue can be controlled with the fabrication of the structure surface of Ti implants.

3. Good wear and corrosion resistance.

4. Improve specific surface properties required by different clinical applications.

The surface modification techniques are a general concept that can be divided into surface treatments and surface coatings, or a combination of both, surface modification classified into [56]:

1. **Mechanical methods**: grinding, polishing, involve physical treatment, shaping, or removal of the materials surface. The typical objective of mechanical modification is to obtain specific surface topographies and roughness, and to remove surface contamination.

   The deposition techniques that represents the processes to build thin film on substrate thin film have a thickness anywhere between a few nanometer to about 100 micrometer. These techniques can be classified in two groups chemical and physics methods as shown in Figure 2.3.

2. **Chemical methods**: include chemical treatment, electrochemical treatment (anodic oxidation), chemical vapor deposition (CVD) ,sol–gel. Electrochemical or biochemical reactions occur respectively at the interface between titanium and a solution. (CVD) is a process involving chemical reactions between chemicals in the gas phase and the sample surface resulting in the deposition of a non-volatile compound on the substrate. In the sol–gel process,

chemical reactions do not occur at the interface between the sample surface and solution or gel, but rather in the solution.

3. **Physical methods**: refer to such methods   as thermal spraying and physical vapor deposition (PVD), where chemical reactions do not occur. In this case, films or coatings on titanium and its alloys are mainly attributed to the thermal, kinetic, and electrical energy. In the thermal spraying process, the coating materials are thermally melted

Into liquid droplets and coated to the substrate at a high speed (kinetic energy). The generation of atoms, molecules or ions from targets can be accomplished by resistance heating, electron beam, sputtering and laser or electrical discharge in vacuum. Glow discharge plasma treatment and ion implantation are also categorized as physical methods [56, 59].
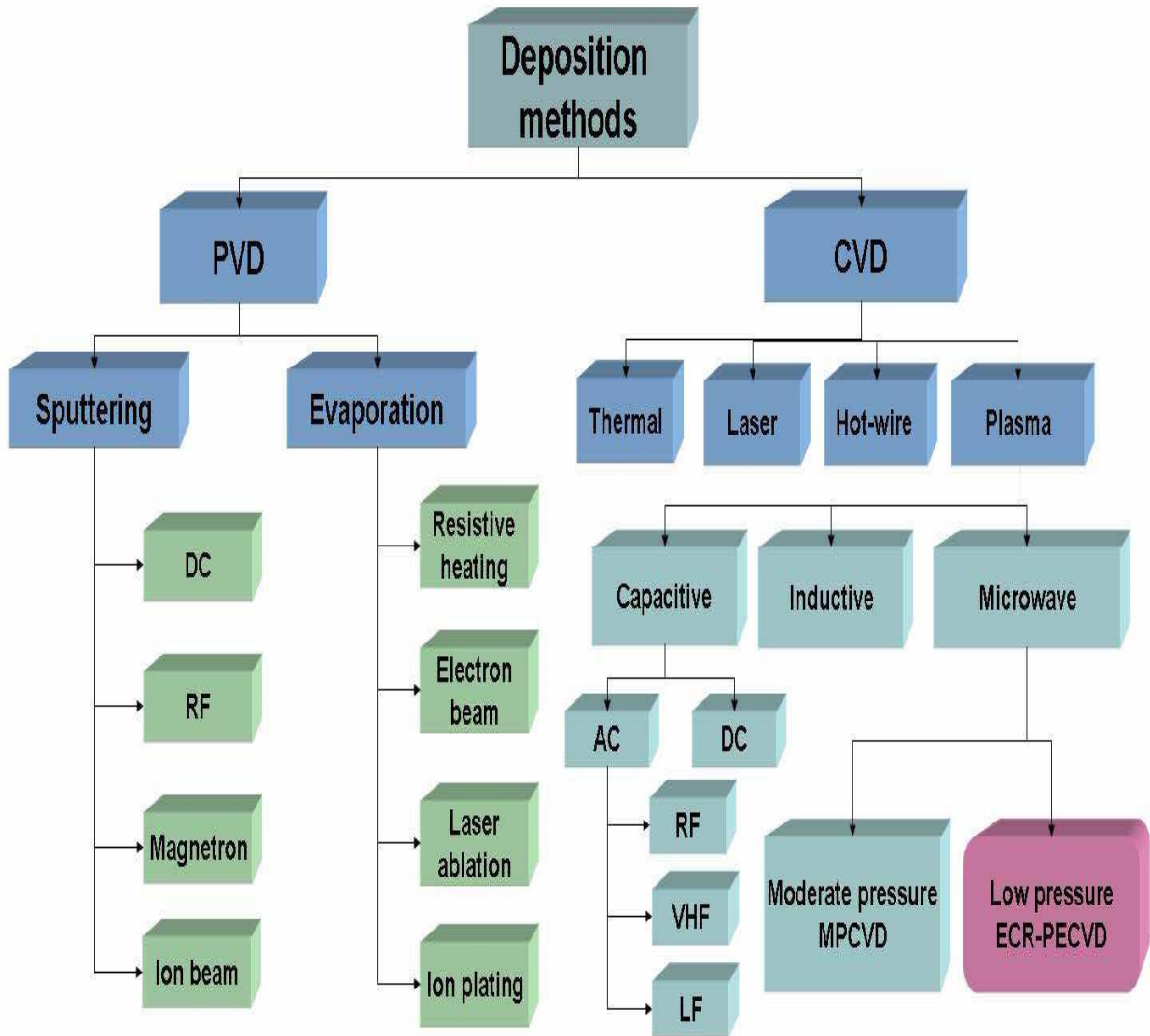
Figure 2.3: Block diagram of deposition techniques [60]

2.5 Plasma and Plasma Properties

Plasma can be defined as a gas containing charged and neutral species showing collective behavior. It consists of electrons, positive - negative ions, atoms, radicals and molecules. On average plasmas are electrically neutral, since any charge imbalance would create electric fields that would tend to move the charges to eliminate the imbalance. As a result, the combined density of electrons and negative ions will be equal to that of

positively charged ions in any given volume of plasma. This property of plasmas is called quasi-neutrality [56].

Sputtering   is a preparation technique where the ejection of a material is due to the transfer of energy from an energetic particle to a surface. The energetic particles, in the mixture form of ionized atoms or clusters of atoms, is passed to a substrate where a film of the target material is deposited. This process has been utilized to more conveniently deposit a wide range of materials since the momentum exchange is a physical process as opposed to a chemical or thermal process [56, 61].

The target is mounted opposite to the substrates in a vacuum chamber. A strong potential difference is applied in a gas, generally of argon, with possibly reactive gases (O_2, N_2, etc.), a precursor gas argon is used in most applications because of its mass compatibility with materials of engineering interest and its low cost. When the target is powered negatively, typically between 0.5 and 5 kV, ionized argon atoms provides the ion bombardment of the target.

The process is then, the ejection of the target atoms is resulted from the argon ion bombardment, their transfer to the substrate with a kinetic energy and the nucleation and growth of the thin film on the substrate surfaces [3], as shown in Fig.2.4.Magnetron sputtering (MS) and RF is a very powerful technique which is used in a wide range of applications due to its excellent control over thickness, preparing large area uniform films, adherence of the films. The magnetic field in the magnetron is oriented parallel to the cathode surface the local polarity of magnetic field is oriented such that E×B drift of the emitted secondary electrons forms a closed loop. Due to the increased confinement of the secondary electrons in this E×B drift loop, plasma density will be much hair compared to a DC or diode device. The

result of the high plasma density and its proximity to the cathode is a high current, relatively low voltage discharge [62,59].

Plasmas have two important characteristics that are ideal for thin film processing:

Firstly, they are sources of chemically active species, radicals and ions that result from the collision of neutral background gases with electrons which are sufficiently energetic to break their chemical bonds. Substrate surface reactions can thus take place at much lower temperatures than in thermal processing.

Secondly, low-pressure plasmas offer the added advantage of a non-collisional sheath, ensuring that the energy of the ions striking the surface can be accurately controlled within a broad range. Energetic ions play a synergetic role in deposition and etching processes and a determining role in sputtering processes [63].
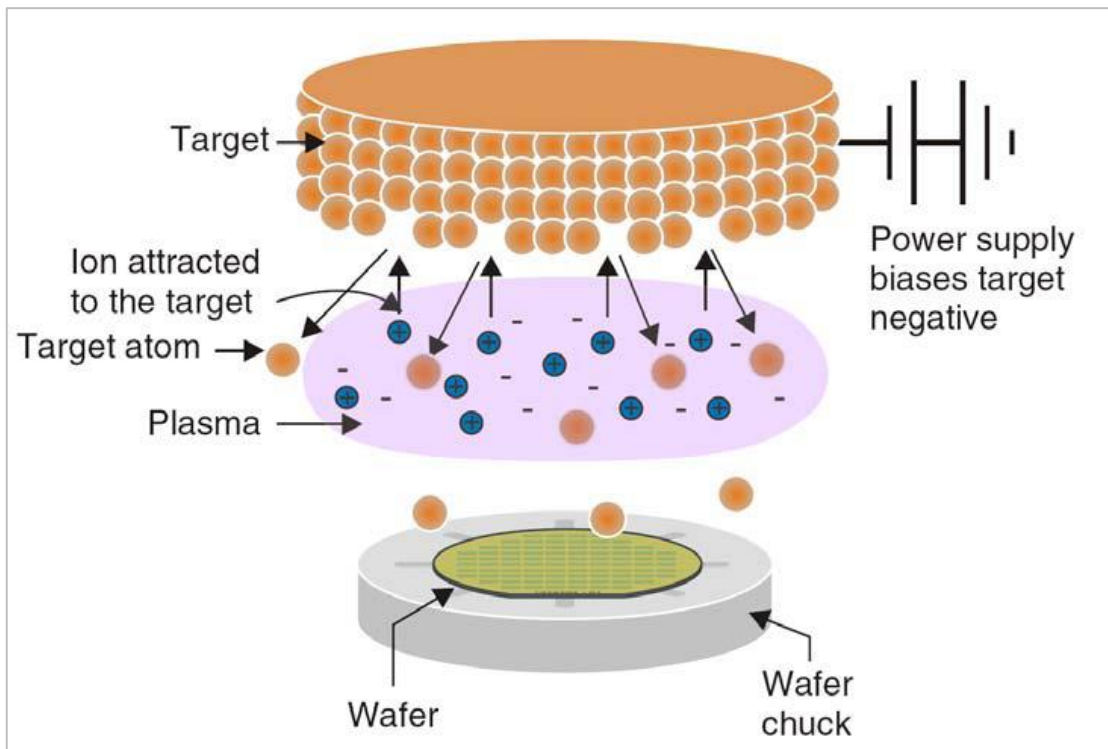
Figure 2.4: Schematic representation of diode sputtering assembly [64]

RF Sputtering Technique

DC methods cannot be used to sputter non-insolating targets because of charge accumulation at the target surface. The application of high frequency voltage can overcome the problem of charge accumulation, this solution by using RF methods typical voltage frequency is 13.6MHz since this has been allocated by the Federal Communications Commission (USA) for industrial-scientific-medical purposes. Sputtering non-conducting materials is based upon the fact that a self-bias voltage, negative with respect to the plasma potential, develops on any surface that is capacitively coupled to a glow discharge. The basis for this potential, which forms as a consequence of the difference in mobility between electrons and ions, is illustrated schematically in Fig. 2.5[64].
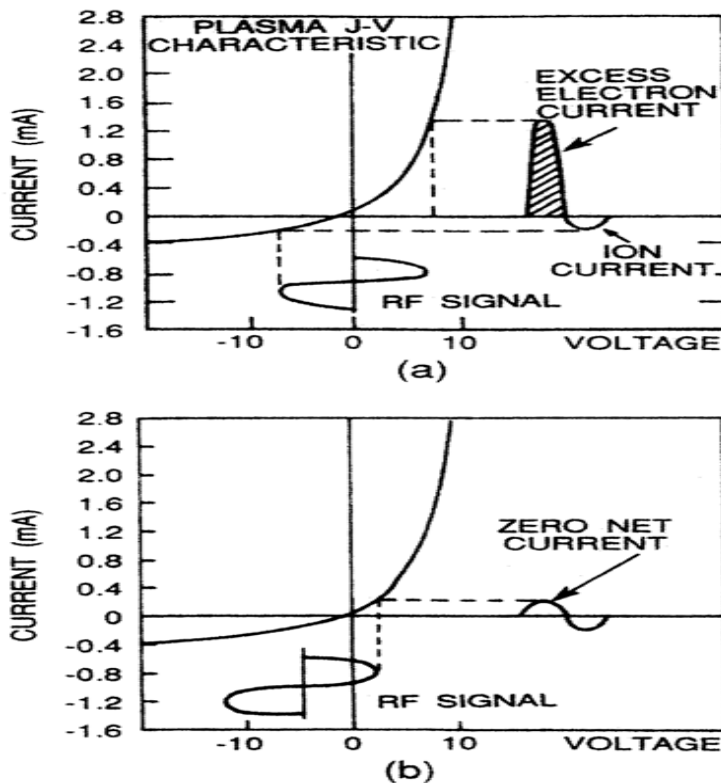
Figure 2.5: Schematic illustration of the development of a negative bias in a RF system : (a) The current-voltage characteristic for an electrode immersed in plasma,(b) When an alternating voltage is applied to an electrode, a positive/negative potential appears on the surface [64].

2.6 Ceramic

Ceramic materials use to cover the implants which used in medical applications, including bio inert ceramics (i.e. alumina and zirconia), and bioactive ceramics (i.e. calcium phosphates, titania, bioactive glasses and glass ceramics). Alumina excellent mechanical properties is for the load-bearing applications, while the bioactivity ceramics leads to the potential for Osteoconduction [65].

2.6.1 Hydroxyapatite HAp

Bone is formed of cells 10% and matrix 90% (organic 40% and inorganic 60%). An organic matrix composed mainly of type1 collagen and a mineralized inorganic matrix (crystals of HAp and CaP). The collagen fibers which form bone are the result of the bonding by means of crossed links of a triple helix of chains of this material [66, 67], as shown in Fig. 6.2.

(a)   (b)
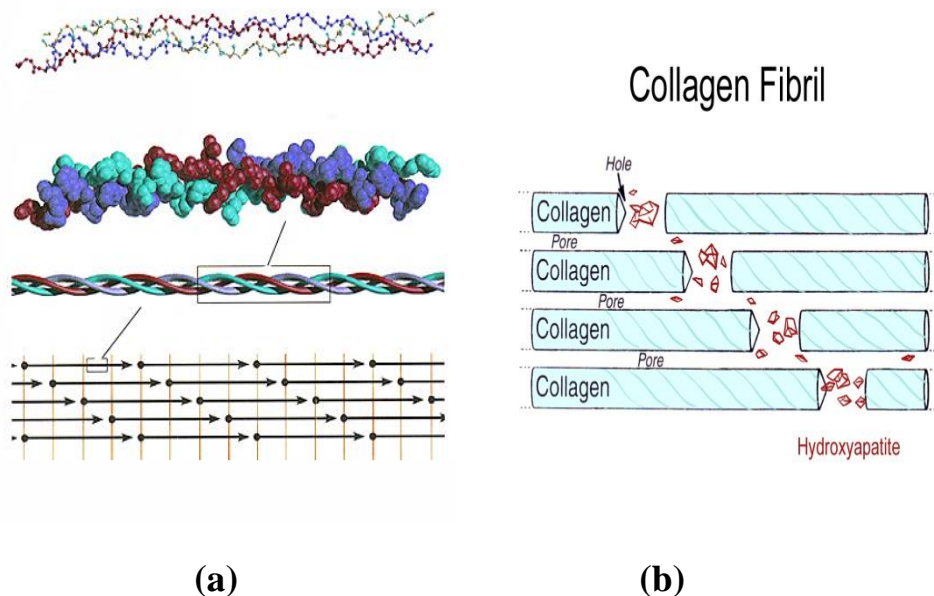
Figure 2.6: (a) Bon Polypeptide triple helix tropocolagen bond together forming, (b) Most HAp fills in holes in collagen[66].

The mineral apatite, can be represented by the formula, $M_{10}(ZO_4)_6X_2$ (or $M_5(ZO_4)_3X$), as a general term that can be applied to the crystal structures. Each component (M, ZO_4, and X) of the common equation $M_{10}(ZO_4)_6X_2$ can be replaced by a large number of different elements or solid states. M or X can also be absent. The most common form found in nature is calcium phosphate apatite, whereby the M and ZO_4 are Ca^{2+} and PO_4^{3-} groups. When the X is OH^-, $Ca_{10}(PO_4)_6(OH)_2$, it is given the name hydroxyapatite. HAp is the key inorganic component of the hard tissues of vertebrae, and is an important substance in bioactive ceramic materials, it is one of many types of calcium phosphate (or calcium orthophosphate) as shown in Table 2.1, but there are several others in this class. The simplest way to arrange these into order is by the calcium-phosphorus composition ratio. At physiological pH (7.2-7.6), HA is most stable.

 OCP is an intermediate that appears during extraction of the HA phase. Within TCP, α-TCP shows a stable phase between 1180 and 1430°C and transforms into its β-phase at higher temperatures.α-TCP, a hypothermic phase material, is often used in the same way as HA, in bioactive ceramics. Its absorptivity when implanted into the body is significantly higher than that of HAp. A material composed of a mixture of HA and α-TCP has also been developed, called biphasic calcium phosphate (BPC).

A metastable amorphous phase material known as amorphous calcium phosphate (ACP) exhibits a significantly higher bioresorbable property than other crystalline calcium phosphate compounds [68, 69].

2.6.1.1 The Crystal Structures of HAP

A schematic diagram of the structure of HA as shows in Fig. 2.7, the structure shown here is the stoichiometric composition of HA where by the unit cell is composed of $Ca_{10}(PO_4)_6(OH)_2$. The core framework of the

structure is constituted mainly of the PO_4^{3-} tetrahedron, with two types of channel structures that lie parallel to the   c –axis at the positions, (x, y) = (0, 1/4) and (x, y) = (1/3, 1/12). The OH ion (z = 0 ± 0.2, 1/2 ± 0.2) and Ca^{2+} ion (z = 0, 1/2) lie within each of these structures. This Ca^{2+} is exposed on the crystal surface, thus playing a large role in the physical properties of HA, such as surface charge, and in interactions with organic compounds.

The stoichiometric crystal structure of HA has a monoclinic system with P21/b as its space group by Ca/P ratio of 1.67, exhibiting lattice parameters, a= 9.4215A°, b= 2a, c= 6.8715A°, gamma =120°. Earlier studies showed that it also could exhibit the hexagonal structure with space group P63/m. However, it is difficult to obtain the exact stoichiometry (Ca/P ratio) in HA because of different Ca/P ratios that can be stabilized depending on the synthesis method and conditions employed [70,71]. Biological apatite is a non-stoichiometric form of HAp, characterized by Ca^{2+} deficiency but containing trace elements.

The trace elements include positively charged ions, Mg^{2+}, Na^+, K^+; and negatively charged ions, Cl⁻ and F⁻. The most common replacement is with the CO_3^{2-} ion which constitutes 5-8% of apatite in bone, by weight. The CO_3^{2-} ion can replace all of the OH⁻ and certain PO_4^{3-} within the HAp structure, termed A-type and B-type replacement, respectively. B-type replacement is common in bones, and is an essential factor in altering the melting point of the biological apatite. Increases in positive charge with the replacement of PO_4^{3-} by CO_3^{2-} are balanced out either by the loss of Ca^{2+} sites or by the introduction of Na^+ ions.

Table 2.1 :The major calcium phosphates [68]

calcium phosphates material	Chemical composite	Ca/P
Monocalcium phosphate anhydrous(MCPA)	$Ca(HPO_4)_2$	0.50
Monocalcium phosphate monohydrate (MCPM)	$Ca(HPO_4)_2.H_2O$	0.50
dicalcim phosphate anhydrous (DCPA.monetite)	$CaHPO_4$	1.00
dicalcim phosphate dehydrate (DCPD.brushite)	$CaHPO_4.2\ H_2O$	1.00
Octacalcium phosphate(OCP)	$Ca_4(PO_4)_2O$	1.33
Alpha tricalcium phoaphate(α-TCP)	$Ca_3(PO_4)_2$	1.50
beta tricalcium phoaphate(β-TCP)	$Ca_3(PO_4)_2$	1.50
Hydroxyapatite(HA)	$Ca_{10}(PO_4)_6(OH)_2$	1.67
Tetracalcium phoaphate(TeCP)	$Ca_8H_2\ (PO_4)_65H_2O$	2.00

Fig. 2.7 shows the crystal structure of hydroxyapatite, where the c-axis is perpendicular to the plane of the paper the x, y, z that are mentioned in the text correspond to the direction of a, b, c in the diagram with defining the repetitive cycle as 1. The numbers in this diagram are the coordinates of the z-axis. The hydrogen atom of OH$^-$ ions on the y = 3/4 plane are hidden behind the oxygen atom [39, 68].
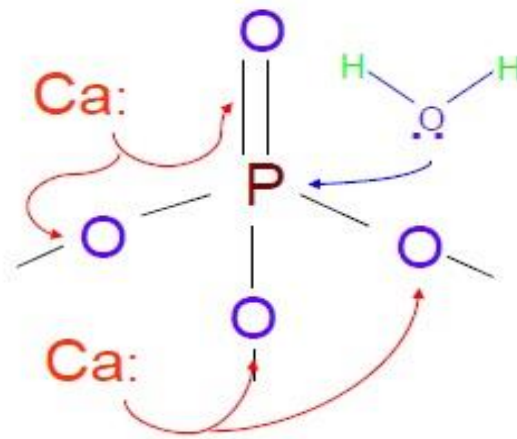
(a)
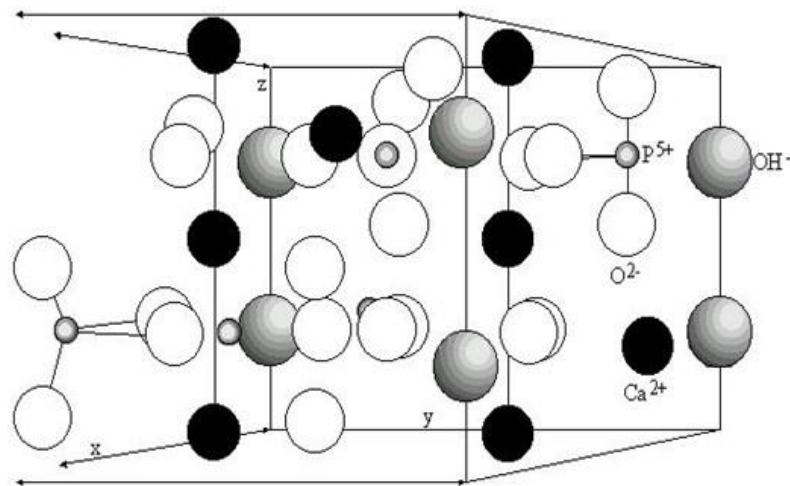
(b)

Figure 2.7:(a) and (b): The crystal structure of hydroxyapatite hexagonal [39]

2.6.2 Titania TiO$_2$

There are three phases of oxide titanium or titania in atmosphere air are anatase, rutile and brookite. Pure Rutile is desirable phase in clinical applications due to the high corrosion protection of metallic implants, a large single crystals can be easily obtained, high biocompatibility and usually stated to be the thermodynamically most stable form of TiO$_2$. Anatase phase also has bioactivity properties. Anatase gradually transforms to rutile depending on temperature that has bioactivity properties. There are

only small differences in Gibbs free energy between anatase, brookite and rutile (4-20 kJ/mol) meaning that the metastable polymer phase is almost as stable as rutile at normal pressures and temperatures. [14, 72].

2.6.2.1 The Crystal Structures of TiO_2

The most important properties of TiO_2 is that it has the crystal structure same as the crystal structure of titanium alloys; so, it is useful to be used for coating it. The structure of rutile and anatase can be described in terms of chains of TiO_6 octahedral.

The two crystal structures differ by the distortion of each octahedron and by the assembly pattern of the octahedral chains. The unit cell of rutile contains two Ti atoms situated at (0, 0, 0) and (½a, ½a, ½c), and four oxygen atoms. The oxygen atoms form a distorted octahedron around every Ti cation.

The unit cells of anatase contains four Ti atoms located at (0, 0, 0), (½a, ½a, ½c), (0, ½a, ¼c), and (-½a, 0, -¼c), and eight oxygen atoms. In anatase, too, the Ti cation is surrounded by a distorted oxygen octahedron, the unit cell structures of the rutile and anatase crystal are illustrated in Fig.(2.8 a and b) respectively and the physical properties are tabulated in Table (2.2)[73,74].

Table: 2.2 Some of the physical properties of anatase and rutile TiO_2 structures at room temperature[37]

Properties	Anatase	Rutile
Crystal structure Space group	Tetragonal P42/mnm (136) c=2.9587 Å, a=4.5937 Å u=0.3048 Å, c/a=0.6441	Tetragonal I41/amd (141) c=9.5146 Å, a=3.7842 Å u=0.2081 Å, c/a=2.5143
Energy gap Eg	3.3 eV	3.0 eV
Mass density ρ	3.894 g/cm^3	4.23 g/cm^3
dTi-Ti	3.79/3.04 Å	3.57/2.96 Å
dTi-O	1.934/1.980 Å	1.949/1.980 Å

(a)   (b)
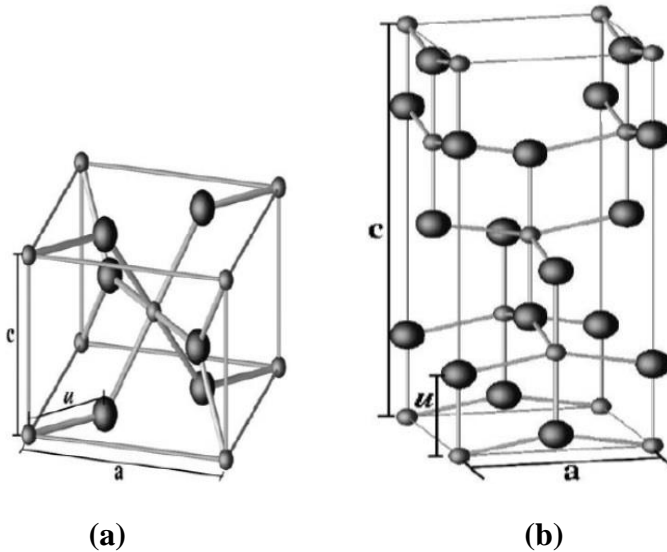
Figure 2.8: (a) **rutile and** (b) **anatase crystallographic unit cells. Small spheres represent Ti atoms, large spheres represent oxygen atoms [73].**

2.6.3 Alumina Al_2O_3

It is a very hard material, wear resistance and its hardness is exceeded only by diamond, high melting point, i.e, above 2000°C (3632°F). Alumina is also an inert substance, and at room temperature, it is insoluble in all

ordinary chemical reagents. These qualities make it useful as a biomaterial. For example, alumina is used for artificial joint replacements; porous alumina is used as a 'bone spacer' and for teeth implants. The most important and wide-range use of alumina is in the field of ceramics [75,76]

2.6.3.1   The Crystal Structures of Al_2O_3

The basic unit cell structure of corundum (the naturally Occurring alumina) is hexagonal. The forms of metastable Al_2O_3 structures, α, ρ, γ, η, θ, χ and *k* Al_2O_3. Those kinds of transition Al_2O_3can be produced from heat treatment of aluminum salts. The crystal structure α- Al_2O_3 which is called corundum structure, ideally consists of close packed planes of large oxygen anions (radius 0.14nm) stacked in the sequence as shown in Figure(2.9) ,the aluminum cations (radius 0.053 nm) have valence of +3 and oxygen anions have valence of -2.There can be only two Al^{3+}ions for every three O^{2-}ions to maintain electrical neutrality [76].
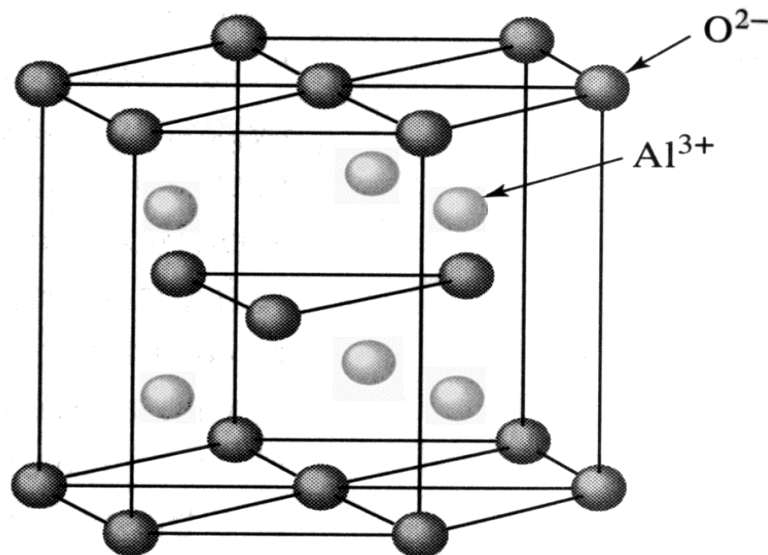
Figure2.9: The crystal structure of α alumina [76]

2.7 Biomimetic and Porosity

Biomimetic are based on the nucleation and growth of calcium phosphate in simulated body fluid, to produce an apatite layer on the surface of Ti implants, increasing their osteoconductivity and consequently favoring Osseo integration. Bioactive coating on the porous surface is an attractive method to improve the quality of the bone-implant interface. Porosity can be defined as the percentage of void spaces in a solid. The Osseo integration obtained with porous Ti is achieved by bone growth into the pores, called "bone ingrowth", which improves micromechanical interlocking, the interlacing of bone tissue within the implant, preventing mobility since it increases the contact area between the biomaterials and bone tissue, resulting in improved implant stability over time, as well as accelerating the process of Osseo integration.

The porous structure must be produced with high porosity to provide sufficient space for cell adhesion and subsequent formation of new bone that permits the transport of body fluids and the proliferation of new vasculature, while providing adequate mechanical properties to withstand stresses during implantation [60].

2.8 Corrosion

Corrosion is the most important example of surface chemistry. It is degradation and transformation of a metallic structure into other chemical structures due to the fact that the interaction with their environment and corrosion of most metals is inevitable [77].

Corrosion of metallic implants causes many problems like:

1. Failure of implant system belongs to additional ions into the body
2. Corrosion fatigue causes weaken for implant.

3. Generation of particulate debris, which may aggravate the body environment.

Corrosion of metal implants is critical because it can negatively affect the mechanical properties and biocompatibility. The materials used must be stable retaining their functional properties and not cause any counteractive biological reaction in the body. Corrosion and surface oxide film dissolution are the two mechanisms which introduce additional ions into the body. The first condition for a material of any type that is to be used in the body is corrosion because metal ion release takes place mainly due to corrosion of surgical implants. It is desirable to keep the metal ion release to a minimum by the use of corrosion-resistant materials.

The corrosion behavior of an implant is effected by:

1. The material of implant itself (e.g. the chemical composition, microstructure, surface condition),

2. The surroundings environment (e.g. pH, temperature, O_2 content),

3. The construction (e.g. presence of crevices).

Changes in these variables can have a further influence on the mode and rate of metal ion release [78].

2.8.1 Gibbs Free Energy

Gibbs free energy G determines the feasibility of a chemical reaction. A react can take place spontaneously when the difference of free energy is negative $\Delta G < 0$. The change of Gibbs free energy per mole of a reacting species is proportional to the difference of electrical potentials ΔE and can be expressed with Faraday's number $F = 96485$ C mol^{-1}:

$$\Delta G = -z\, F\, \Delta E \qquad\qquad (1)$$

Each mole of a reacting species of valence z transports a charge of Q = z F.

The negative sign in equation (1) is used to conform to the convention that a positive potential results in a negative free-energy change for a spontaneous reaction. The more negative the value of ΔG, the greater the tendency for the reaction to go [79].

2.8.2 Electrochemical Kinetics of Corrosion

Corrosion processes are controlled both by thermodynamics and kinetics, which are about the fundamental feasibility of the reaction and the rate, respectively. It is important to know how fast corrosion takes place. So, to develop more corrosion-resistant alloys and to improve methods of protection against corrosion, an understanding of the fundamental laws of electrochemical reaction kinetics is essential.

The rate of electron flow to or from a reacting interface is a measure of reaction rate. The proportionality between current, I, in amperes, and mass reacted, m, in an electrochemical reaction is given by Faraday's Law [78]:

$$mass\ loss\ m(g) = \frac{Ita}{zF} \qquad (2)$$

Where a is the atomic weight (11.97 amu for titanium), and t is the time. Dividing equation (2) through by t and the surface area, A, yields the corrosion rate;

$$r = \frac{m}{tA} = \frac{ja}{zF} \qquad (3)$$

Where j, defined as current density (I/A). This equation shows proportionality between mass loss per unit area per unit time ($mg/cm^2/day$) and current density ($\mu A/cm^2$). Units of penetration per unit

time result from dividing equation (3) by the density, D(4.5 g/cm^{3}for cpTi and 4.4 g/cm^3 for Ti-6Al-4V) of the alloys,(z) is the number of equivalents exchanged (1 for titanium) . For corrosion rate in millimeter per year, equation (3) becomes

$$C_R \ = 0.00327 \frac{ja}{zD} \ (in \ \frac{mm}{year}) \qquad (4)$$

2.9 Corrosion Test Methods

The biocompatibility of a material interaction with surrounding medium under real conditions of exposure as well as the resulting deterioratiotion of both components. Alloys proposed for implants systems can be evaluated using *in vitro* test corrosion direct current (DC) and alternating current (AC) or impedance electrochemical test methods.

2.9.1 Open Circuit Potential (OCP)

It is one of the simplest electrochemical tests available, measuring the open circuit potential (OCP), also referred to as the equilibrium potential or corrosion potential. The OCP is by definition the electrical potential difference between two conductors in specific electrolyte with zero current flow between them [81]. Monitoring OCP over time can provide vital information about the system being studied. And the system has reached a steady state and when transitions between different states, such as a passive and trans passive behavior will occur. Properties of the oxide formed on the test electrode can be evaluated by monitoring of the OCP which typically results in a positive shift in the OCP, inductive of the formation of a passive film (i.e. a surface oxide protecting the metal from further oxidation). The formation of porous oxide films, which can hinder

but not prevent further oxidation, typically results in a decrease in the OCP [82, 83].

2.9.2 Linear Swap Voltage (LSV)

A LSV plot is one of the most popular DC techniques for valuation of corrosion rate. The induction of anodic and/or cathodic Tafel lines for charge transfer controlled reactions gives the corrosion current density, i_{corr}, at the corrosion potential, E_{corr}. This method is based on the electrochemical theory of corrosion processes [80].

It is performed on a metal specimen by polarizing the specimen about 300 mV anodic ally (positive- going potential) and catholically (negative - going potential) from the corrosion potential, E_{corr}. The resulting current is plotted on a logarithmic scale as shown in Fig. (2.10).The corrosion current, I_{corr}, is obtained from a Tafel plot by extrapolating the linear portion of the curve to E_{corr}. The corrosion rate can be calculated from I_{corr} by using equation (4). The term i_o is a function of reaction, the concentration of reactants, the electrode materials, the temperature and surface roughness. The potential of the intersection between anodic reaction rate and the cathodic reaction rate is identified as E_{corr}, and the current at this intersection is defined as i_{corr}. The slop of the V-I curve can be measured. The slope is called the polarization resistance, Rp and it is related to the corrosion rate by:

$$i_{corr} = i_a = \frac{B_a B_b}{2.303(B_a + B_b)R_P} \qquad (5)$$

Where B_a & B_b are constant that are characteristic of the corroding metal and which can be measured or estimated.

This technique is called linear polarization
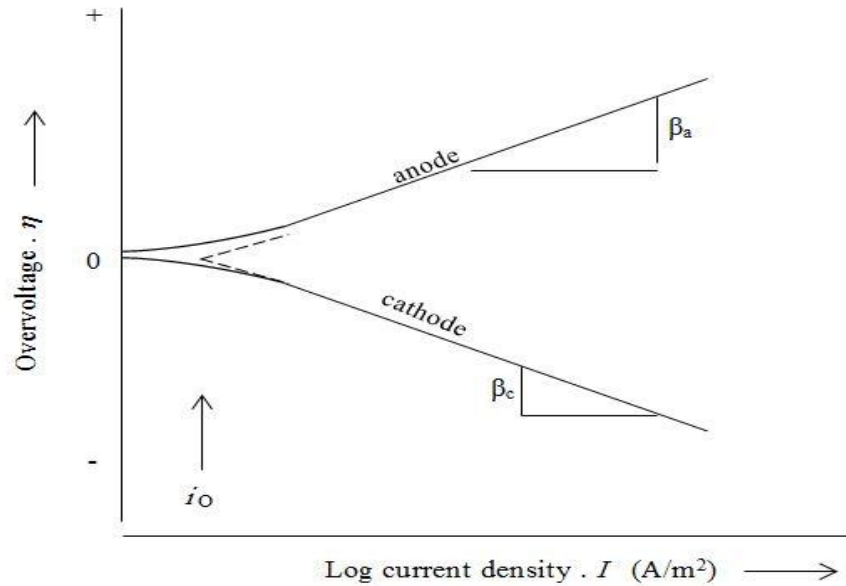
Figure 2.10: Experimentally measurable anodic and catholic polarization curves [78].

2.9.3 Electrochemical Impedance Spectroscopy (EIS)

Impedance electrochemical test system is one of the most popular AC techniques that can provide precise, error-free kinetic and mechanistic information by using a variety of techniques and output formats (Nyquist plots, Bode plots, Randles plots, etc.). This method can be used to make measurement in low conductivity solutions where DC techniques are subjected to potential-control errors. During EIS experiments, a small amplitude AC signal is applied to the system being studied. Therefore, it is a nondestructive method for the evaluation of a wide range of materials, including coatings, anodized films and corrosion inhibitors. EIS measurements can provide information regarding the kinetics of electrochemical corrosion system [84]. Some characteristics of coatings, such as corrosion behavior, porosity, solution absorption and/or film delimitation, can be predicted by EIS [85]. An EIS measurement, an alternating voltage, is applied to the corroding metal, and the impedance, Z is measured because both magnitude and the relative phase angles of

the voltage and current have to be accounted for the impedance is measured for a number of frequencies that span a range from a few mHz to 100 kHz, and the result is complex number (the impedance) for each of the hundreds to thousands of frequencies that are used. In EIS, an AC voltage of varying frequency is applied to the sample. It is useful to think of the frequency as a camera shutter that can be very fast (high frequency) for fast reactions and very slow (low frequency) for slow reactions. This is the technical feature that allows EIS to get so much information on an electrochemical reaction in one experiment. This is why EIS is more useful for coatings than dc electrochemical techniques. EIS can quantitatively measure both resistances and capacitances in the electrochemical cell. A resistance corresponds to electron transfer reactions such as corrosion. The capacitance of a metal electrode in contact with an electrolyte is important information for any electrochemical system [77].The primary advantage of impedance techniques is that a purely electronic circuit model can be used to represent an electrochemical system. Fig. 2.11 a shows a typical three-circuit element, Randles equivalent circuit. R_Ω is the uncompensated resistance of the electrolyte between the working and the reference electrodes, Rp is the polarization or the charge transfer resistance at the working electrode/electrolyte interface. Cdl is the specific double-layer capacitance at the working electrode/electrolyte interface [7].

2.9.3.1 Nyquist Plot

The Nyquist is a plot of imaginary component of the impedance (Z") against the real component of the impedance (Z') Fig.2.11 b. The high frequency intercept, the resistance (R_Ω), and the low frequency intercept,

sum of R_Ω and R_p, can be used to determine R_p. The corrosion current density can be obtained using the Steam-Geary equation (Equation 5) [7].
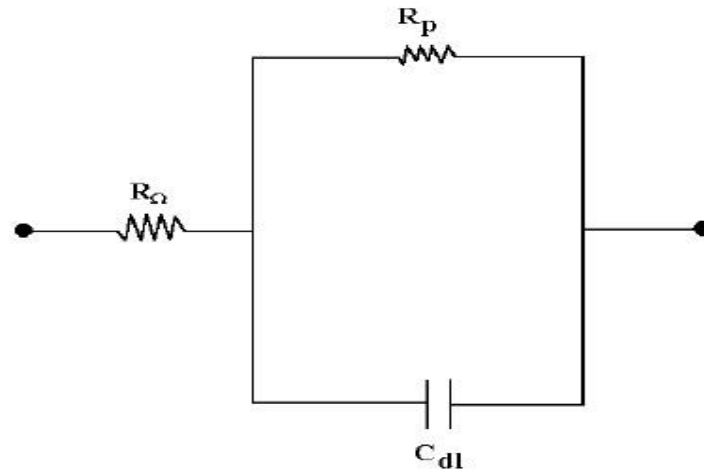
(a)
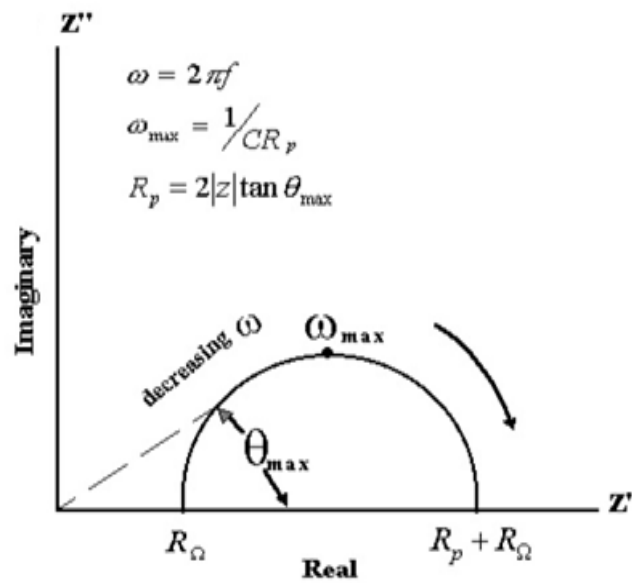
High frequency:$Z'' \to 0 \Rightarrow Z' \to R_\Omega$

Low frequency:$Z'' \to 0 \Rightarrow Z' \to R_\Omega + R_P$

(b)

Figure 2.11: (a) Schematic for Three-Element Randles equivalent circuit, (b) Nyquist plot for Randles equivalent circuit [86].

2.10 Electrochemical Polarization

The change from open circuit potential as a result of current across the electrode/electrolyte potential is called polarization $\boldsymbol{\eta}$. For cathodic polarization $\boldsymbol{\eta_c}$, because the electrons are supplied to the surface and building up in the metal due to the slow reaction rate the surface potential becomes negative to electrode potential E_p ,(E_P can be defined as the potential of an electrode in an electrolyte as measured against reference electrode). Hence, $\boldsymbol{\eta_c}$ is negative. For anodic polarization, electrons are removed from the metal which results a deficiency in a positive potential change due to the slow liberation of electrons by the surface reaction, and $\boldsymbol{\eta_a}$ must be positive. As anode increases its potential as more current flows from it to the electrolyte, while cathode's potential decreases as current flow into it. Both electrodes in the cell polarize until they reach essentially the same potential, corrosion potential.

At anodic polarization, the anodic processes on the electrode are accelerated by changing the specimen potential in the positive (noble) direction, but at cathodic polarization, the cathodic processes are accelerated by moving the potential in the negative (active) direction. Various types of polarization describe the resistance elements throughout the corrosion cell. Polarization can be divided into four different types, activation polarization, concentration polarization, resistance polarization, and combined polarization [78]

A- Activation Polarization

It is a mechanism by which the corrosion rate is reduced in some systems. It occurs when one of the steps in the corrosion process has a high activation barrier so that the whole process is slowed considerably. Activation polarization involves electrochemical process that has been controlled by the reaction sequence at the metal-

electrolyte interface. Alien some steps in a corrosion reaction control the rate of charge or electron flow, the reaction is said to be under activation or charge-transfer control [87].

B- Concentration Polarization

This polarization occurs when the rate of corrosion is limited by the diffusion of ions within the electrolyte. If the corrosion reaction proceeds more rapidly than at which ions can be supplied to the cathode (or removed from the anode), then the local ion concentration changes with time. This polarization occurs due to either a decrease in ion concentration at the cathode, or an increase in metal ion concentration. This is the region of concentration polarization , see Fig. 2.12 [88].
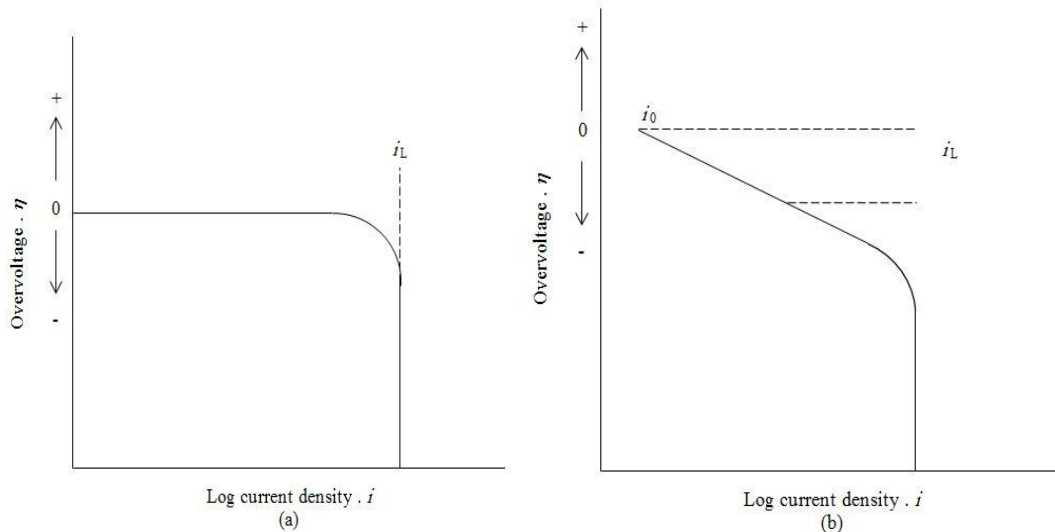
Figure 2.12: For reduction reactions, schematic plots of overvoltage versus logarithm of current density for, (a) concentration polarization, and (b) combined activation-concentration polarization [88].

In the region of concentration control, the reaction rate is no longer dependent on the potential (driving force) but rather becomes dependent on either the rate at which reactants species arrive at the electrode or the rate at which products of the reaction can be removed from the vicinity of

the electrode surface. The reaction rate is controlled by the mass transfer of reactant and products of the reaction, and this mass transport is essentially independent of potential [89].

C-Resistance Polarization

In discussing activation and concentration polarization, no account was taken of ohmic resistances. For some electrode reaction the effects of ohmic resistance can be very considerable. This is especially significant when the reaction itself or a complementary reaction produces films on the electrode surface. The total potential drop across such resistance is called resistance polarization, η_R. This over potential is defined by Ohm's Law as [90]:

$$\eta_R = IR \qquad (9)$$

Where I is the current and R is the resistance of the electrolyte path between anode and cathode and is directly proportional to the path length. In typical corrosion processes, the anodes and cathodes are immediately adjacent to each other so that resistance polarization makes only a minor contribution to the overall polarization as indicated in Fig. (2.13).
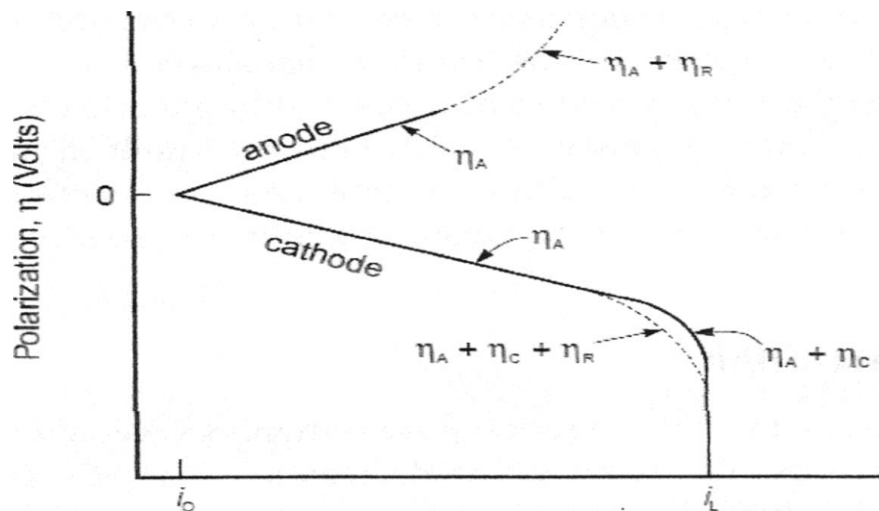
Figure 2.13: Polarization curves showing contributions for η_A η_C and η_R

D-Combined Polarization

Both activation and concentration polarization usually occur at an electrode. At low reaction rates, activation polarization usually controls, while at higher reaction rate concentration polarization becomes controlling. Total cathodic polarization is the sum of activation and concentration polarization. Because concentration polarization is usually absent for anodic polarization of metal dissolution reactions, activation polarization represents the total polarization [91].

2.11 Passivity

A condition in which a piece of metal, because of an impervious covering of oxide or other compound, has a potential that is much more positive than that of the metal in the active state. The effect is valuable in conferring corrosion resistance on bare metal surfaces even in aggressive environments [92] .Passivation leads to a marked reduction in the rate of the anodic reaction. In simple terms, the rate of the anodic reaction in steady-state conditions will be the rate of dissolution of the passive film. The passive current density which is the rate of the anodic reaction in the passive region is usually relatively independent of potential, since it is controlled by the rate of dissolution of the passive film. Where there is a region of solubility of the corrosion product between the region of stability of the metal and of the passivating oxide film, then an *active-passive* transition will be observed. At potentials just above the equilibrium potential for the metal, the metal will corrode actively, and activation kinetics will apply. As the potential moves up into the region where the passive oxide film is stable, then the surface will passivate, and the current will fall rapidly to the passive current density. When the

potential exceeds the equilibrium potential, the oxygen evolution reaction starts to occur on the surface of the passive film. The rate of this reaction will depend on the electronic resistance of the passive film (since electrons must pass through the film to permit the oxygen evolution reaction to occur) and on its electrochemical reactivity. If the metal oxide can be further oxidized to a more soluble state, trans passive (meaning 'above passive') corrosion can occur [93].

2.12 Corrosion of Surgical Implants

2.12.1 Electrochemical Aspects

The body environment is very aggressive in terms of corrosion since it is not only aqueous but also contains chloride ions and proteins. A variety of chemical reactions occur when a metal is exposed to an aqueous environment. The chemical reactions that occur on the surface of a surgically implanted alloy are identical to those observed during exposure to seawater (namely, aerated sodium chloride). These metallic components of the alloy are oxidized to their ionic forms and dissolved oxygen is reduced to hydroxide ions

$$M \rightarrow M^{n+} + ne \qquad 10 \ (oxidation)$$

$$O_2 + 2H_2O + 4e \rightarrow 4OH^- \quad 11 \ (reduction)$$

is the general reaction for the oxidation of the metal atom. The electrons that are released are conducted through the metal to another site where they are consumed in the reduction process (Equation 11).

2.12.2 Forms of Corrosion

There are many causes that contribute to the corrosion of metals when placed inside the human body. After surgery, the pH surrounding the

Implant is reduced to a pH between 7.3-7.6 typically due to the trauma of surgery. Infectious micro gains and crevices formed between components can reduce oxygen concentration, both of which contribute to the corrosion of the implant [94].

Corrosion of implants in the aqueous medium of body fluids takes place via electrochemical reactions. All the surgically implantable metallic materials, including the most corrosion-resistant materials, undergo chemical or electrochemical dissolution at some finite rate, due to the complex and corrosive environment of the human body. The body fluid constitutes water, complex compounds, dissolved oxygen and large amounts of sodium, Na^+ and chloride, Cl^- ions and other electrolytes like bicarbonate and small amounts of potassium, calcium, magnesium, phosphate, sulphate and amino acids, proteins, plasma,.. etc [95].

Corrosion can affect the metal in a variety of ways which depend on its mixture and the precise environmental conditions prevailing, and a broad densification of the various forms of corrosion in which five major types have been identified, is presented in the following[96]:

1-Uniform (General)Corrosion: It is the uniform thinning of a metal without any localized attack. Corrosion does not penetrate very deep inside.

2-Galvanic (two–metal)Corrosion: Galvanic corrosion occurs when two metals with different electrochemical potentials or with different tendencies to corrode are in metal-to-metal contact in a corrosive electrolyte, as shown in Fig. 2.14
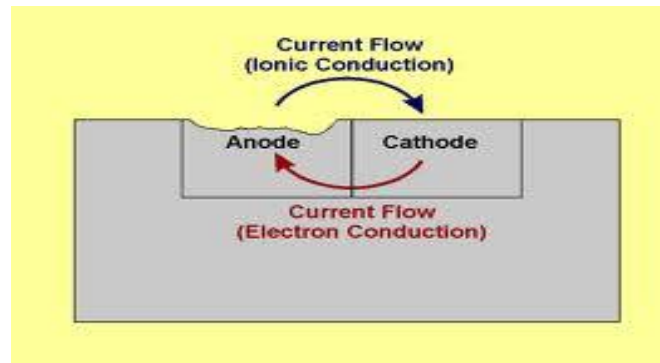
Figure 2.14: Galvanic (two–metal) Corrosion

3-Crevice Corrosion: This is a localized form of corrosion, caused by the deposition of dirt, dust, mud and deposits on a metallic surface or by the existence of voids, gaps and cavities between adjoining surfaces. An important condition is the formation of a differential aeration cell for crevice corrosion to occur, as shown in Fig. 2.15.
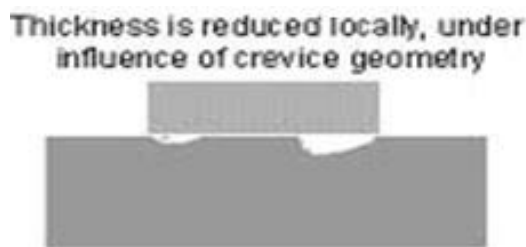
Figure 2.15: Crevice Corrosion

4-Pitting Corrosion: It is a form of localized corrosion of a metal surface where small areas corrode preferentially leading to the formation of cavities or pits, and the bulk of the surface remains unattached, as shown in Fig. 2.16.
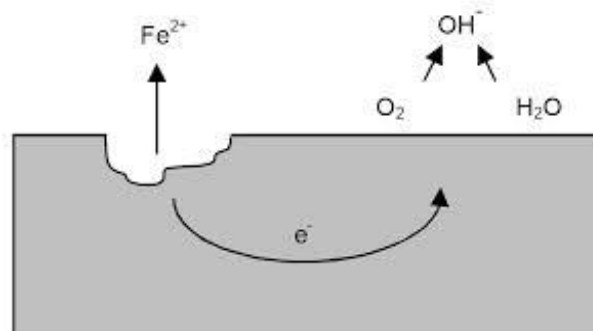
Figure 2.16: Pitting Corrosion

5-Corrosion wear and Corrosion fatigue: Wear is a loss of material with the generation of particles resulting from relative motion between two opposed surfaces. Corrosion fatigue is the mechanical degradation of the material under the joint action of corrosion and cyclic loading.

2.13 Corrosion of Biomedical Metals and Alloys

Over the past decades, quantitative analyses of basic biomaterials properties have been utilized to better optimize biocompatibility profiles for surgical implant devices. Correlations between results from preclinical investigations have provided critical comparisons of cause-effect relationship between synthetic material properties and longer-term device function [86].

All metals and alloys are subjected to corrosion when in contact with body fluid. Based metals and alloys used in medical and dental devices are corrosion resistant due to the presence of a protective surface oxide film. A number of types of failures have been observed in medical implants, some related to the effect of the environment on the implant and others to the effect of the metal on the living system. Under certain conditions, titanium and titanium alloys are remarkably resistant to corrosion because of the formation of stable self-healing, oxide film on metal surfaces because of high affinity of titanium for oxygen that insulates the base material from the surrounding environment [97]. In the passive state, titanium is covered with a nonstoichiometric oxide film, and the average composition of which is TiO_2. Semiconducting properties of the passive film are generally attributed to oxygen anion vacancies and Ti^{3+} interstitials that function as donor states and give *n*-type semiconducting characteristics to the oxide [98].

CHAPTER THREE

Materials and Methods

3.1 Introduction

This chapter includes the materials that were used in the work including preparation, modification and surface examination techniques. The chapter consists of two parts; the first part (pilot study) was done in the laboratories of Ministry of Sciences and Technology in Iraq, it includes the preparation of TiO_2 target manufactured in laboratory and the deposited on cpTi and Ti-6Al-4V alloy substrate as single layer, where the coating is done using the RF sputtering, and results were analysed and the *in vitro* test (corrosion tests LSV) were done. The second part (research study) was done in the laboratories of Murdoch and Curtin Universities, Australia and KAIST University, South Korea. The work includes the use of TiO_2, Al_2O_3 and HAp as target for RF sputtering. These targets were purchased, and single, multi and triple layers of these compounds were deposited on substrate of cpTi and Ti-6Al-4V alloy. The work done in Murdoch University lab was sample preparation which was coated with the above mentioned compounds using RF sputtering in KAIST University and analysed by XRD,EDS,SEM,XPS and Ramman techniques. The *In vitro* work (corrosion tests OCP, LSV, EIS) and biometric were done in Murdoch and Curtin Universities laboratories all the spectroscopic technics for analysis like XRD,EDS,SEM,XPS and FTIR techniques.

3.2 Experimental Works includes TiO_2 as a Target (pilot study)

A. Materials

1. Titanium alloy cpTi and Ti-6Al-4V manufactured from (BAOJI JINSHENG METAL MATERIAL CO.CTD), GR2 ASTM F67 and ASTM F136 respectively(Appendix).

2. Titanium oxide powder 99.99% pure and particle size less than 20nm rutile and anateis phase manufactured from (sigma aldrich).

3. Chemical materials used *In vitro* tests: NaCl, $CaCl_2$, $NaHCO_3$, KCl, K_2HPO_4, $MgCl_2$ $6H_2O$, Na_2SO_4(sigma aldrich).

B. **Surface modification**

1. Wire-cut (Alibaba - machine-7740_1479395532.htm, Denmark).

2. Grinding process: using (Struers- DAP-U system, Denmark).

3. Polishing process: Silicon carbide papers (Kement Strurer, Denmark).

4. Etching and cleaning process: using ultrasound (BRANSON5510 German).

5. RF magnetron sputtering (TORR .CRC-600 Sputtering System).

6. Furnace DAIHAN Scientific CEBER .

C. **Equipment**

1. X-ray Diffractometer. (XRD Shimadzo6000, Japan).

2. PH meter WTW (Wissenschaft Technisch Werkstatten) D- 82388

3. SEM(JEOL-JSM-5600 USA)

4. Corrosion system (PARASATE 2273, Princeton Application Research),USA.

3.2.1 Materials Preparation

In order to enhance the bone bonding ability and corrosion resistance, the surface of the implant materials should be modified. It is necessary to prepare uniform surface and requires careful specimen preparation .Titanium alloy (cpTi and Ti-6Al-4V) had the composition as in appendix A and B respectively   according to the manufacturer.

Specimen preparation (was done according to the ASM Metals Handbook)[99]

Surface condition of a specimen plays an important role in corrosion resistance. Hence, it is necessary to prepare uniform surface and requires careful specimen preparation. Specimen preparation for microstructure evolution, electrochemical studies and surface analysis involve the following steps:

A. Cutting: The cpTi and Ti-6Al-4V alloy rods were cuted with a circular shaped specimens, (dimension 20 mm diameter and a 1.8 mm thickness).

B. Polishing: The mount specimens were grinded with SiC emery papers with different grits in the flowing steps :(120, 180, 240, 320, 500, 600, 800, 1000, 1200, and 1800 of grain size) to get flat and scratch free surface.

C. Etching: Finally, the polished specimens were etching in the solution (HF: 10g, HNO_3: 30g, deionized water: 60g) for 3 min to remove the oxide layer and remaining of SiC and cleaned ultrasonically in ethanol and deionized water for 20 min at temperature 25°C respectively, finally the substrate were dried and stored in plastic containers.

3.2.2. Target

Weight of (20g) of titanium oxide powder with particle size 21nm Fig.(3.1 a), was mixed with 5 drops of alcohol inside ceramic crucible for 15min. Then the mixture pressed in cylindrical stainless-steel mold with (dimension of 51mm diameter and 7mm in high) as can be shown in Fig.(3.1 b) the pressing was done , under 5.1MPa pressure for 6,8 and 10 min by using hydraulic press as shown in Fig.(3.1 c). Pressing is mechanical process use to reduce the porosity and vacancies between the particles and to produce a disc at 5cm diameter and a 5mm thickness as shown in Figs. (3.1 d and e) . The samples sent to sintered which include heating the disk to a temperature in the range of 30% − 75 % of the

material's melting temperature (the melting temperature 1843°C for TiO$_2$) The sample was sintered using tube furnace for 2 and 3 h at 1200°C [100]. It has been found that the sample produced under 5.1MPa pressure for 10min and sintered 3h at 1200°C   is not brittle and strong enough for sputtering.
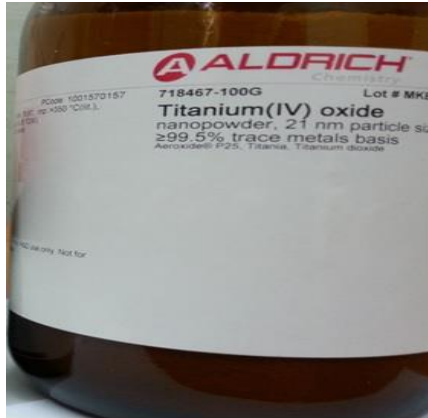
(a)

(b)

(c)

(d)
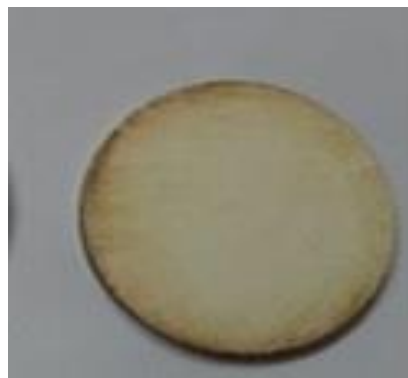
(e)

Figure 3.1 :(a) The titanium powder, (b) stainless-steel mold ,(c) piston hydraulic, (d) target of sputtering before and(e) after sputtering.

3.2.3 RF Sputtering

RF sputtering   was done in a vertical chamber made from stainless steel have two upper position for targets and the substrates lower position inside the chamber the cpTi and Ti-6Al-4V alloy were introduced inside the sputtering chamber and the chamber window was tightly closed. The high vacuum was performed inside the chamber then waiting for 4-5 hours to reach (3×10^{-5} torr). The position of the substrates was in front of the wanted target at fixed distance10 cm between target and the substrate (D10). Argon gas with flow of 27,8 sccm was used as shows in Fig.(3.2). The substrate was heated gradual to reach balance temperature of 100°C, the substrate was rotating during the deposition in order to increase the uniformity distribution. Thickness thin film was controlled by using thickness monitor.

Thin film of TiO_2 was deposited on the substrates of cpTi and Ti-6Al-4V alloy with working conditions, as tabulated in Table (3.1) depending on the creation of the plasma which is necessary for deposition.

Table 3.1 : The TiO_2 target coated on substrates (cpTi and Ti-6Al-4V) alloys as single layer

Experiment No	Power (W)	Pressure (Torr)	Substrate Tempter (^{o}C)	Distance between target& substrate(cm)	Time of deposition t_D (min)
1	180	7×10^{-3}	100	10	61.96
2	120	7×10^{-3}	100	10	118.06
3	110	7×10^{-3}	100	10	210.83
4	55	7×10^{-3}	100	10	88

Figure 3.2 :RF magnetron sputtering system

3.2.4 Heat Treatment

The thermal treatments of the samples were performed in tubular furnace and the temperature accuracy of the furnace was controlled within $\pm 2^{o}$C. The annealing process was done to the coated   samples for 2 hours at $400^{°}$C under atmosphere [16].

3.2.5 Surface Examination and Characterization Instruments

3.2.5.1 Phase Analysis Studies

The crystalline nature of the materials, which were used in this study, was tested by X-ray Diffraction using Cu Kα radiation. The 2θ angles were swept in step of one degree, the locations of peaks in the XRD profiles were compared to reference spectra. The diffraction patterns were indexed according to the ICDD powder diffraction files (PDF) that listed in Table 3.2.

Table 3.2:Tested materials by X-ray Diffract meter with standard PDF files

Material	Powder Diffraction File(PDF)
Ti	44-1294
Rutile TiO_2	21-1276
Anatase TiO_2	21-1272
$Ca_3(PO_4)_2$	04-014-2292
$\alpha Ca_3(PO_4)_2$	0 90348
$Ca_5(PO_4)_3(OH)$	00-024-0032
$Ca_5(PO_4)_3(OH)$	00-024-0033
$Ca_4H(PO_4)3.25H_2O$	44-0778
Al_2O_3	040877

3.2.5.2 Scanning Electron Microscopy (SEM)

A scanning electron microscope (SEM) is a type of electron microscope that produces images of a sample by scanning it with a focused beam of electrons. The electrons interact with atoms in the sample produce various signals that can be detected and that contain information about the sample's surface topography and composition. The electron beam is generally scanned in a raster scan pattern, and the beam's position is combined with the detected signal to produce an image. The most common SEM mode is detection of secondary electrons emitted by atoms excited by the electron beam. The number of secondary electrons depends on the angle at which beam meets surface of specimen i.e. on specimen topography. By scanning the sample and collecting the secondary electrons with a special detector, an image displaying the topography of the surface is created. A film coated on medical alloy cpTi and Ti-6Al-4V was examined by SEM (JEOL-JSM-5600).

3.2.6 *In vitro* **Electrochemical Reaction Test**

The *in vitro* test was performed by corrosion test .The electrochemical reaction samples with its environment of SBF, as shown in Table (3.3), were carried out using potentiostat/galvanostat (PARASATE 2273, Princeton Application Research) provided with electrochemical Interface controlled by commercial POWER SUITE software. All the potential measurements were made with reference Ag Ag/Cl as a saturated calomel electrode (SCE) and Platinum was used as counter electrode(CE). The specimen was scanned in the positive direction at sweep rate of 10 mV/sec and the current was monitored with respect to the potential. This technique was used for evaluating corrosion parameters for different specimens with different surface coating.

Table 3.3:The concentration of SBF[44]

No	Material	Wight in gm/l
1	sodium chloride NaCl	8.036
2	calcium chloride $CaCl_2$	0.293
3	sodium bicarbonate $NaHCO_3$	0.352
4	potassium chloride KCl	0.225
5	dipotassium hydrogen phosphate trihydrated $K_2HPO_4 \cdot 3H_2O$	0.230
6	magnesium chloride six hydrated $MgCl_2 \cdot 6H_2O$	0.311
7	Sodium kpretait Na_2SO_4	0.072

3.3 Experimental Works includes TiO_2, Al_2O_3 and HAp as Targets (research study)

The material and surface modification save as mention in the pilot study as mention in the pilot study paragraph 3.2 **.**

C. Surface examination

1- EDS (Energy Dispersive X-ray Spectroscopy) PHILIPS XL series, Japan.

2- SEM (Scan Electron Microscopic) HITACHI 5-4800 and sputter coulter mission with platinum material under vacuum BAL-TEC, SCD-005, Japan.

3- Alpha step profiler optical 3D micro scan VSM, KLATe, ASIQ3, F=47-63 HZ.

4- XRD (X-Ray- Diffraction) Rigaku Ultima JV, Japan.

5- Raman spectrometer (labram aramis, HORIBA, USA)

6- XPS (X-ray Photoelectron Spectroscopy) XPS-KRATOS AXIS ULTRA DLD-2014 model, MANCHESTR, UK.

7- PH meter. WTW (Wissenschaft Technisch Werkstatten) D- 82388

8- Corrosion system Biological. (SP 300)

Fig. (3.3) includes the diagram for the plan experimental works (second part) and the RF sputtering.

(a)

(b)
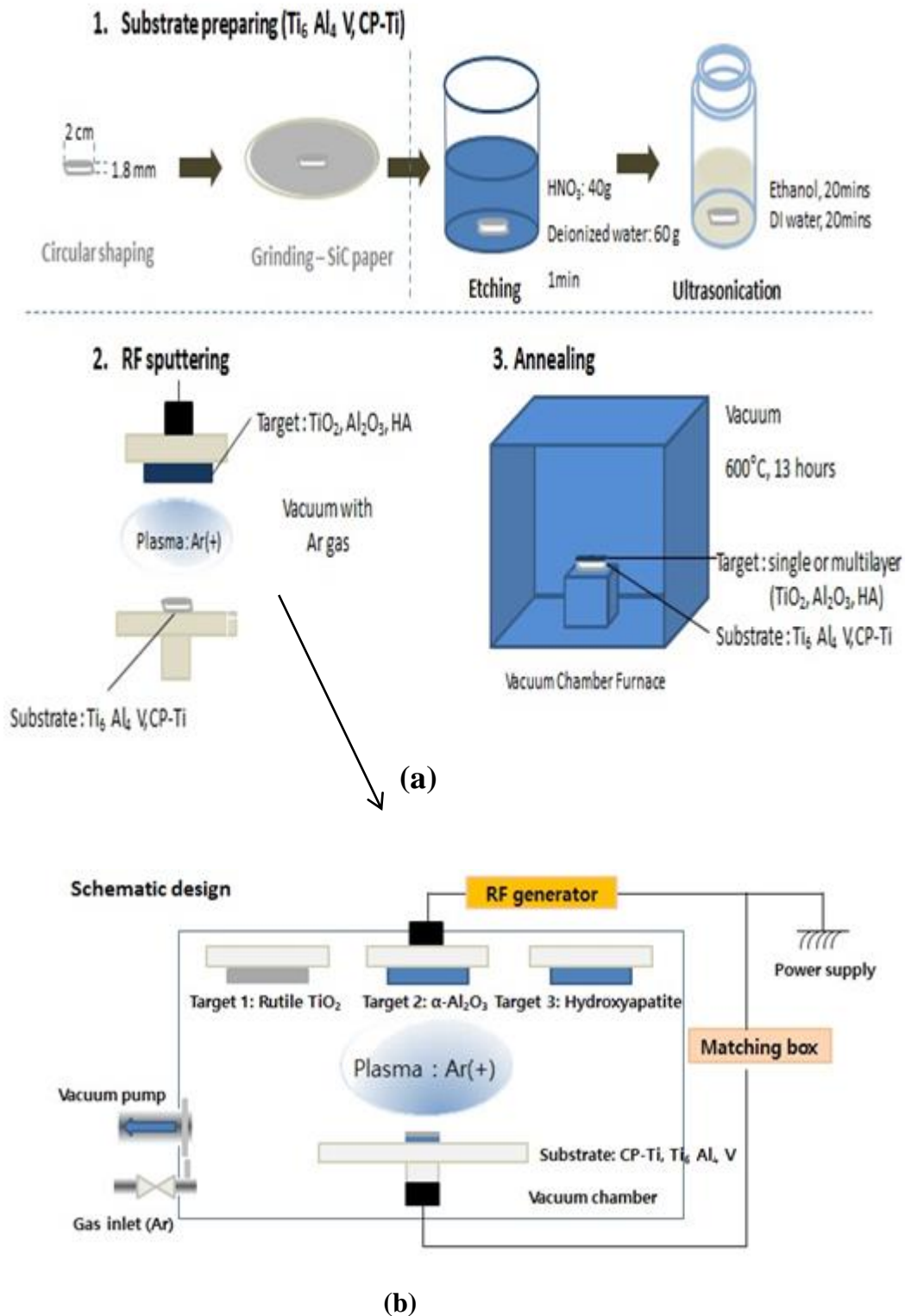
Figure 3.3: (a) plane diagram for the experimental works (research study) and (b) diagram for RF sputtering system .

3.3.1 Materials Preparation

Samples preparation was done followed the same steps mentioned in section 3.2.1 with addition to the following:

- SiC paper with 2500μm grain size, see Fig. (3.4).
- Etching: the same steps repeated but the substrates disks were placed in 40% nitricacid and rinsed with deionized water 60% (7.1g nitricacid HNO_3 with of purity 70% and 43g deionized water) as shown in Fig. (3.5).

Figure 3.4: Grinding paper and mission
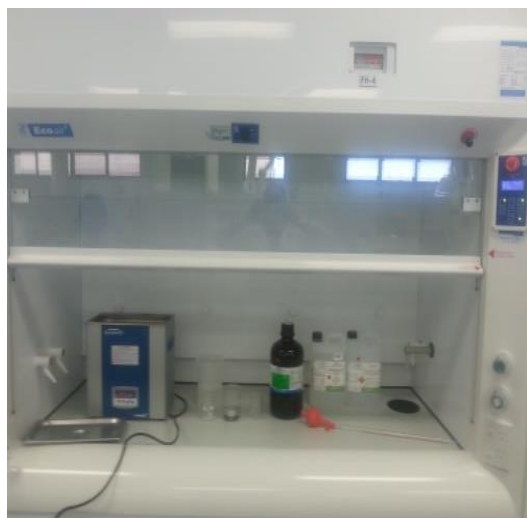
(a)   **(b)**

Figure 3.5: (a) and (b) the ultrasonic etching and clean for the substrates.

3.3.2 Targets

Targets provided from VTFM (Vacuum Thin Film Materials)

1-Titanium oxide (TiO_2) has 4~5μm particle size, rutile phase, and with purity is 4N5 (99.995%)

2-Hydroxyapatite (HAp) has size 2μm particle size and with purity is 3N (99.9).

3-Aluminum (Al_2O_3) has 1um particle size, alpha phase, with purity is 5N (99.999%). as shown in Fig. (3.6).The size of all targets 3" × 3mmt.

Figure 3.6: Targets (TiO_2, HA, Al_2O_3)

3.3.3 RF Magnetron Sputtering

RF sputtering system is shown in Fig.(3.7 a)made from stainless steel , small cylindrical horizontal chamber with dimensions (150 mm diameter and 80mm   in high) Fig.(3.7 b) and the main   process chamber are cylindrical vertical in shape(Figs. 3.7 c&d) with dimensions (500mm diameter and 400mm in high) had four upper position for targets fixation (Fig. 3.7 e).To enhance the conductivity, a copper foil was fixed below the sputtering targets and to protect the target from damage. The substrate was

inserted inside the small horizontal chamber (after etching and cleaning) The window was closed followed by evacuating the chamber up to 20 min to reach to balance in vacuum $3 \times 10^{-7} torr$ between horizontal and vertical chambers The substrates then were pushed mechanically under vacuum inside horizontal sputtering chamber. The position of substrates was opposite to wanted target. High purity argon (99.999%) was introduced through a needle valve and the gas flow was maintained at a value of (50 sccm).The substrate was heated to a final temperature 300°C with a gradual heating rate of 2°C /min and this was taken about30 min. Before the deposition was started pre-sputtering with Ar was carried out for about 5min under sputtering pressure of 2×10^{-2} torr to remove the surface oxidation and contamination from the target. The substrate target distance was changed depend on the type of targets and the deposition time was controlled to obtain a uniform film thickness. In all our experiments, we were used two types of substrates (cpTi and Ti-6Al-4V alloy) coated with (TiO$_2$, Al$_2$O$_3$, HA) using RF magnetron sputtering in presence of Ar gas at different distance between the target and the substrates the work conditions are tabulated for each experiments. The selected condition for the formation of rutile TiO$_2$ and HAp film was a substrate temperature of 300°C which is the required the temperature for HAp film layer to be deposited [12].The best work conditions were selected depending on the EDS analysis.
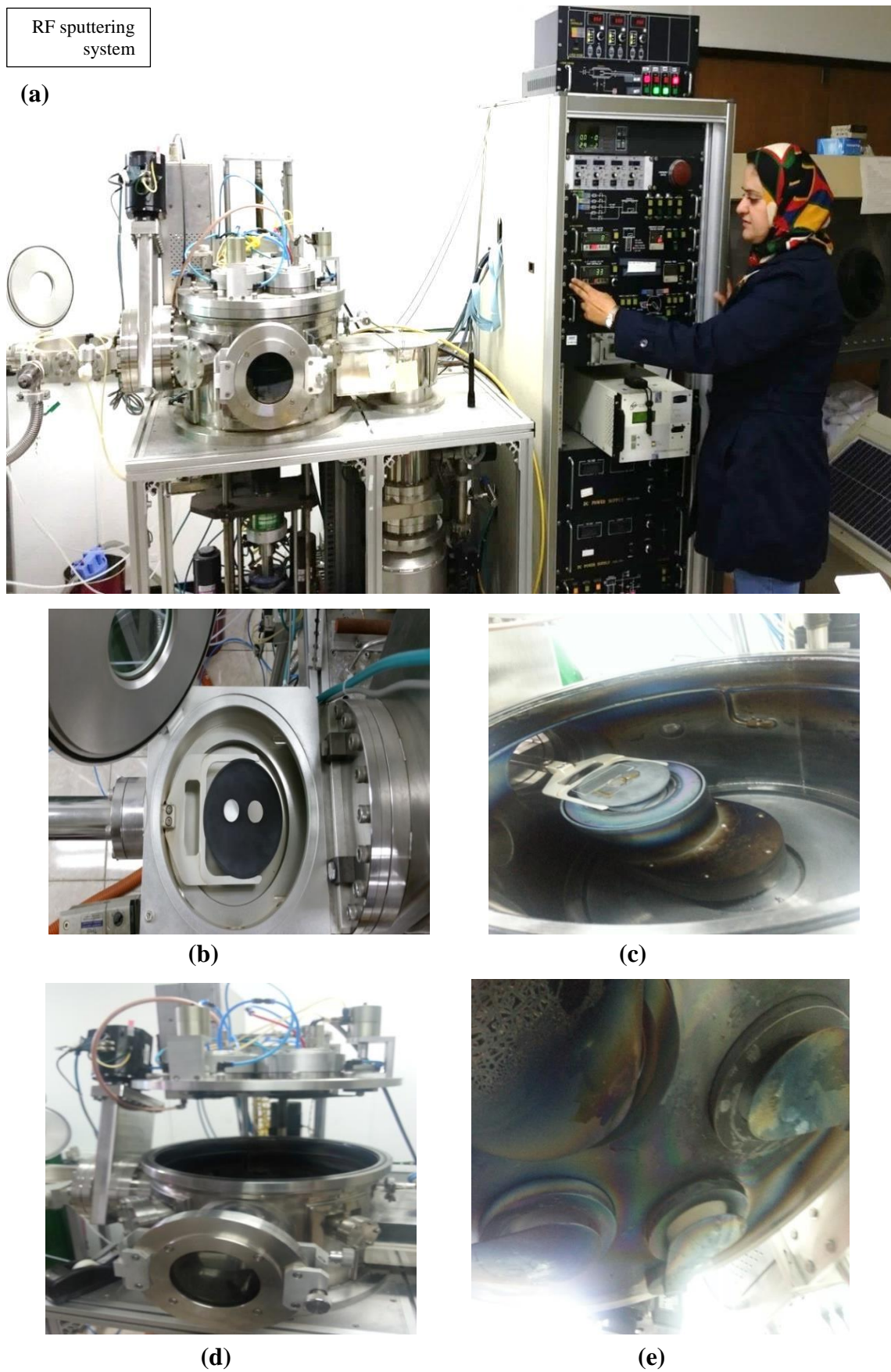
Figure 3.7: (a) Sputtering system, (b) Substrate chamber,

(c) and (d) Sputtering chamber and (e) Targets positron.

The substrates were prepared as follows:

3.3.3.1 Single Layer

A. Hydroxyapatite (HA)

A substrate of cpTi and Ti-6Al-4V alloy were coated with HA at different distance between target and substrates (D9 and D7) with working conditions as tabulated in Table (3.4). The thickness of thin film was determined by using SEM and Alpha Optical Micro scan.

Table 3.4: The condition of cpTi and Ti-6Al-4Valloy coated with single layer HAp

Experiment No	Power (W)	Pressure (Torr)	Substrate Tempter (^oC)	Distance between target& substrate (cm)	Time of deposition(hour)
1	150	5.5×10^{-3}	300	9	2
2	150	5.5×10^{-3}	300	9	4
3	150	5.5×10^{-3}	300	9	7
4	150	5.5×10^{-3}	300	9	10
5	150	5.5×10^{-3}	300	7	2
6	150	5.5×10^{-3}	300	7	4
7	150	5.5×10^{-3}	300	7	7
8	150	5.5×10^{-3}	300	7	10

B. Tetania (TiO$_2$)

Thin films of TiO$_2$ were deposited on substrates of cpTi and Ti-6Al-4V alloy using TiO$_2$ target under process conditions: power (150W), pressure(5.5×10^{-3} Torr)**,** substrate tempter at $300^{\circ}C$, distance between target& substrate7 cm(D7) and deposition time 2 hours. The thickness of thin film was determined by using XPS.

3.3.3.2 Multilayer (TiO$_2$+Al$_2$O$_3$)

Thin films were deposited on substrates cpTi and Ti-6Al-4V alloy using TiO$_2$+Al$_2$O$_3$ targets. The TiO$_2$ was used as the first deposited layer on the substrates which was depend on working conditions of TiO$_2$ as mentioned above in single layer, then under continues vacuum using Al$_2$O$_3$ target with same working condition of TiO$_2$, the second layer of Al$_2$O$_3$ was deposited film.

3.3.3.3 Three layers (TiO$_2$+Al$_2$O$_3$+HA).

Table 3.5: The condition of cpTi and Ti-6Al-4Valloy coated with triple layer

Experiment No	Power (W)	Pressure (Torr)	Substrate Tempter (^{o}C)	Distance between target& substrate(cm)	Time of deposition (hour)
1	150	5.5×10^{-3}	300	7	2
2	150	5.5×10^{-3}	300	7	4
3	150	5.5×10^{-3}	300	7	7

The cpTi and Ti-6Al-4V alloy substrates were coated with a triple layer of TiO$_2$+Al$_2$O$_3$ +HA, the deposition   was started with TiO$_2$ as the first and Al$_2$O$_3$ as second layer depend on the same working conditions of the multilayer in the section 3.3.3.2 .The third layer was HAp deposited on the last final Al$_2$O$_3$ layer and the same process condition was used as can be seen in table in Table (3.5).

3.3.4 Heat Treatments of the Samples

Annealing was done for all coated specimens using a vacuum furnace with heating value 2°C/min to reach an annealing temperature 600°C, Fig. 3.8. The specimens were kept at this temperature for 2 hours and then allowed to colliding to the room temperature [51].

(a)

(b)

Figure 3.8: (a) and (b) Heat treatment vacuum furnace

3.3.5 Surface Examination and Characterization Instruments

3.3.5.1 Energy Dispersive X-ray Spectroscopy (EDS)

This technique sometimes called energy dispersive X-ray analysis (EDXA) or energy dispersive X-ray microanalysis (EDXMA), is an analytical technique used for the chemical characterization or elemental analysis of a sample or small area. A sample is exposed to an electron beam inside SEM, these electrons collide with electrons within the sample, causing some of them to be knocked out of there orbits. The vacated positions are filled by higher energy electrons which emit X-ray in the process. The number and energy of the X-rays emitted from a specimen can be measured by an energy-dispersive spectrometer EDS which is shown in Fig. (3.9) which are powerful tool for microanalysis of elements energy. The dispersive spectrometer (EDS, PHILIPS XL series, japan). With electron probe at an acceleration voltage 15 KV was employed in this study.

Figure 3.9: Energy Dispersive X-ray Spectroscopy (EDS)

3.3.5.2 Scanning Electron Microscopy (SEM)

The thin film coated on medical alloys cpTi and Ti-6Al-4V alloy was examined by (SEM, HITACHI 5-4800 japan) as shown in Fig. (3.10 a). To avoid electrical charging due to low electrical conductivity of coated surfaces(ceramics), they were initially covered with a very thin layer of platinum under vacuum by sputter coater mission (BAL-TEC, SCD-005) as shown in Fig. (3.10 b). Also SEM used to measure the thickness of thin film by inserting the samples in holder, as shown in Fig. (3.10 c).

(a)

(b)   **(c)**

Figure 3.10: (a) Scanning Electron Microscopy (SEM) ,(b) sputter coater device and (c) holder samples .

3.3.5.3 Phase Analysis

The X-ray Diffraction was used to analysis the uncoated and coated surface using (XRD- Rigaku Ultima JV ,japan, with 20 KV,2mA and 0.04KW with a monochromatic radiation scanned Cu Kα (1.54056 Å) radiation occupying a scan speed of 2° per minute and a step scan of 0.01 . Table (3.2) illustrated these materials, the indexing of the data was carried out using XRD powder diffraction files (PDF) released by ICDD as shown in Fig. (3.11).The software programs used for analysis the results were:

1. MD 1 Jade software version .5
2. Theoretical model TOBAS–XRD software program for calceolate the concentration of apatite in samples.
3. Origin lab program.

Figure 3.11: The X-ray Diffraction Facilities

3.3.5.4 X-ray Photoelectron Spectroscopy (XPS)

XPS is a powerful surface science technique that is used to investigate   the elemental and chemical composition   of surface. XPS uses X-ray to excite electrons out of the sample carrying information about their original electronic environment these electrons only come from the outer 2-5nm of the sample, making XPS highly sensitive to the surface. Electrons ejected from the surface are energy filtered via a hemispherical analyzer (HSA) before the intensity for a defined energy is recorded by a detector. Since core level electrons in solid-state atoms are quantized, the resulting energy spectra exhibit resonance peaks characteristic of the electronic structure for atoms at the sample surface. The main points of the technique suggested, are as follows. The spectral information covers the amount of the material of the coating, and that of the substrate. Since quantitative XPS-analysis is greatly affected by surface roughness which is expressed in the variations of the intensity ratio between the surface coating and substrate signals, the knowledge of the surface topography is urgent. Low energy X-ray illuminates a sample and ejects photoelectrons and the energy distribution of these photoelectrons is measured by a hemispherical electron spectrometer. (XPS-KRATOS AXIS ULTRA DLD) the Monochromatic radiation scanned AlKα X-rays (hν=1486.6 eV) were used to excite the photoemission, and the analyzed sample was conducted in a vacuum chamber, ~10^{-10} torr controlled by(CASA lab software version 10.2x) as can be shown in the Fig. (3. 12). The samples were positioned with respect to the analyzer at the electron takeoff angle normal to the surface, and the analyzer was set to constant pass energy Ep= 160eV, to remove the effect of charge from the sample films. The binding energy(BE) scale all XPS spectra   was   calibrated   by   measuring   the   reference   peak   of   C1s   at

BE=284eV ,and the XPS results for all samples were analyzed using NIST XPS database.

(a)
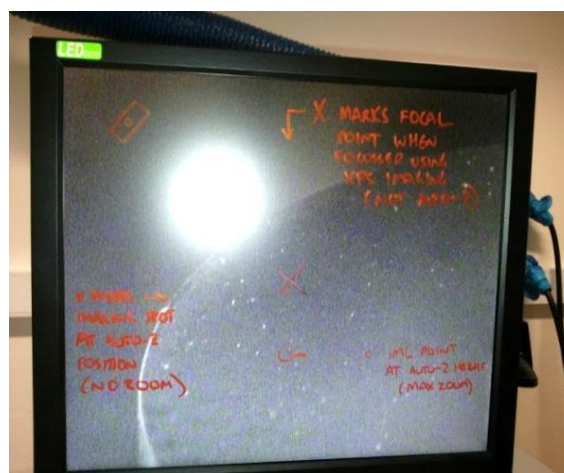
(b)   **(c)**

Figure 3.11:(a) XPS system ;(b) Sample inside system and(c) System screen to select the analyzing point on the sample.

3.3.5.5 Fourier Transform Infrared Spectroscopy (FTIR)

FTIR is a powerful tool for identifying types of chemical bounds in a molecule by producing an infrared absorption spectrum (where T+R+A=1).FTIR is a method where infra-red radiation causes the atoms within the sample to vibrate relative to each other. A molecule can only exist in distinct vibrational states with defined energies. The difference in the energies of these states allow analysis of the vibrational character of the bonds in the sample. The different coated and uncoated specimens were analyzed using NICOLET IS50 series FTIR spectrometer (Fig.(3.12))at depth 3-10 nm, DATR 1 bounce Diamond/ZnSe with applied force 100 N Infrared spectra were recorded in the range of 550 -4000 cm^{-1}.

Figure 3.12: Fourier Transform Infrared Spectrometer (FTIR)

3.3.5.6 RAMAN Scattering

Micro-Raman spectroscope LabRam Arams800, Horiba Scientific, JobinYvon Technologya, France (Fig. 3.13)was utilized to collect Raman spectra of hydroxyapatite in the triple layer of the coated cpTi and Ti-6Al-

4V alloy at D7 and t_D 10 and 7 respectively . The samples were fixed in micrometric manipulator of the confocal microscope Olympus BX41 .The sources of optical excitations laser Diode 514.53nm, 20mW, and radiating green light. The spectrometer was calibrated with the use of a silicon band of at 521 cm^{-1}. The slit of the spectrometer has the size of 100 μm and the diameter of the analyzed spot was approximately 1μm. The spectra were processed using LABSPEC software.
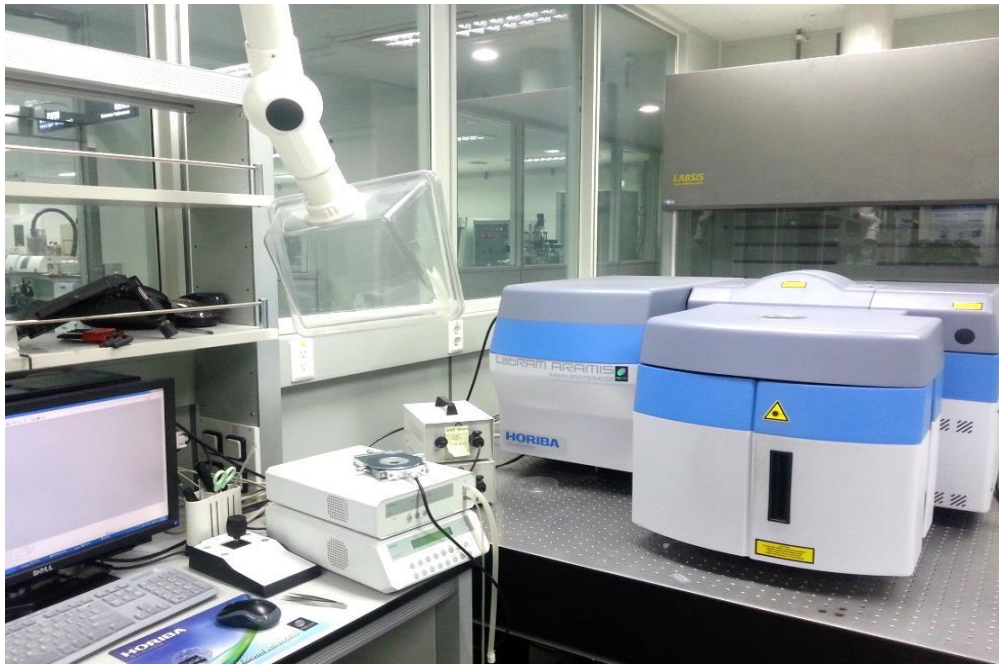
Figure 3.13: RAMAN Scattering Instrument

3.3.6 Alpha Optical Step

The Alpha-Step IQ Profiler (Fig. 3.14 a) is a computerized, high-sensitivity surface profiler that measures roughness, waviness, and step height in a variety of applications. It features with up to 1Å or less resolution, over short distances as well as waviness in a scan over a full surface. The computer offers powerful measurement control, data storage, analysis, and networking. This instrument   was used to measure the coating thickness for all coated cpTi and Ti-6Al-4V alloy specimens (single and triple layer).

The Alpha-Step IQ software is compatible with Windows XP. A minimum of 256 MB of RAM is required to ensure proper screen resolution of 1024x768 with16-bit colors(Fig.. 3.14 b).

(a)

(b)

Figure 3.14: (a) and (b) Alpha Optical Step

3.3.7 Biomimetic Immersion Test

In this study, Simulated Body Fluid (SBF) was prepared according to the concentration shown in Table (3.3) by dissolving the content in 1000 ml of distilled water and the solution was buffered to pH 7.4 at $25^{\circ}C$[101]. The biocompatibility test was done for samples HAp coated alloy as single layer for experiment number 8 in Table (3.4) and HAp coated on cpTi and Ti-6Al-4V alloy as triple layer for experiment number 3in Table (3.5).The samples were immersed in SBF for one month as shown in Fig.(3.15)and the apatite layer growth.

(a)   **(b)**
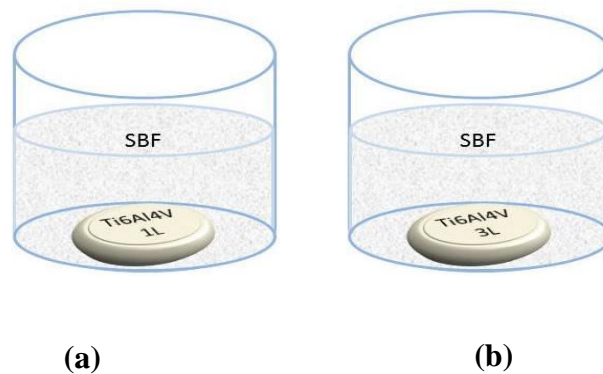
Figure 3.15: The samplesTi-6Al-4V were immersed in SBF for one month after coated with (a)HAp as single layer ,(b)(TiO$_2$+Al$_2$O$_3$+HAp)

3.3.8 In vitro Electrochemical Tests

The electrochemical studies were carried out in SBF using potentiostat/galvanostat (Biological since instrument EN61010) provided with electrochemical Interface controlled by (EC lab software version 10.2x) (Fig. 3.18). All the potential measurements were made with reference (RE) Ag Ag/Cl as saturated calomel electrode (SCE). Platinum was used as counter electrode(CE). The working electrode (WE) specimen was scanned in the positive direction from -2 to +2 volts, with scan rate of 1.67 mV/sec and the current was monitored with respect to the potential with different surface coatings as shown in Table (3.6)

(a)

(b)

Electrochemical cells
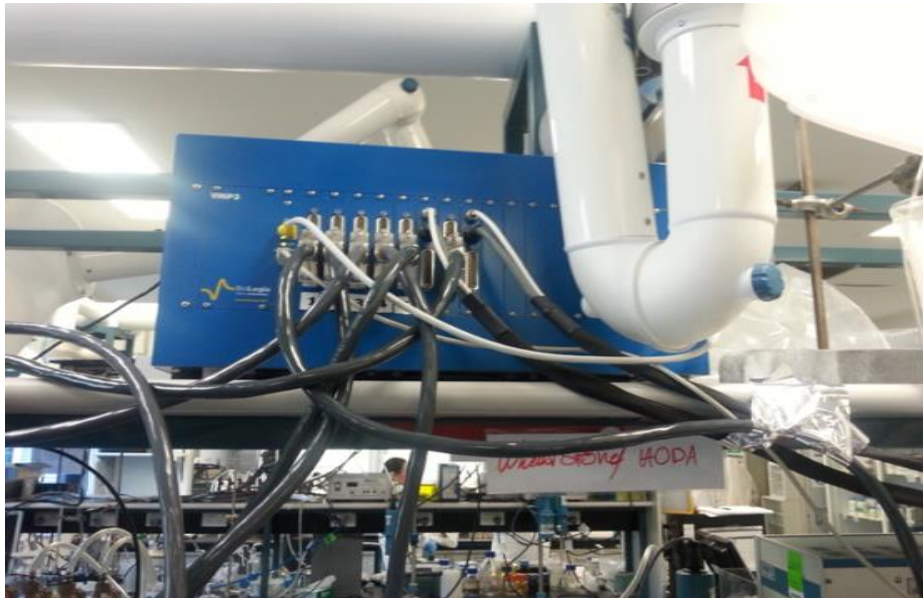
(c)

Figure 3.18: (a) Potentiostate device, (b) and (c) Electrochemical cell

Table 3.6: Medical alloy which were tested by corrosion device with their Surface modification types

Medical alloy types	Surface coated type
cpTi	Uncoated
Ti6Al4V	
cpTi	HA coated as Single layer
Ti6Al4V	
cpTi	$TiO_2+Al_2O_3+HA$ coated as Three layer
Ti6Al4V	

CHAPTER FOUR

Results and Discussion

4.1 The Results and Discussion For TiO$_2$(pilot study)

AFM was used to determine the surface roughness of cpTi and Ti-6Al-4V substrates after the specimen were grinded ,the roughness value was found to be Ra = 0.4939μm which range is very closed to the surface roughness used byD.D. Deligianni et al [100]. Fig. (4.1 a)represents the cpTi andTi-6Al-4V alloy substrate   treated with different surface modifications, grinding and etching were done as was explained in the materials preparsion. Surface modifications Figu. (4.1 b) was deposition of ceramic particles as single layer of TiO$_2$ on cpTi and Ti-6Al-4V alloy with works conditions listed in Table (3.1).
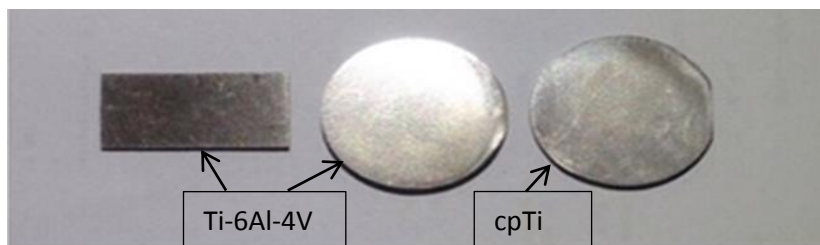
(a)
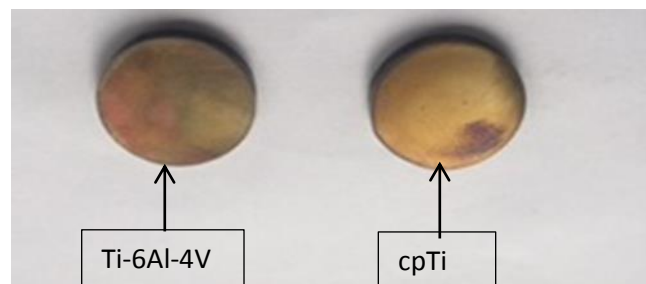
(b)

Figure 4.1: (a) the substrate cpTi and Ti-6Al-4Valloy before coating, (b) the substrate cpTi and Ti-6Al-4Valloy after coating with TiO$_2$ film.

4.1.1 Thickness of TiO₂ Film

To determain the thickness of TiO_2 films RFsputtering system thghickness monitor was used and are demonstrated Table (4.1).

Table 4.1: Thickness of TiO₂ film coated on substrate

Experiment No.	Substrates	Thickness of film(nm) using thikness moniter of RF sputtering
1	1-cpTi 2-T-i6Al-4V	100
2	1-cpTi 2-Ti-6Al-4V	200
3	1-cpTi 2-Ti-6Al-4V	300
4	1-cpTi 2-Ti-6Al-4V	500

4.1.2 XRD Single Layer High Thickness Film TiO₂

The structure of TiO_2 coated on cpTi specimen was characterized by XRD for single layer high thickness film (500nm)   according to the condtions work listed in   Table (3.1), Fig. 4.2. XRD   pattern shows   that there is more than one peaks of(101,220, and 110) rutile TiO_2 at $2\theta^o$(36.0, 56.6 and 27.4)compared to the other typs of titania crystals structars (anatase and brookite) there is only one peak of (101) anatase at $2\theta^o$ (25.2). Thermal treatment at 400^oC shows rutail crystalline phase [17]. The rutile phase is more important than other types of titania for medical application.This is due to the crystal structureof both typs, the energy gap for anatase are more than the energy gap for rutail, this makes the anatase more pores and its used in optical application while the rutail is with low energy gape and more stable for that its used for medical applications [19].
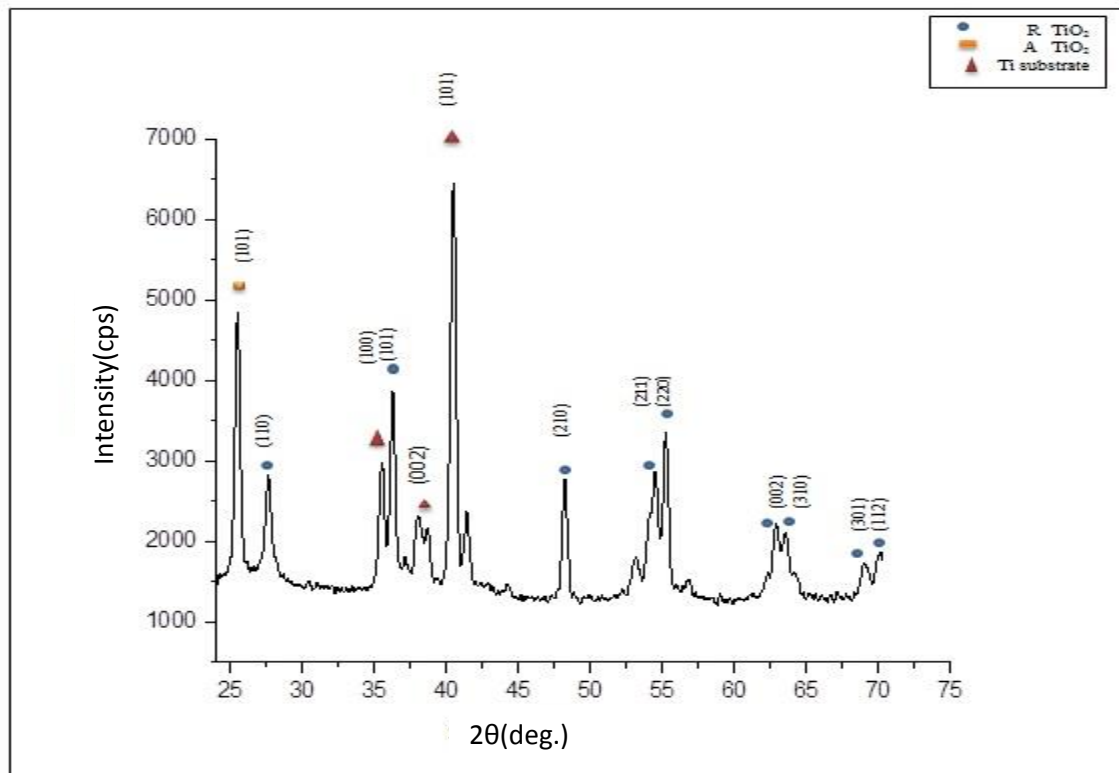
Figure 4.2: XRD patterns of cpTi alloy coated with TiO$_2$ with thickness 500nm.

4.1.3 Morphology of Thin Film TiO$_2$

Fig.(4.3 a) rpresents the uncoated cpTi and Ti-6Al-4V alloy respactivly. The Fig.(4.3 b) show thick and cracked coating covers the cpTi substrat where as uniform and crack free coating are seen in Fig. (4.3 c) cover the Ti-6Al-4V alloy substrate surface. The appearnce of the cracks on cpTi are due to the residul stress comes from accumulation of TiO$_2$ on one phase cpTi (α phase) where as there was no crack in the TiO$_2$ coated layer formed on Ti-6Al-4V alloy. The reasons for this behaviour due to Ti-6Al-4V are twophase alloy (α+β). The coating layer TiO$_2$ cover the β phase (V)wich isneedle phase as shown in Fig. (4.3 c) .The other phase wich is α phase (Ti,Al) represent the matrix the azlloy.
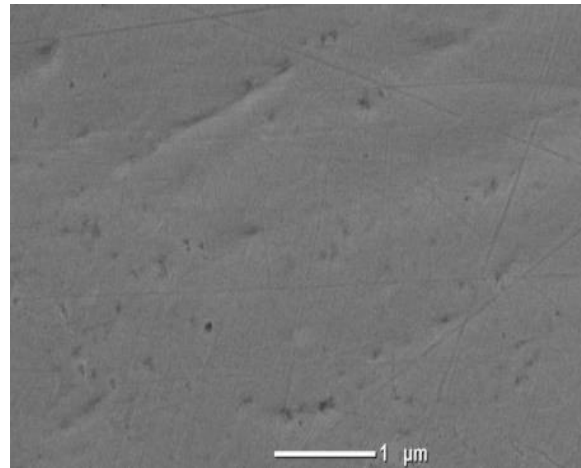
(a)
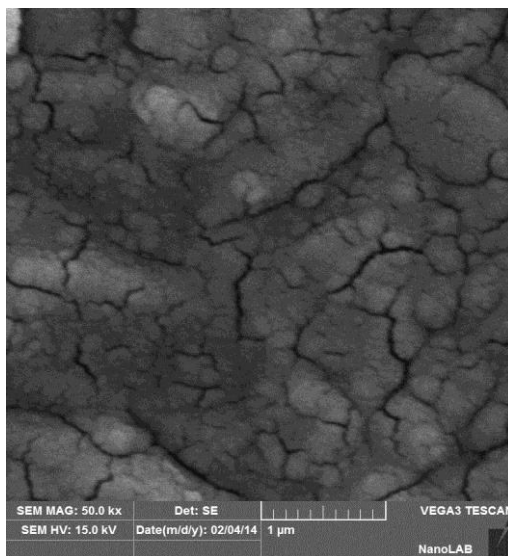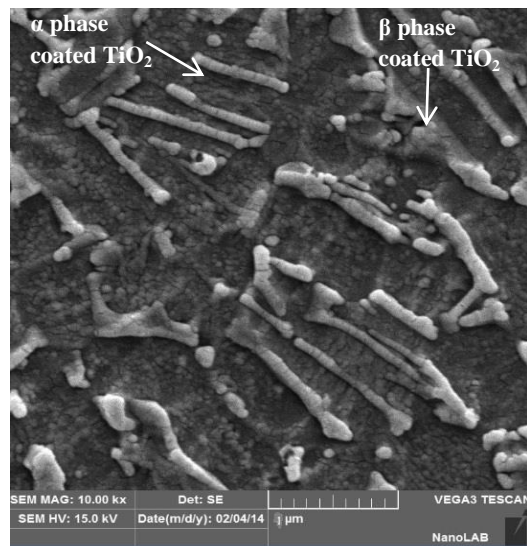
(b)   **(c)**

Figure 4.3: Top viewSEM (a) cpTi uncoated,(b)and(c) film TiO$_2$ with thickness 500nm coated on surface of cpTi and Ti-6Al-4V alloy respectively.

4.1.4 *In vitro* Tests Coating MorpHology of Thin Film TiO$_2$

The *In vitro* corrosion test for the samples of cpTi and Ti-6Al-4Valloy coated with TiO$_2$ with thickness of 200,300 and 500 nm were performed in Simulated Body Fluid (SBF) with concentrations listed in Table(3.3) .

 Figus. (4.4 and 4.5) represent the LCV behaviour of the uncoated and TiO$_2$ coated cpTi and Ti-6Al-4V alloy with 200,300 and 500nm layer thickness.Table (4.2) showed demonstrart the corrosion parameters period

from Figs. (4.4 and 4.5). There are a clear improvement in the polarization behaviour after coating in the values of E_{corr} , I_{corr} and C_R. The value of E_{corr} after coating is shifted   towards the positive noble direction of potential. With increases in the thickness of TiO_2 film ,the value of I_{corr} reduced and moved to be more negative . Corrosion ratio are also reduced, which mean increasing in the resistance corrosion .

The apperance of cracks and poros in the layer deposited on cpTi shown   in the micrograph SEM Fig.(4.3 b) did not prevent the improvement in corrosion resistance of cpTi .From Figs. (4.4 and 4.5) and the datas in Table (4.2) cpTi and Ti-6Al-4V alloy show approximately the same positive corrosion behaviour but for Ti-6Al-4V alloy shows more improvement .This gives an indication that the alloy with two phases give better improvement with TiO_2 depostion. Corrosion current density I_{corr} of samples in this work reduces in comparison with samples resoults of outher group worked on TiO_2 coatings on NiTi alloy using Electrophoretic Deposition Process[17,48].
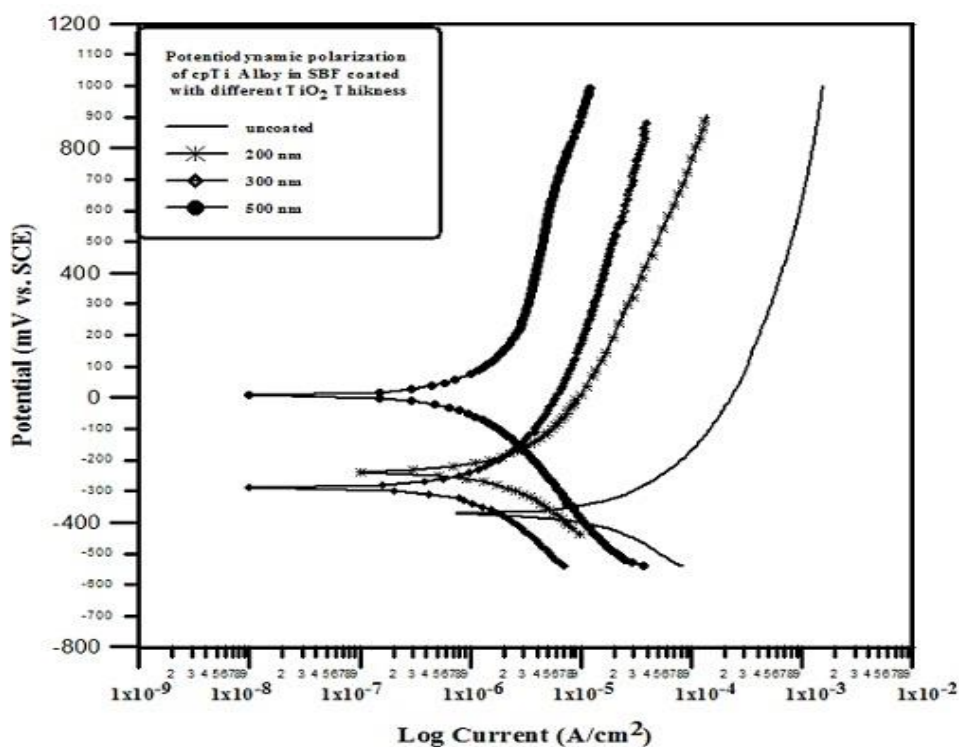
Figure 4.4: LSV pattrens for the uncoated and TiO$_2$ coated cpTi with different thickness in SBF solution .
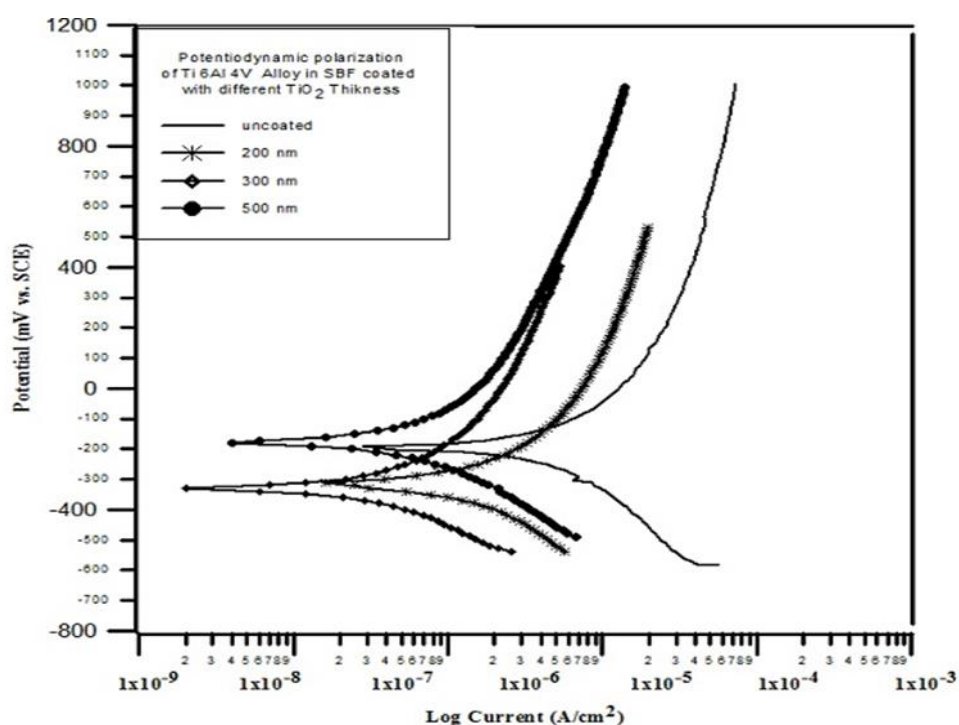
Figure 4.5: LSV pattrens for the uncoated and TiO$_2$ coated Ti-6Al-4V alloy with different thickness in SBF solution.

Table 4.2: Corrosion parameters for cpTi and Ti-6Al-4V alloy uncoated and coated with different thickness TiO$_2$

No	Thickness (nm)	Substrates	log I$_{corr}$ (A/cm^2)	I$_{corr}$ (A/cm^2)	E$_{corr}$ (V)	Corrosion rate C$_R$ (mmpy)
1	uncoated	cpTi	8×10^{-5}	-4.09	-3.9	6.958×10^{-5}
		Ti-6Al-4V	2.5×10^{-6}	-5.602	-2	2.223×10^{-5}
2	200	cpTi	9.6×10^{-6}	-5.01	-2.3	8.350×10^{-5}
		Ti-6Al-4V	8×10^{-7}	-6.09	-2.3	7.116×10^{-6}
3	300	cpTi	7×10^{-6}	-5.15	-3	6.088×10^{-5}
		Ti-6Al-4V	3.5×10^{-7}	-6.45	-3.5	3.113×10^{-6}
4	500	cpTi	5×10^{-6}	-5.30	zero	4.349×10^{-5}
		Ti-6Al-4V	3×10^{-7}	-6.52	-2.2	2.668×10^{-6}

4.2 The Results and Discussion For TiO$_2$, Al$_2$O$_3$ and HAp (Research study)

Fig. (4.6) shows the Ti-6Al-4V substrate deposited with single layer HAp and TiO$_2$ respactivly ,double layer (TiO$_2$+Al$_2$O$_3$) and triple layers (TiO$_2$+Al$_2$O$_3$+HAp)Using RFsputtering.
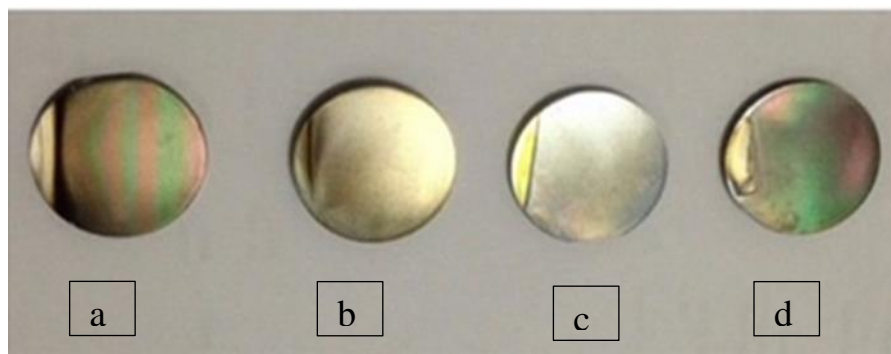
Figure 4.6: Substrates Ti-6Al-4V alloy Coated with :(a) Single layer HAp,(b) Single layer TiO$_2$ (c) multil layer(TiO$_2$+Al$_2$O$_3$) and (d) triple layers (TiO$_2$+Al$_2$O$_3$+HAp).

4.2.1 Chemical Composition

4.2.1.1 Energy Dispersive Spectroscopy of Uncoated cpTi and Ti-6Al-4V Alloy

In order to investigate the chemical composition of the cpTi and Ti-6Al-4V alloy two specimens were used to characterized composion using Energy Dispersive X-ray spectroscopy. Figs. (4.7 a and b) shows the EDS patterns of the as resived cpTiand Ti-6Al-4V alloy respactivly .The patterns shows transition energies 4.508KeV and 4.93 KeV which belong to Ti Kα and TiK_β respectively energy transitions elements O Kα are 0.5 KeV, as shown in Fig 4.7a.

The Fig. 4.7b shows another energy transition that represents V Kα 4.946 KeV which is almost over lapped with Ti$K_\beta$energy.The Al$K\alpha$ appears at energy of 1.48 KeV.The resoults whight concentration for EDS cpTi and Ti-6Al-4V alloy are tabulated in Table (4.3).

(a) **(b)**
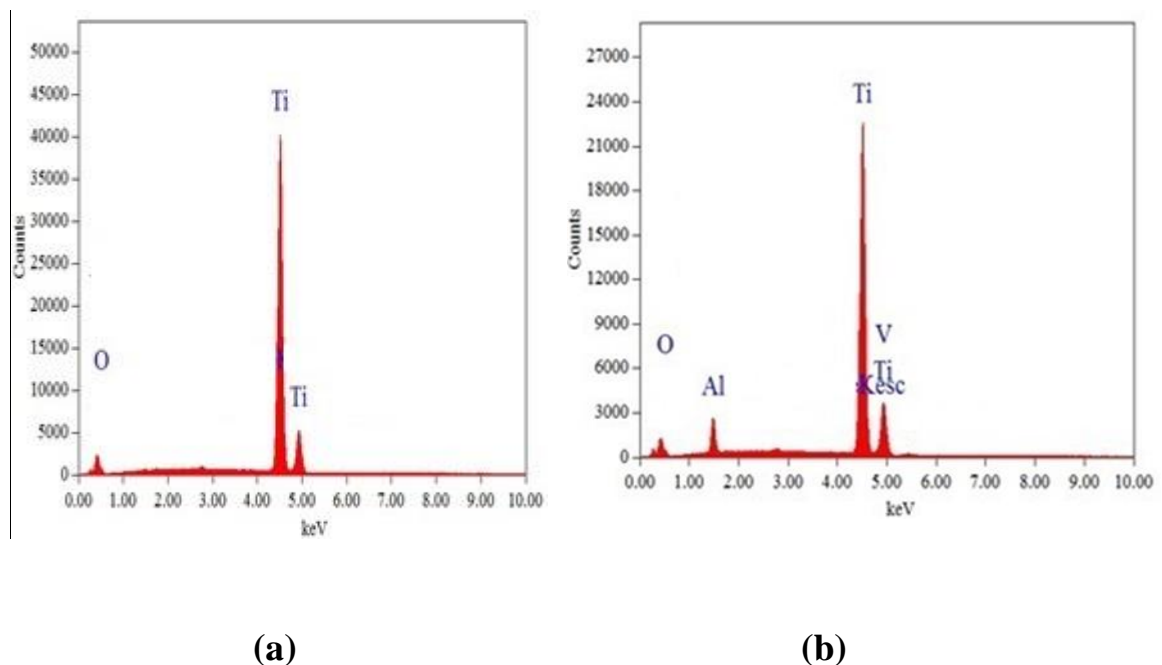
Figure 4.7: EDS spectra for (a) cpTi and (b) Ti-6Al-4V alloy un coated .

Table 4.3:Whight concentrations for cpTi and Ti-6Al-4V alloy determined by EDS

Ti		Al		O		C		V		Fe	
Wt%	At%	Wt%	At%	Wt%	At%	Wt%	At%	W%	At%	Wt%	At%
cpTi											
95.99	86.47	---	---	0.62	1.67	3.28	11.77	----	-----	0.11	0.09
Ti-6Al-4V alloy											
85.54	69.86	3.91	5.67			6.57	21.42	3.87	2.97	0.11	0.07

EDS for HAp Coated on cpTi   and Ti-6Al-4V Alloy

The HAp coated on cpTi and Ti-6Al-4V alloy with two types single and triple. The single is divided into low thickness film HAp coated at D 9 cm and high thickness film HAp coated at D7 cm. The triple layer high thickness film HAp is coated at D7 cm distance between target and substrate.

4.2.1.2 EDS of HAp Single Layer Low Thickness

Fig.(4.8 a and b) shows EDS patterns for cpTi and Ti-6Al-4V alloy respactivly coated with single thin HAp layer. The energy transitions elements Ca Kα and P Kα are 3.69 KeV and 2.01 KeV respectively ,energy transitions elements O Kα   are 0.5 KeV.The pattrens show   the accumillation of Ca and P specimen surface due to the appearance of Ca and P comparing to the uncoated specimens in Fig. 4.8. This gives an indication that rigid layer of Ca and P formed by sputtering. The concentration of the elements is listed in Table 4.4 related to all experiments depend on work conditions shown in Table 3.4 at D9 cm.

(a)   (b)
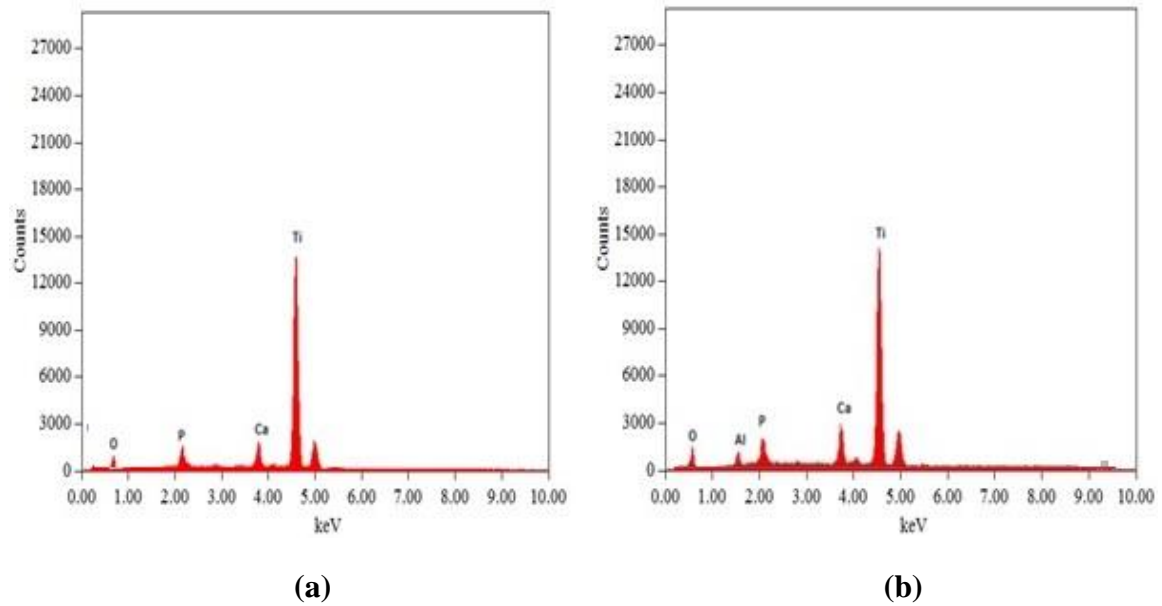
Figure 4.8: EDSspectra of single layer HAp for t_D 10 hours an D9 coated on

(a) cpTi and (b)Ti-6Al-4V alloy

Table 4.4: Concentrations   single layer HAp for t_D (2, 4, 7 and10) hours coated on cpTi and Ti-6Al-4V alloy determined by EDS

Experiment No	Time of Deposition t_D (hours)	Ti		O		Ca		P	
		Wt %	At%	Wt%	At%	Wt%	At%	Wt%	At%
cpTi +HAp									
1	2	73.25	53.41	17.06	37.24	06.16	5.98	03.53	3.98
2	4	75.32	55.45	16.63	36.72	05.57	4.91	02.48	2.83
3	7	66.17	45.8	20.02	20.02	09.22	7.36	03.06	3.27
4	10	74.98	55.07	16.80	36.95	05.21	4.57	03.01	3.42
Ti-6Al-4V alloy +HAp									
1	2	67.42	47.14	18.90	39.57	07.53	6.29	04.02	4.35
2	4	73.75	53.67	16.86	36.73	05.09	4.43	02.34	2.64
3	7	60.79	40.83	21.21	42.65	11.01	8.83	03.58	3.72
4	10	75.05	55.31	16.49	36.39	05.14	4.52	03.31	3.78

These weights concentration are adopted to as a measure to increasing the thickness of thin film HAp. Non leaner or oscillatory relation ship between Ca, P concentration weight with increasing t_D sputtering, possibly accrue presputtering phenomena at this distance thin film HAp grow with low thickness.

4.2.1.3 EDS of HAp Single Layer High Thickness

Fig. 4.9 a and b shows EDS patterns for cpTi and Ti-6Al-4V alloy respactivly coated with single layer film HAp. Also, the energy transitions elements Ca Kα and P Kα are 3.69 KeV and 2.01 KeV respectively and energy transitions elements O Kα are 0.5 KeV. The concentrations of the elements listed in Table 4.5 related to all experiments that depend on work conditions as shown in table 3.4 at D7 cm. A linear relation ship between Ca, P weight concentration and increasing with increasing the t_D sputtering, the coated at this distance is successful to grow high thickness thin film HAp.

(a)   (b)

Figure4.9: EDS spectra of single layer HAp for t_D 10 hours and D7 coated on (a) cpTi and (b) Ti-6Al-4V alloy

Table 4.5: Concentrations single layer HAp for t_D (2, 4, 7 and10) hours , D9 and

D7 respactively coated on cpTi and Ti-6Al-4V alloy determined by EDS.

Experiment No	Time of Deposition t_D (hours)	Ti		O		Ca		P	
		Wt%	At%	Wt%	At%	Wt%	At%	Wt%	At%
cpTi + HAp									
1	2	75.53	56.15	5.25	33.94	4.43	3.94	1.67	1.94
2	4	46.85	30.24	22.42	43.33	20.09	15.50	6.47	6.46
3	7	22.03	13.34	25.06	45.32	36.58	26.14	14.13	13.20
4	10	21.24	12.40	23.32	40.77	37.86	26.42	13.83	12.13
Ti-6Al-4V alloy +HAp									
1	2	69.24	48.99	18.24	38.55	5.53	4.67	1.57	1.72
2	4	47.18	30.59	21.29	42.55	18.87	14.62	6.97	6.93
3	7	13.02	7.68	26.22	46.31	40.38	28.47	14.82	13.52
4	10	10.17	5.77	24.74	41.65	43.98	29.55	15.84	13.78

4.2.1.4 EDS of Triple Layer HAp

Fig. 4.10 a and b shows EDS patterns for cpTi and Ti-6Al-4V alloy respactivly alloy coated with triple layer HAp.The concentrations of the elements for all experimental conditions mentioned in table 3.5 are listed in Table 4.6 . EDS patterns show that the deposition of Ca and P in triple layer is similar to that of the single layer at same distance between the target and the substrate but with low weight concentration because the depositing on cpTi and Ti-6Al-4V alloy as in single layer which is different from depositing on thin film ($TiO_2+Al_2O_3$) as in triple layer .

Thin film contains a number of pours and O_2 cavity,when depositing Ca and P atoms this leads to the formation of bounds with the two layers coverd the($TiO_2+Al_2O_3$) coverd the specimen. There are pecks belong to the energy transition of the substrates AlKα that appears at energy of 1.48 KeV which belong to the second layer of Al_2O_3 coated.In general, from

Tables(4.4), (4.5) and)(4.6),the decrese in the value of the weight concentration of titanium element is due to the coverage of the spacimen by the layer of HAp and this leads to increase in thickness of film. The form HAp is $Ca_{10}(PO_4)_6(OH)_2$ where the weight concentration of Ca is more than P with ratio Ca/P equile to 1.67. The increase in this ratio belongs to the double increasing in concentration of Ca than P, some researchers suggested that during the sputtering, the calcium Ca atoms, which have a little more mass, displace the atoms of less mass, in particular phosphorus P on the surface[36].

Other authors reported that phosphorus was pre sputtered from the growing surface film by negative oxygen ions with the energy determined by the potential drop in the cathode dark sheath[102]. The source of the oxygen that can concentrate in creament comes from the TiO_2, Al_2O_3 and HAp targets and also from increasing in the oxide layer thickness due to exposure of samples to air, heat of sputtering system and normalize heat annealing, this good feature to increasing air cavity or pours for compatoblity with tisuss bone and increasing passivation layer samples so increasing corrosion resistance. In creasing the deposition time t_D to 7 hours leads to the appearance of the increase on the energy transition for Ca at energy of 4.01 KeV which represents the CaK_β as can be shown in Fig .(4.10)in both substrates . Also there is a small peck at energy of 3.31KeV that represent in the KKα which belongs to the other target in the sputtering system located near the HAp target.From concentration of Ca and P ,the thickness of thin film on Ti-6Al-4V alloy more than on cpTi alloy.From EDS test in table 4.6 the Ca and P concentration on Ti-6Al-4V alloy more than cpTi.

(a)   (b)
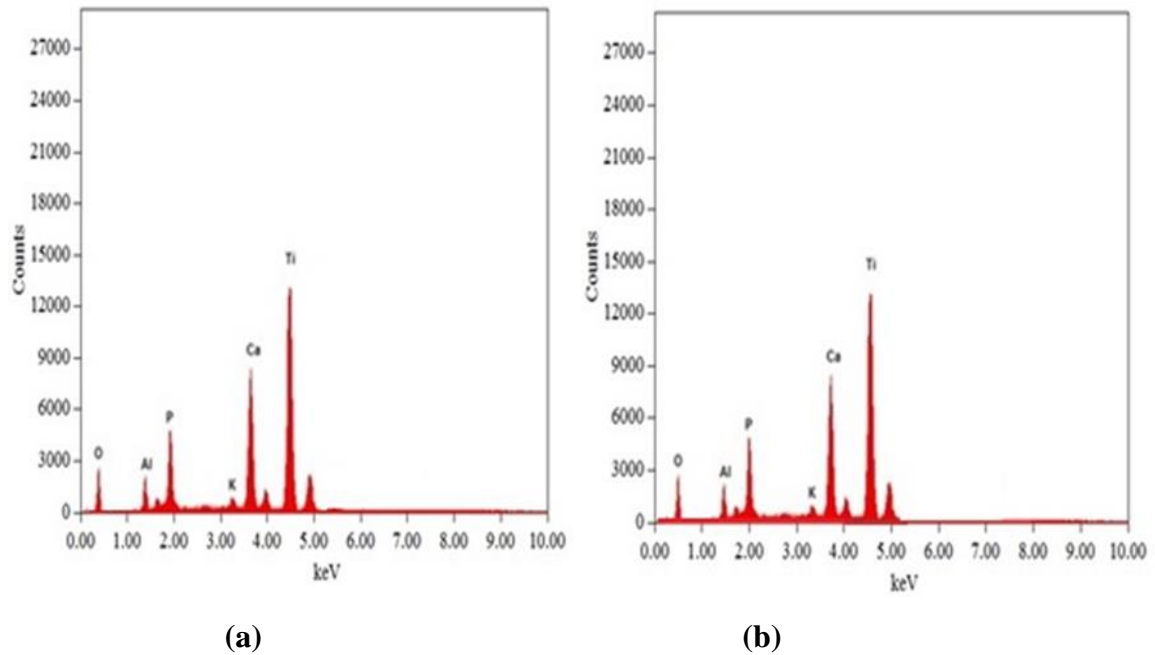
Figure 4.10 :EDS spectra of triple layer HAp for t_D 7 hours and D7coated on (a) cpTi and (b) Ti-6Al-4V alloy
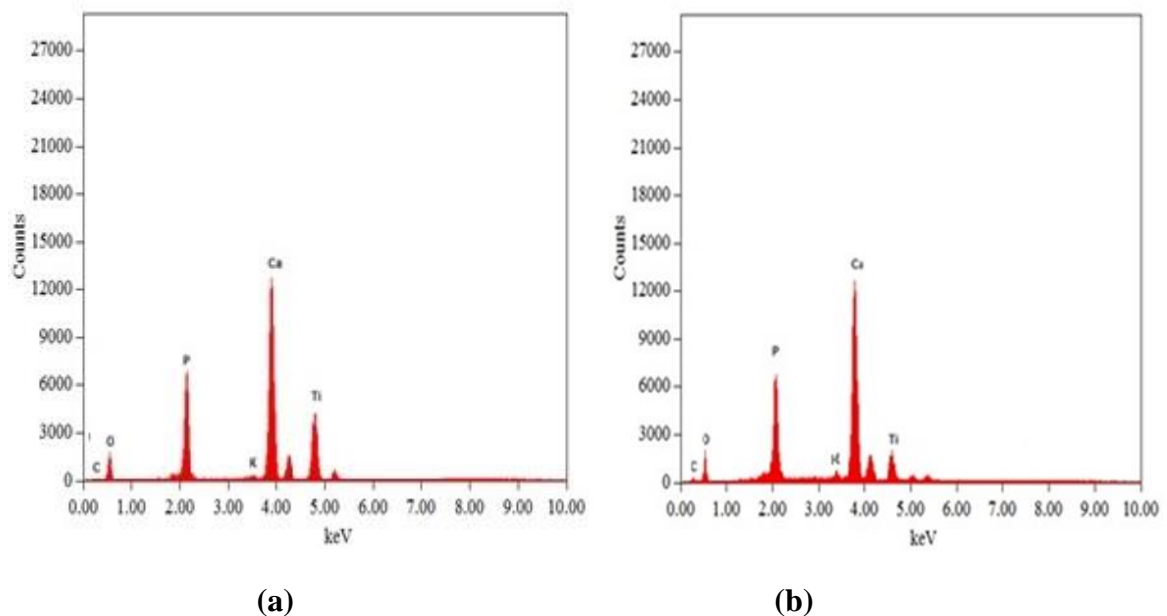
Table 4.6: Concentrations   triple layer HAp for t_D (2,4 and 7)hours coated on cpTi and Ti-6Al-4V alloys determined by EDS.

Experiment No	Time of Deposition t_D (hours)	Ti		Al		O		Ca		P	
		Wt.%	At%	Wt.%	At%	Wt.%	At%	Wt.%	At%	Wt.%	At%
cpTi +TiO$_2$+Al$_2$O$_3$+HAp											
1	2	70.4	51.02	2.88	3.71	16.30	35.38	6.98	6.05	3.43	3.85
2	4	54.88	35.83	1.61	1.87	22.72	44.41	13.23	10.32	6.07	6.13
3	7	46.02	29.08	3.1	3.48	23.73	44.90	17.42	13.16	7.30	7.14
Ti-6Al-4V alloy+TiO$_2$+Al$_2$O$_3$+HAp											
1	2	74.4	55.0	1.38	1.82	15.84	35.06	5.49	4.85	2.87	3.28
2	4	46.65	29.6	7.28	3.67	23.4	44.44	16.48	12.49	7.28	3.26
3	7	43.37	27.22	2.49	2.77	23.4	44.44	19.61	14.71	8.24	8.0

4.2.2 Structral Analysis

The structural was carried out for coated and uncoated samples using XRD.The HAp coated film formed on cpTi and Ti-6Al-4V alloy was performed by XRD for both types single and triple layer thin films.

4.2.2.1 XRD of HAp Single Layer Low Thickness

Figs.(4.11) and(4.12) show the XRD pattrens of uncoated and HAp coated cpTi and Ti-6Al-4V alloy for t_D 2,4,7 and 10 hours . Heat treatment for the coated specimence at 600°C[35,40,51] shows a crystalline phase but there is a little shift for all peaks toward higher $2\theta°$. This resulted from the heat effect and also the overlapped of Ti substrate peak with Miller indices (*hkl*) (101) with the peak of Octa Calcium Phosphate (OCP) (-4-22). It can be seen from Figs(4.11) and(4.12) that peaks of αTi and (OCP) when t_D was 4 hours for cp Ti and (2 and 7) hours for Ti-6Al-4V alloy.This gives an indication that these samples are covered with coated film according to the EDS results   peak in Fig. (4.8) of high crystalline of these sample.

Depend on results of EDS Fig. (4.8) and Table (4.4), the intensity of peak HAp(211)various un depend on the increasing in t_D and the same thing can be seen for the (112) peak also the same phenomena can be noted for CP peaks(1211),(3012),(2212) and(143). The diffraction angle of the Ti (102) ,the peak is shifted from its original position and reduced in intensity with increasing its time working inside the sputtering system.This caused by the dissolution of oxygen in the subsurface which increases the lattice parameters [78].

Figure 4.11: XRD patterns of the uncoated and HAp coated cpTi alloy for different   deposition time t_D(single layer) low thickness.

Figure 4.12: XRD patterns of the uncoated and HAp coated Ti -6Al-4Valloy for different time deposition time t_D(single layer) low thickness.

4.2.2.2 XRD of HAp Single Layer High Thickness

The X-ray diffraction patterns in Figs. (4.13) and(4.14) have more than one peak of HAp comparing to other calcium phosphate crystals. This is in good agreement with the EDS results in Fig. (4.9) and Table(4.5). Heat treatment at 600°C resulted in high crystalline and there are shiffting in the(101)αTi of the cpTi and Ti-6Al-4V alloy substrats rested in the formation of (404) of CP at $2\theta°$ (41.06)which dominating in the three deposition time started from 2 hours can be seen in Figs.(4.13) and(4.14).

The major phase that dominated the depostited single HAp layer are HAp comparing with the other CP compound phases .It can be seen that the (211), (112) and (002) at $2°\theta$(31.77,32.19 and 25.87) HAp peaks are the highiest intensities in all specimens coated at different t_D.

For the two substrats   at t_D10 hours the HA peaks intensities are increase with holding time , there was an improvement in the coating crystallization and the strong HAp was at (112), (211) and (002) with a 100% intensity of HA at (112) which over lapped with (211).This preferred orientation suggested that high coating and chemical reaction between the different components were occured.

 The (002) HAp peak at $2\theta°$ (25.8)was stronger compared to (112),(211) HAp peaks around $2\theta°$ (31.7)specially for the HA coating Ti-6Al-4V alloy Fig. (4.15). From the XRD wide scan spectra it can be concluded that longer times of deposition resulted in a higher crystalline phase content and a wider variety of growth directions. And this strongly agreement with the review Study done by [34].
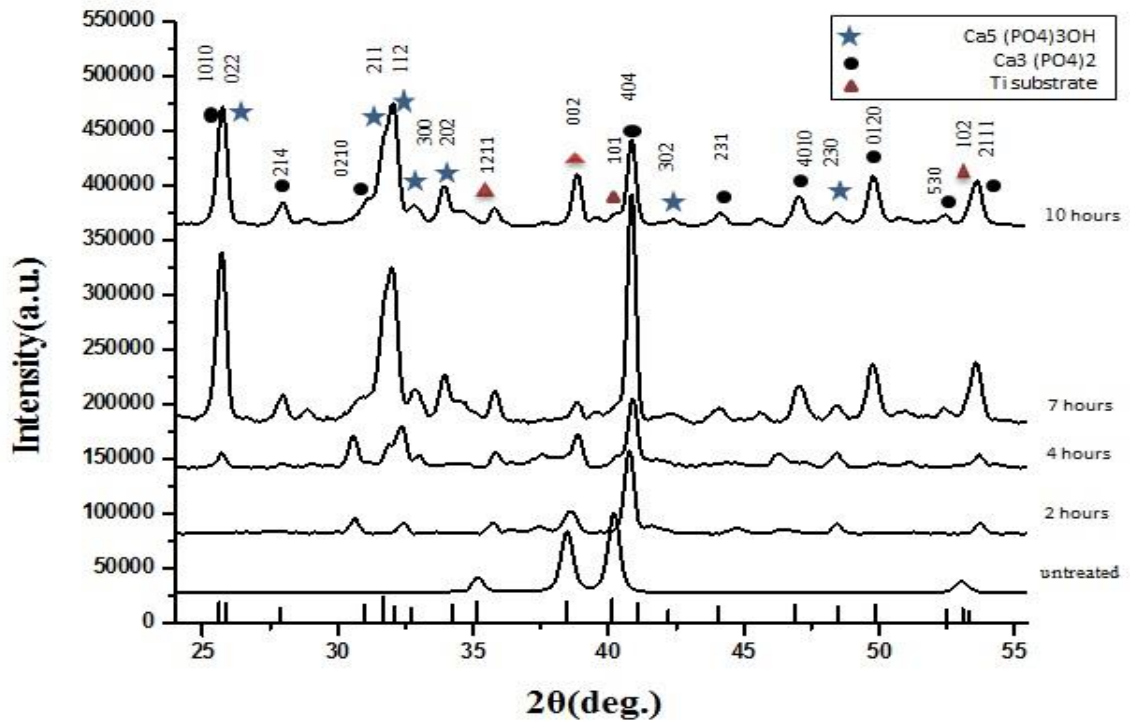
Figure 4.13: XRD patterns of the uncoated and HAp coated cpTi alloy for different deposition time t_D(single layer) high thickness
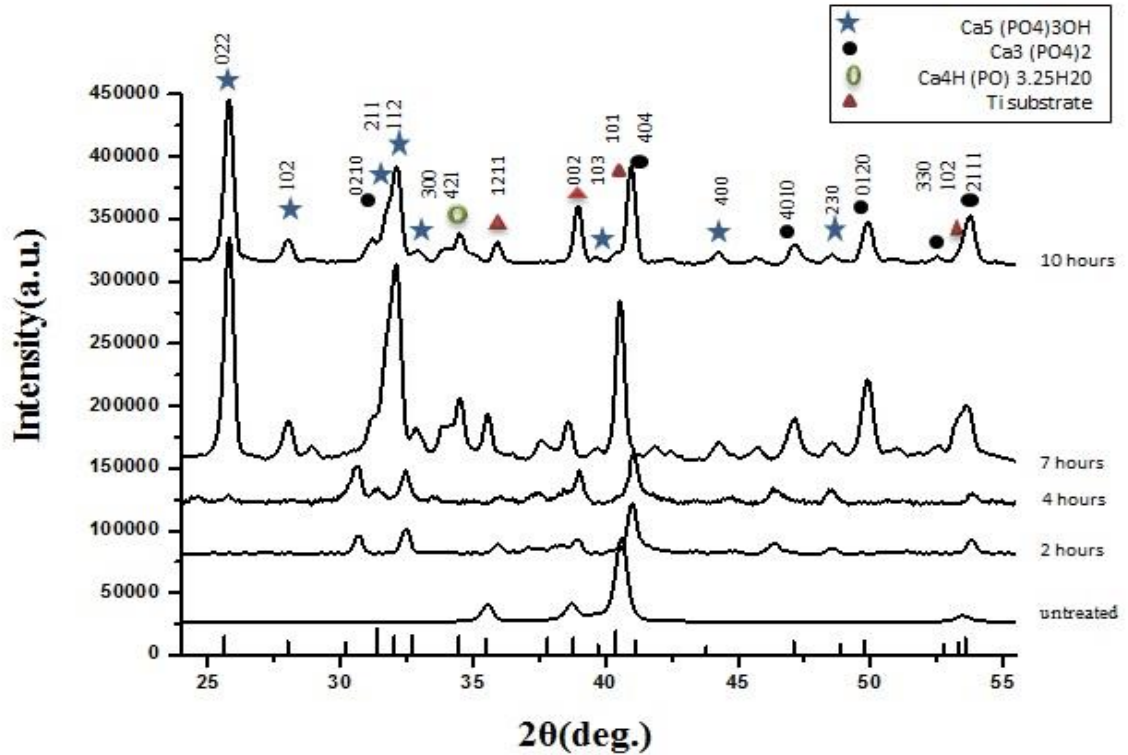
Figure 4.14:XRD patterns of the uncoated and HAp coated Ti -6Al-4Valloy for different deposition time t_D(single layer) high thickness.

4.2.2.3 XRD of HAp Triple Layer High Thickness

The Triple –layer coated specimens shows that the layer consisted of an alternating layers of TiO_2 and Al_2O_3 coated on Ti and its alloys, followed by depositing of a HAp as the third layer. From Figs. (4.15) and(4.16), it is noted that phase composition of the coating detected by XRD was contined Al_2O_3 phase at $2\theta^{\circ}$ (47.56) and(200)TiO_2 at $2\theta^{\circ}$ (39.18). In the XRD pattrns of cpTi specimeans coated with triple layer with HAp at t_D 7 hours show the formation of different ceramic compound inclouding (080)TCP at $2\theta^{\circ}$ (34.6) ,(2-32)OCP at $2\theta^{\circ}$ (38.6),(404)CP at $2\theta^{\circ}$ (41.1) and HAp (211) at $2\theta^{\circ}$ (31.7) ,HAp (002) at $2\theta^{\circ}$ (25.8) .Ther are other peaks appeard dominted by HAp phase for example(112),(102) and(4010) ..ect at $2\theta^{\circ}$ (32.1,28.1 and 46.9) respectively.

The presence of (200)TiO_2 at $2\theta^{\circ}$ (39.18) in Fig. (4.15) for cpTi suggested the thickness of the natural oxide film layer on the sample. This was resulted from the oxgen of ceramic material and the exposer of the sample to the atmosphere and heat that came from the plasma inside the sputtering system for long time and annealing. The TiO_2 layer generally consist of (TiO_2, Ti_2O_3 and TiO) [3,8] in addion to that formed the first layer TiO_2 during the deposition.

In Fig. (4.16) presence peak Al_2O_3 on Ti-6Al-4V alloy phase at $2^{\circ}\theta$ (47.56) as result from natural oxide layer for Ti-6Al-4V in form (Al_2O_3, TiO_2) add to coated with second layer Al_2O_3. The reduce in intensity at increasing t_D HAp means that the chemical reaction between Al_2O_3 , HAp layers XRD showed improvement in coated.
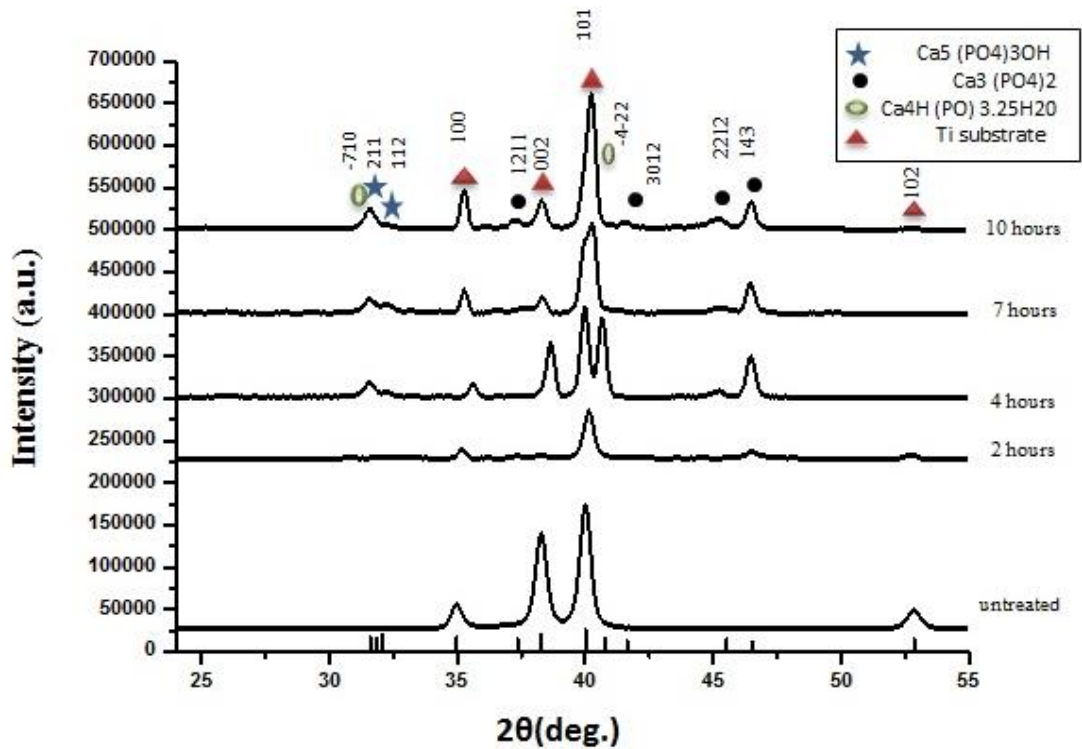
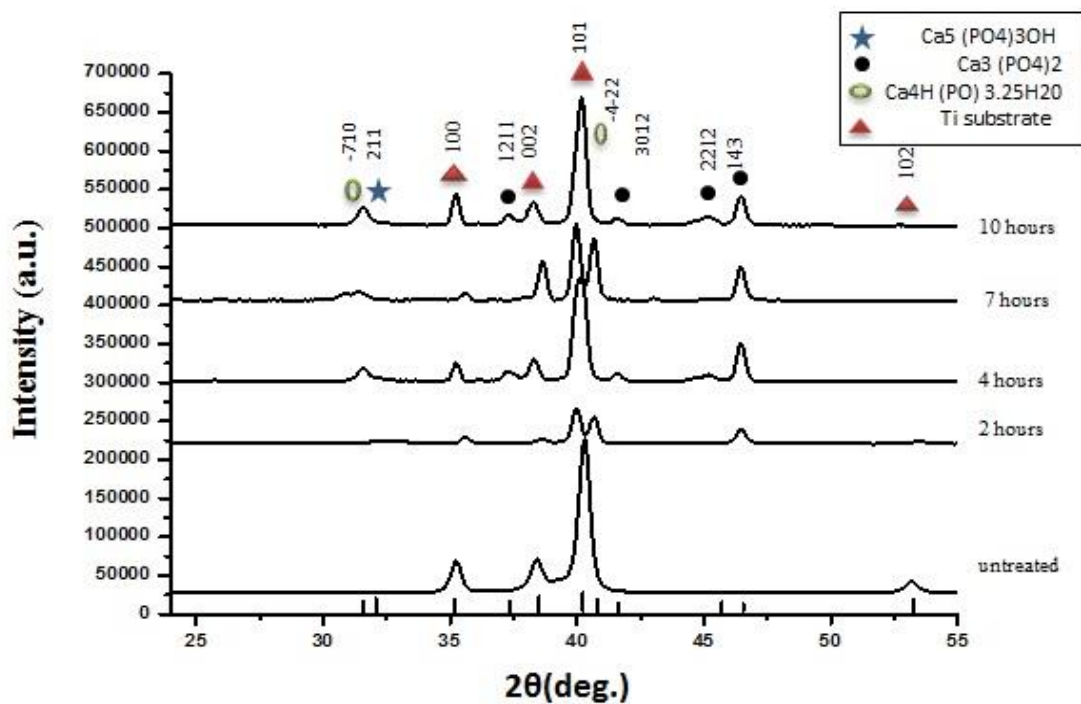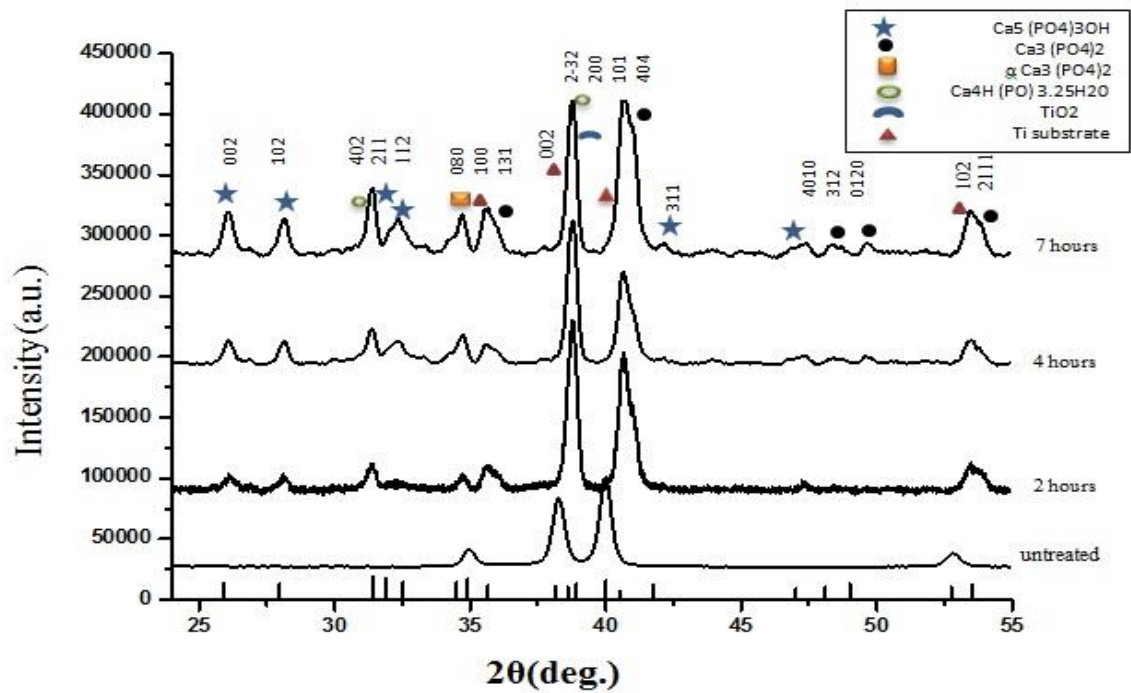**Figure 4.15: XRD patterns of the uncoated and HAp coated cpTi for different deposition time t$_D$(triple layer) high thickness**
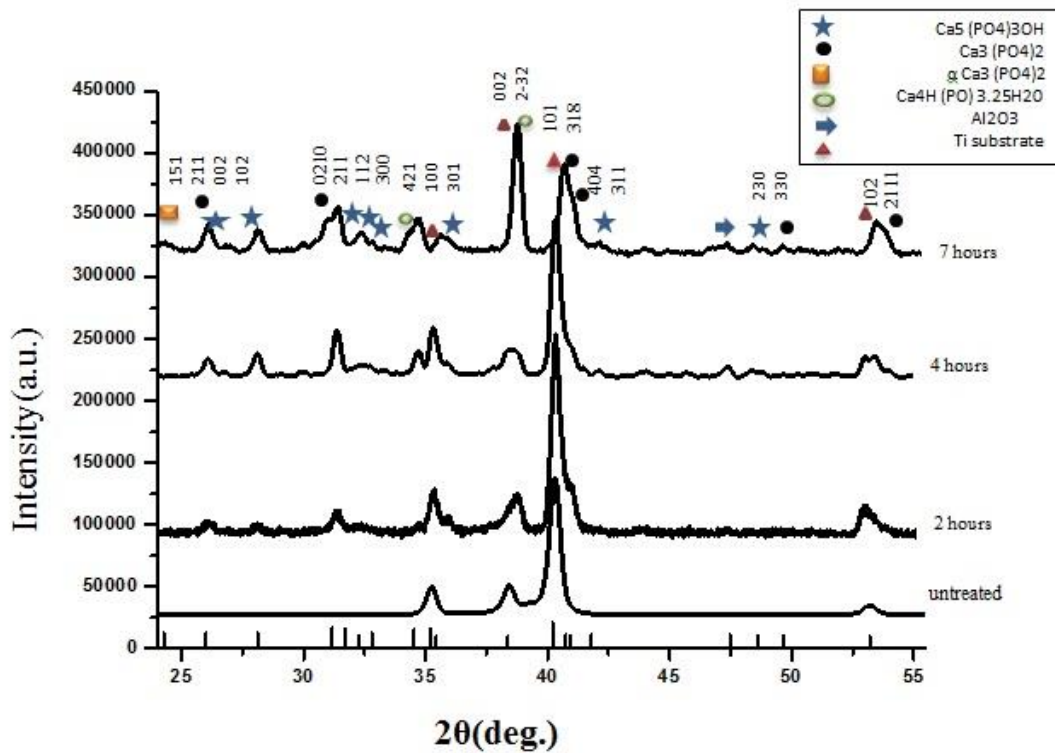
Figure 4.16: XRD patterns of the uncoated and HAp coated Ti -6Al-4Valloy for different deposition time t$_D$(triple layer) high thickness

The intensity of HAp thin film was increased with the increasing of t_D, but appeard lower if compared with intensity single layer for sa67890me condition work.The deposition directory on the alloy surface are different than the deposition on alloy surface coated with ceramic layer (Al_2O_3) which can give a pores layer.The HAp layer are higher in bonding when it was coated on ceramic coated initialy layer. A strong structural interdependence appeard between the covering HAp layer and the Al_2O_3 substrate. Howevery similar observations were also made by other researches Zhou &Mercioniu [50,52] .Particaly of HAp reduce from micro to nano through RFsputtering, this means that the number of particles increase so that the intensity of the peak increased. The grain size growth, narrow-scan spectra of the (002), from $25^°$ to 27° peak have been recorded the particle size calculated using Scherer equation in X-ray diffraction the full-width-at-half-maximum (FWHM) results[43], as shown in Table (4.7).

$$\text{Scherrer's relation: } a = \frac{o.9\lambda}{B\cos\theta}$$

Table 4.7 : The particle size HAp film for t_D 7 hours coating cpTi & Ti-6Al-4V alloy .

Sample thickness	Titanium alloy coated with HAp	HAp crystal size (nm)
Single layer low thickness At D9	cpTi	15.7
	Ti-6Al-4V	16.4
Single layer high thickness At D7	cpTi	26.6
	Ti-6Al-4V	12.8
Three layer high thickness At D7	cpTi	22.0
	Ti-6Al-4V	10.2

where a is the crystal size , *B* is the FWHMof the peak, and θ is the diffraction angle. From Tables(3.4)and(3.5) chapter three, it is noted that the time deposition for HAp single layer high thickness is approximately more than three layers, moreover,it can be seen that the (FWHM) of the HAp(002)   at $2\theta^o$ (25.8)   decreases when t_D was increased, for that the crystal size of the HAp single layer high thickness was more than that of three layers. The HAp crystallites grow fixedly in size with longer t_D. The present study indicated that "the HAp with crystal size <100 nm at least in one direction are with high surface activity and ultrafine structure similar to the mineral found in hard tissues"[103]. The phase concentrations of single and triple layered HA of D 7 cm were calculated using theoretical model TOPAS–XRD program as shown in Table (4.8). The concentration of apatite thin film on cpTi and Ti-6Al-4V alloy for single more than triple layers.The results in Table (4.8)show that the HAp phase concentration in the single layer are higher than that in the triple layer(see AppendixC) .This is due to the bonding effects which can be varied according to the different thermal expansion.Therefor in this single layer, the bonding will occure between ceramic (HAp) and metal (Ti) which will be higher in bonding between ceramic(Al_2O_3) and ceramic (HAp) in the triple layers.

Table 4.8: The concentration of apatite for t_D 7 hours in single and triple layer coating cpTi- Ti-6Al-4V alloy .

Concentration of Apatite in thin film	
Single layer HAp coated	Triple layer HAp coated
cpTi alloy	
81.29%	11.55%
Ti6-Al-4V alloy	
83.45%	19.40%

4.2.3 Thickness and Morphology of Thin Film Using SEM

The thickness of thin film HAp coating Ti-6Al-4V alloy was characterized by using side view SEM for single and triple layer. The morphology of thin film HAp coating cpTi and Ti-6Al-4V alloy was characterized by using top view SEM for single and triple layer.

4.2.3.1 Thickness of thin film HAp.

The thermal expansion coefficient of Ti alloy substrate are (8.7×10^{-6}/K), for TiO_2 (7.249×10^{-6}/K) ,for Al_2O_3 (8.2×10^{-6}/K) and for HAp (13.6×10^{-6}/K). Addition TiO_2 on the substrate to reduce thermal expansion mismatch between substrate and other layer of coating. Al_2O_3 has been chosen as a second layer between TiO_2 and HAp, because it has nearly thermal expansion to TiO_2 ,also it has been confirmed that the existence of Al_2O_3 in the HAp coating leads to lower the thermal expansion coefficient of the composite coating into effect and contribute in the increase of interfacial bonding strength. The HAp was used as top layer to increase surface biocompatibility [50,53].

It is clear from the Fig. (4.17 a) for a single layer ,HAp has thickness of 290nm when the D 9cm,while in Fig.(4.17 b) the HAp as thickness became 598 nm when the D7cm also it was observed thin layer between substrate and the HAp layer about 112 nm representing the natural oxide layer.

It was conformed by different authors [46,48]in both case multilayer and composite shows uniform thickness for TiO_2 layer coated on Ti surface which was approximately not more 200nm and for HA were approximately not more 800nm, while for Al_2O_3 not more 600nm thickness. As aspect ratio Al_2O_3 on TiO_2 around 600nm which make it acceptable.

In Figure (4.17 c) to t_D 4hours HAp,the total thickness 1.21 μm, the TiO_2, Al_2O_3 and HA represent the 177nm,542nm and 387nm respectively from

the total thickness. Due to diffusion bounds, complex chemical layer form between the three layers,. The mixing between Al_2O_3 & TiO_2 at tempreture 1150°C creat complex composit chemical layer as bonding thin layer which is very clear between Al_2O_3 on TiO_2 layer about 126nm.
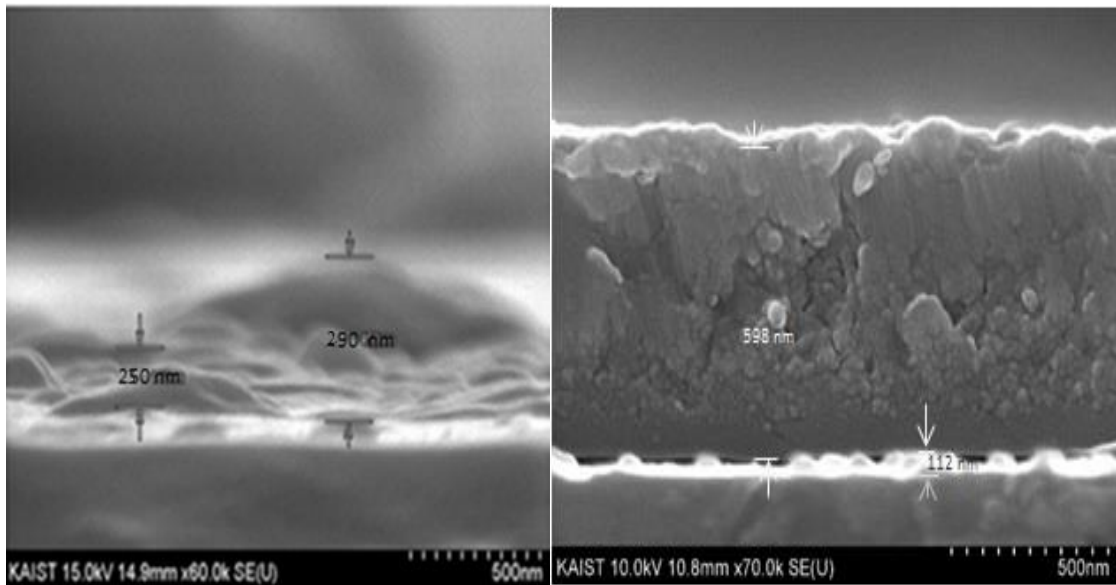
(a)   (b)
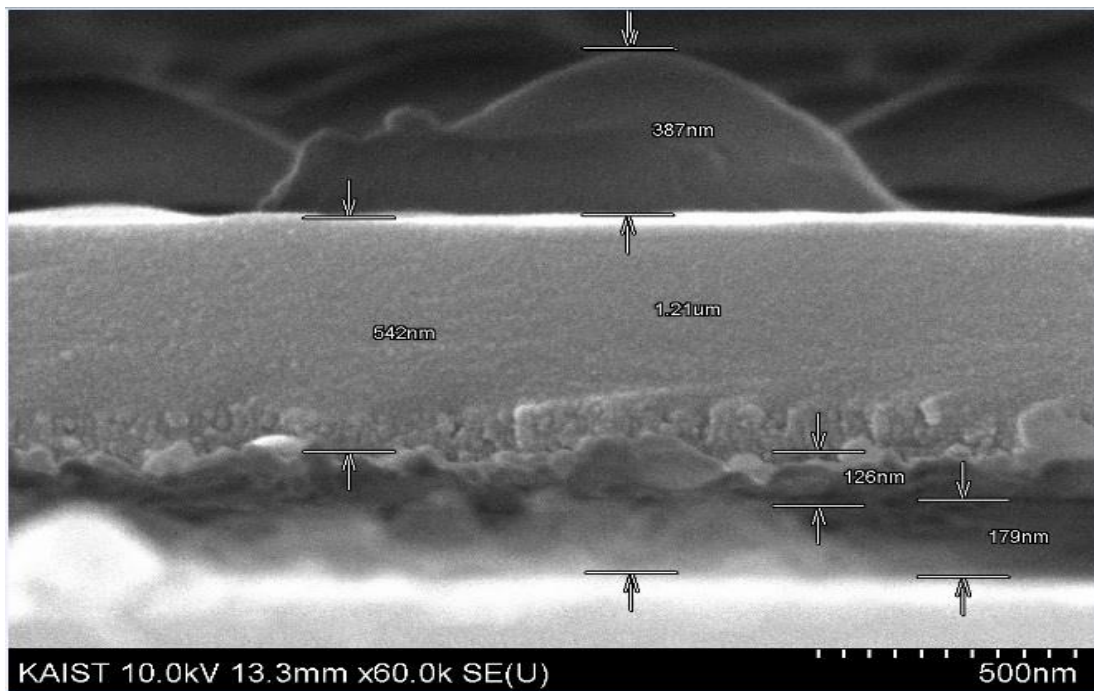
(c)
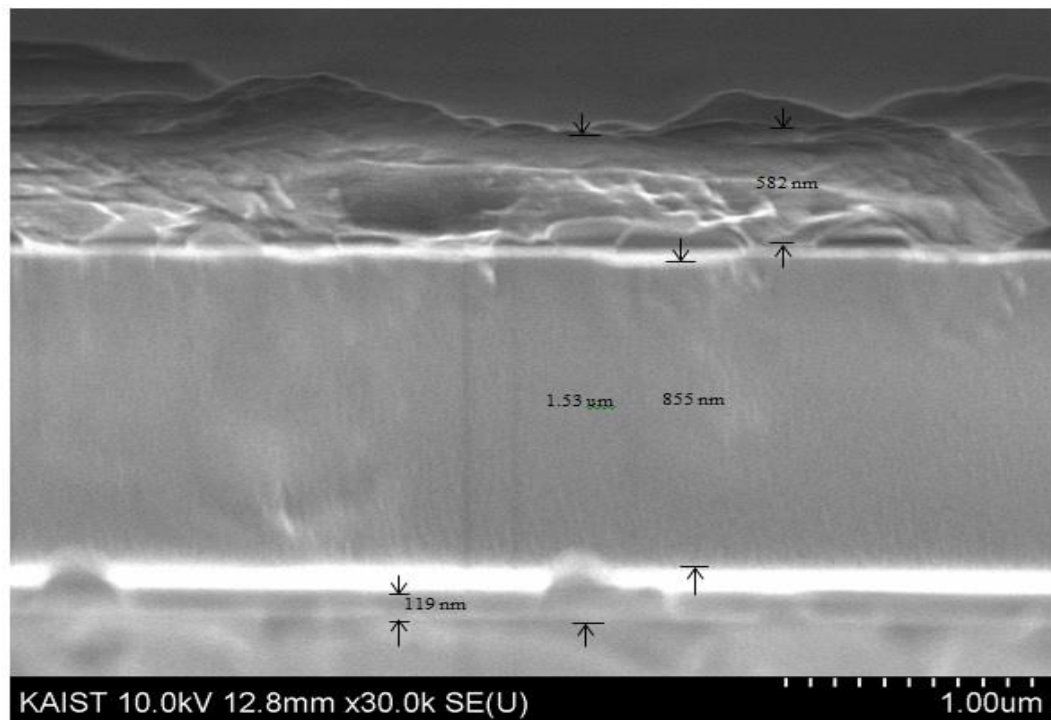
(d)

Figure 4.17: Cross section SEM micrograph of HA coated on Ti-6Al-4V alloy :
   (a) at D9 cm distance as single layer for t_D 10 hours,(b) at D7 cm distance
   as single layer for t_D 10 hours ,(c) at D7 cm distance as triple layer t_D 4
   hours,(d) at D7 cm distance as triple layer t_D 7 hours .

In Fig. (4.17 d) for t_D7 hours ,the thickness was 1.53 μm, the total thickness of the layers of TiO_2 and Al_2O_3, multilayer 855 nm, whereas 542nm is the thickness of the HAplayer from the total thickness.

Also there is a thin layer 119 nm represents the natural oxide layer TiO_2 which is contained the natural oxide film along with depostedTiO$_2$ layer.This increases in the TiO_2 layers thickness are able to improve the interfacial bonding strength[45]. Also the dense oxide layer is beneficial in preventing the ion release from the melalic substrate.Addition to SEM which was used to measure the thickness of the thin films for both single and multi and triple layer, Alpha step profiler optical 3D micro scan was also used to measure the thickness as shown in Table (4.9). From this

table, the value of thickness is increased with increasing t_D and the layer thickness deposited on Ti-6Al-4V alloy are significantly more than that on cpTi alloy. These results in agreement with results of EDS in Tables (4.5) and (4.6) XRD.The different in thickness values between SEM and Alpha optical for Ti-6Al-4V alloy approximately±3nm which is almost acceptable increasing the thickness value may lead to the surface smoothing HAp so that the difference in the measuring value between two technique reduced .

Table 4.9:Thickness of film coated on cpTi and Ti-6Al-4V alloy

as single and triple layers.

Types of Deposition HAp layer	Time of Deposition t_D HAp hours	Total thickness of thin film on cpTi alloy(nm)		Total thickness of thin film on Ti-6Al-4V alloy	
		SEM	Alpha optical	SEM	Alpha optical
Single Layer	4	----	277(nm)	---	290(nm)
	7	----	369(nm)	---	388(nm)
	10	----	578(nm)	598(nm)	595(nm)
Triple Layer	2	----	988(nm)	1.00(um)	1.03(um)
	4	----	1.12(um)	1.21(um)	1.19(um)
	7	-----	1.49(um)	1.53(um)	1.55(um)

4.2.3.2 Morphology of Thin Film HAp Layer

A) Single Layer Thin Film HAp

Fig.(4.18) presents the SEM micrograph of HAp which was built by RF magnetron sputtering on whole surface of cpTi and Ti-6Al-4V alloy.It can be seen that the coating is with uniform distribution of HAp which is fully covered the substrate surface. Mostly spherical particle morphology is observed in all samples produced. Fig.(4.18 a and b) at distance 9 cm shows that the entire substrate surface is covered by the deposition of HAp with low thickness.Such a set of sphere-like islands with small grain size was also obtained by other authors who worked on NiTi alloy coated

with HAp by using RF sputtering [102] . There is no large agglomerates and no grow in grain size at increasing t_D.This was observed in contrary of what happened with other group worked on Ti-6Al-4V alloy coated by HAp that is larger agglomerates can be seen after 60 min [34]. Fig. (4.18 c and d) represent single layer HAp coating on cpTi and Ti-6Al-4Valloy at D7 cm and 10 hours t_D.The morphology particle shapes of the surface are similar to that of the one obtain by [104]when they produced HAp powder. It can be seen from SEM photograph Fig.(4.18 c and d) the thickness of HAp layer and the grain boundries is continue to grow in size with increasing t_D. These results are in agreement with other group worked on TiO_2 coating by RF sputtering[18]. Also, it is observed larger agglomerates and some porosity on the surface, this agglomeration is due to the appearance of (CP) with increasing thickness of thin film as shown in Fig.(4.18 c and d) [40]. The layer grain size shown in SEMcomparing with that measured with Scherrer's equation are due to agglomeration of particles. The interest of using RF sputtering are to produce alyers with nano size with multiphase of HAp. Annealing process cause different orientations of their crystallographic planes, as explained by the XRD spectra Figures (4.11), (4.12), (4.13),(4.14), (4.15) and (4.16). Due to the annealing process, the grain size increases, smaller inter grain pores, thickening of the material increase , and the more clear brittle fractures are shown in Fig. (4.18 c and d) specially for cpTi Fig. (4.18 c) [43]. This can best be understood by noting that, the HA has phase (hcp) and cpTi alloy containing single αphase (hcp) while Ti-6Al-4V alloy contain double phase major (α phase (hcp)) and manor (β phase (bcc)) so larger agglomerates can be seen into the deposition process on cpTi higher than Ti-6Al-4V alloy.The porous surface improves fixation via the growth of bone into the coating forming a mechanical interlock alloy[18].
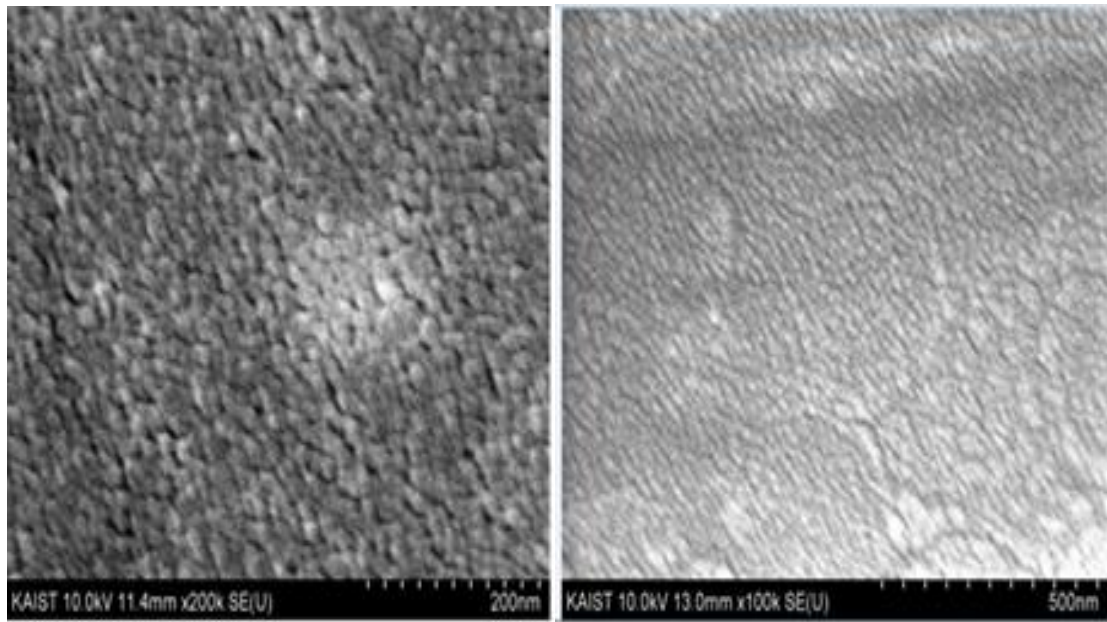
(a)   (b)
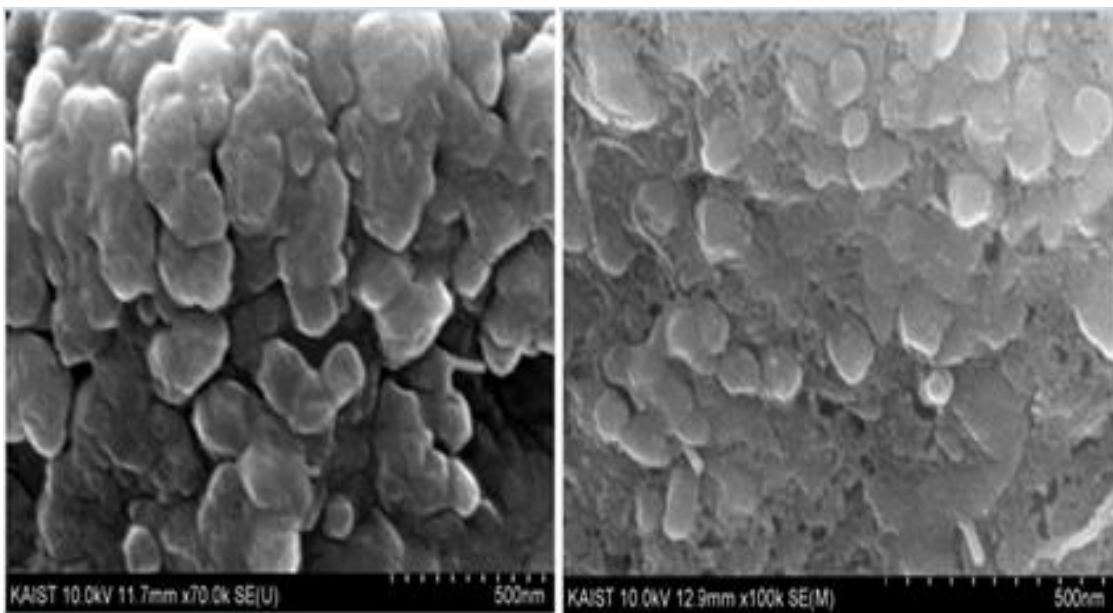
(c)   (d)

Figure 4.18: Top-view SEM image of HA as single layer   for t_D10 hours coated on:(a) cpTi   at D9cm ,(b) Ti-6Al-4Valloy at D9 cm,(c) cpTi   at D7 cm , (d) Ti-6Al-4Valloy at D7 cm.

B) Multilayer TiO_2+Al_2O_3 Film

Fig. (4.19) shows that thin films were deposited on substrates (cpTi and Ti-6Al-4V) alloys respectively using two targetsTiO_2&Al_2O_3. The TiO_2 is used as the first layers deposited on the substrates then under continues vacuum using Al_2O_3 target deposed as second layer on TiO_2 thin film as explain in section (3.3.3.2) Multilayer TiO_2+Al_2O_3 targets.

There is clear different in the morphology of coated layer between cpTi and Ti-6Al-4V alloy in spite of the layer of TiO_2 , the surface roughness which is affected by the natural oxide film of the alloy. Because cpTi with single phase, the growth of the crystal will be with large and agglomerates as shown in Fig. (4.19 a) ,while if there is another phase, this will affect the growth of HAp crystal and limit the agglomerates which is clear in Ti-6Al-4Valloy Fig.(4.19 b).

Fig. (4.19 a) there is a grow the fibrous strings TiO_2towards up belong to TiO_2first layer.
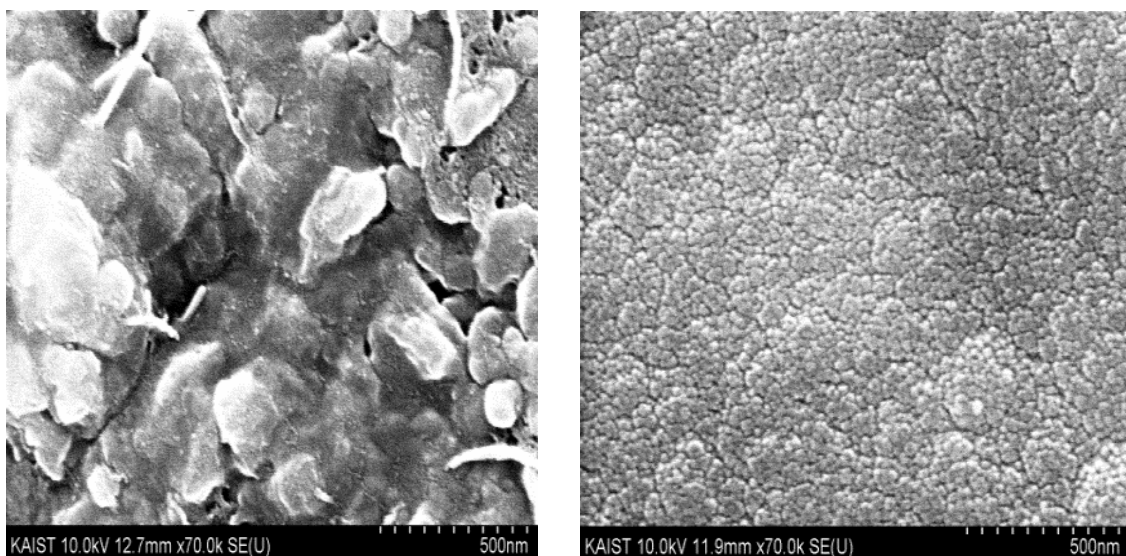
(a)	**(b)**

Figure 4.19: Top-view SEM image of multilayer of $TiO_2$and $Al_2O_3$and coated on:

(a) cpTi ,(b) Ti-6Al-4Valloy at D7 cm and t_D 4 hours.

C) Triple Layer High Thickness HAp

Fig. (4.20 a and b) show the SEM micrographs for cpTi and Ti-6Al-4Valloy coated with triple layer of $(TiO_2+Al_2O_3+HAp)$.The cpTi morphology in Fig. (4.20 a)shows big grains of HAp with long boundries which are similar to that observed by Gerard Edd *et al* [104]. In general the HAp was deposited on the surface of the two substrates and covered fully the surface.The HAp grains on Ti-6Al-4V alloy were very fine which is due to the two phase α and β.Alloy in Fig. (4.20 b) prevented the growth of the grains, as it was observed with worked other group [105].Comparing to the single layer HAp depostion Fig. (4.20 c and d), it is obvious that triple layer shows no agglomerates with hair area of grains boundres .
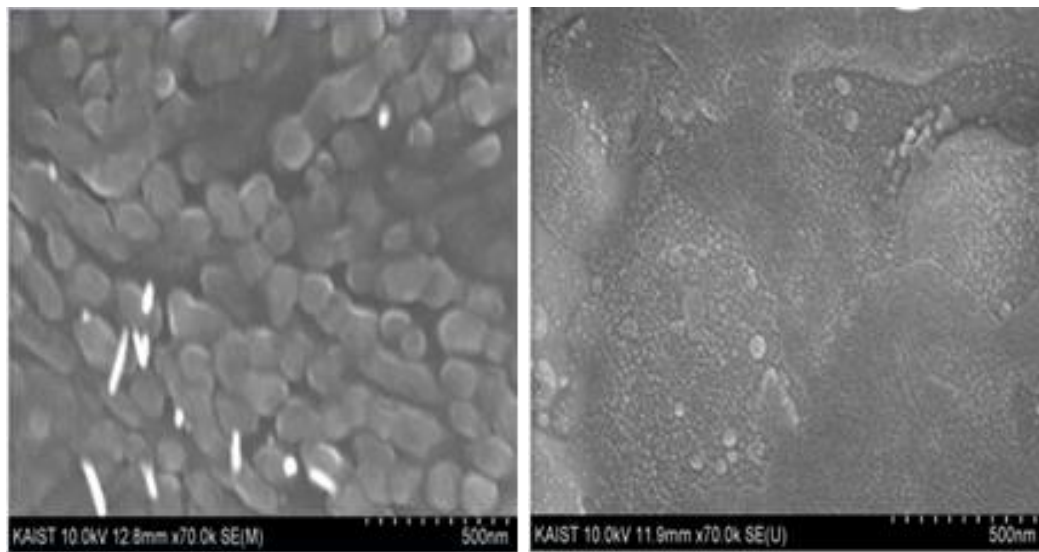
(a)   (b)

Figure 4.20: Top-view SEM image of HAp coated (a) cpTi and (b) Ti-6Al-4Valloy as   triple   layer at D7 cm for t_D 7 hours.

This may come due to the base Al_2O_3 layer that deposited befor the HAp layer in the triple layer depostion. For two substraites, the volume of grain boundries are widening associated with the oxidation reaction of $Al \rightarrow Al_2O_3$, Ti $\rightarrow TiO_2$ add to first layer TiO_2 and of the second one Al_2O_3

of partially compensates for the annealing shrinkage and prevents the formation of cracks.In Fig. (4.20 a), there are a fibrous strings grow of TiO$_2$ grown towards up and this agreement with XRD results. The SEM observations suggest that longer t$_D$ are favour for the synthesis of higher quality, small size grainsof HAp films.

4.2.4 Elemental Depth Profile at TiO$_2$ Layer Using XPS

The depth profile of the XPS technique was used to investigate the surface of Ti-6Al-4Valloy and the elemental depth profile chemistry of a sample coated with TiO$_2$ layer. The results of XPS are illustrated in Fig. (4.21) which shows the thickness of TiO$_2$ layer coated on the substrate of Ti-6Al-4Valloy.The profil shows the Alomnium (Al) is in high concentration on the surface with atomic percent 85% and this is due to the TiO$_2$ layer covers the surface.This concentration is reduced with each time 100s and in this time the concentration of O$^+$ start increasing to percent 40% with Ti 15% and finally O$^+$ concentration reached to the steady state at this trace element of each time about 220s indicating that each reached to the substrate .From this depth profile measurement, we can conclude that the surface of Ti-6Al-4Valloy coated with TiO$_2$ layer was mainly composed of TiO$_2$ up to reaching time 220s.With reference to SEM Fig. (4.17 c) the above atomic perecent for TiO$_2$ layer after 1100s are about 179m in thickness.
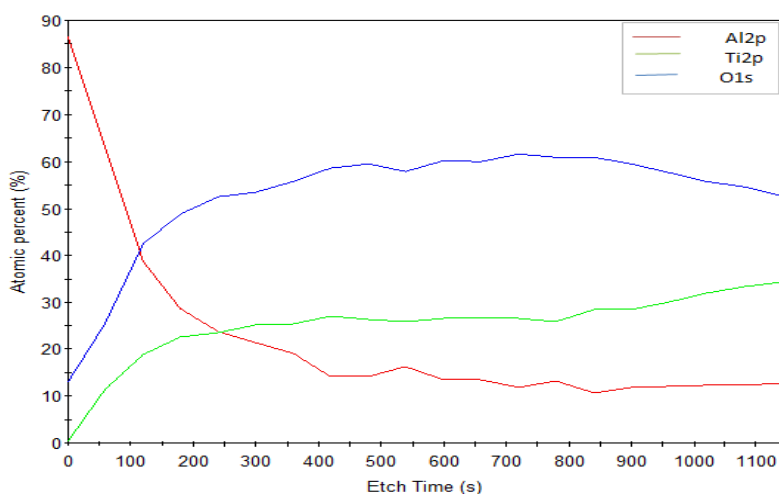
Figure 4.21: Atomic percent ves. Etch Time of TiO$_2$ layer coated Ti-6Al-4V alloy

4.2.5 FTIR Analysis

The FTIR was used to determine the various functional groups in the phosphate and carbonate substitution in the triple layer HAp coated on cpTi and Ti-6Al-4V alloy as triple layer at D 7 cm for t$_D$ 10 hours are shown in Fig. (4.22). The FTIR spectrums of standard (STD) HA powders were poplished   by authors[106],this was certain by PO$_4$$^{-3}$ (v3(1190-976), v1(953-6), v4(600-520)),OH$^-$(3571,632)andCO$_3$$^{-2}$ (v3(1665-1380), v2(885-880)) as shown in Table(4.10). The assigned peaks for the HAp coated on cpTi and Ti-6Al-4Valloy as triple layer are shown inFig.(4.22). The peak standard HAp and the data obtained from this Figure are given in the Table (4.10). The peaks analysis of the PO_4^{-3} (1087.5,1021.4,985.2 963) for first sample HAp coated on cpTi and the peaks (1090,1033,963) for second sample HAp coated on Ti-6Al-4Valloy revealed the presence of asymmetric v3 phosphate bands P-O in the region 1190-976 cm^{-1} which characterized the structure of apatite also conformed by Ravi Krishna Brundavanam *et al*[107]. The peak 1090cm^{-1} is very strong bands close to peak standard HAp in the group of phosphate. Depnding on standard HAp peak, band at 3569 and 3571 cm^{-1} for first and second samples

respactivelay are an indication of the vibrational modes of OH⁻ groups. On the other hand bands at 1434.7 for first sample and 1470 for second sample are attributed to the presence of CO_3^{-2} functional group, the carbonate ion comes from the reaction of HAp samples with atmospheric carbon dioxide [108].The shifting in all beaks might attribute to the process of rehydroxylation during the annealing[78].

Table 4.10: Infrared band positions for hydroxyapatite powders

Sample identity	Phosphate bands (cm⁻¹)			Carbonate bands (cm⁻¹)		Hydroxyl stretch 3571, 632 (cm⁻¹) m
	v_3 1190-976 vs	v_1 953-6 s	v_4 600-520 s,m,vs	v_3 1665-1380 w	v_2 885-880 vw	
3L HAp coated on cpTi	1087.5 1021.4 985.2 963.1			1434.7		3569
3L HAp coated on Ti-6Al-4V alloy	1090 1033 963			1470		3571

1190-976 cm⁻¹   P-O stretching vibration

953-956 cm⁻¹   P-O stretching vibration

600-520 cm⁻¹   P-O bending vibration
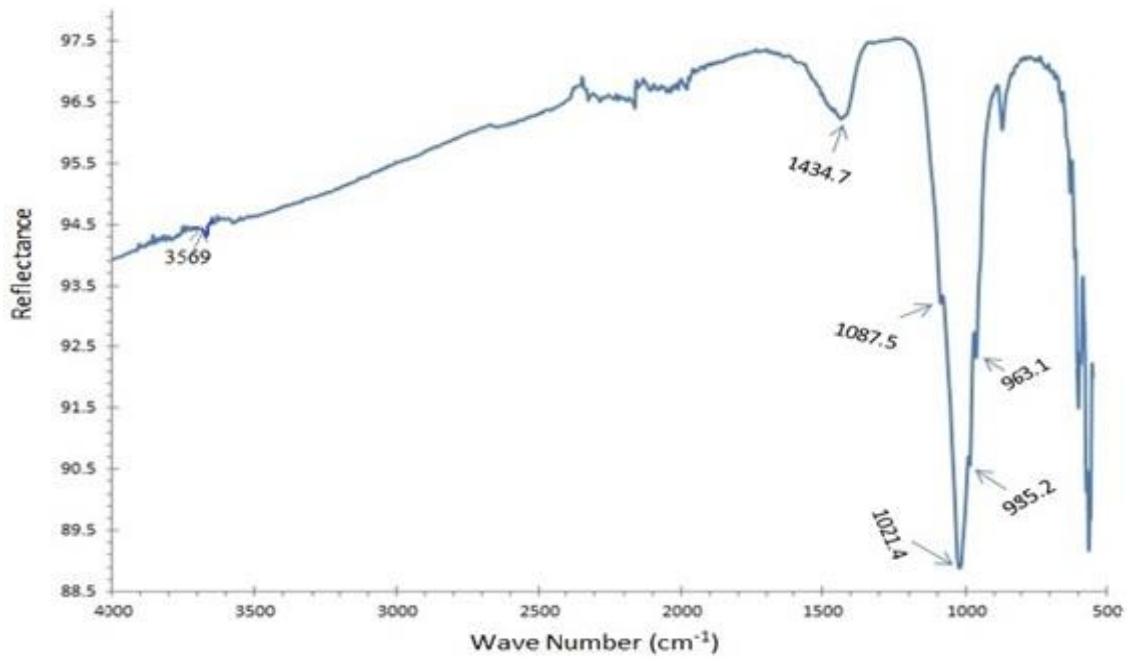
(a)
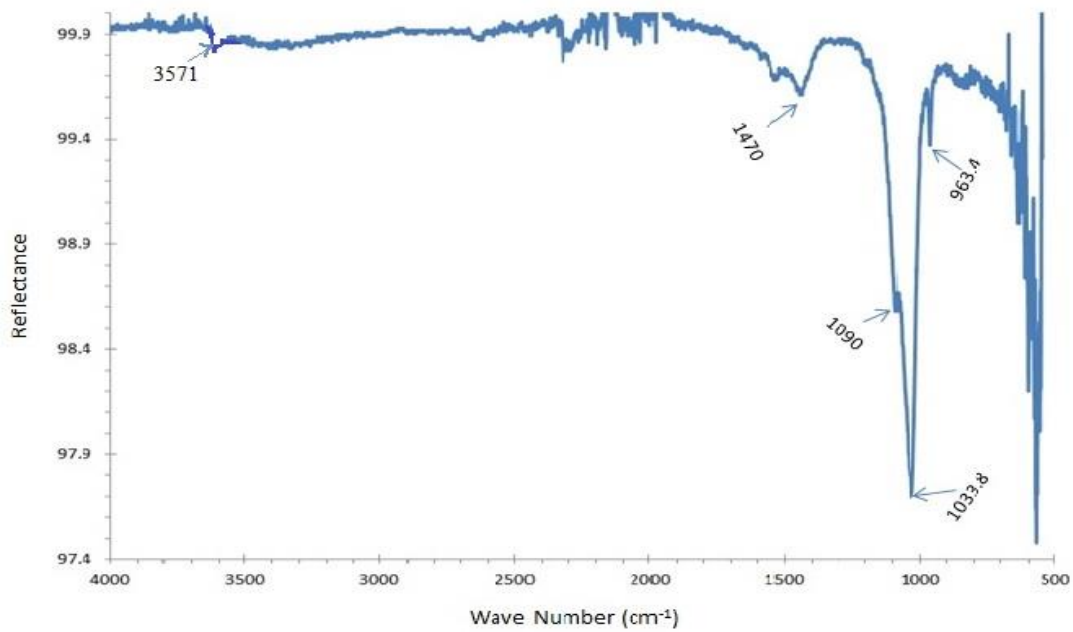
(b)

Figure 4.22: Typical FTIR spectrum of HAp coated (a) cpTi and (b) Ti-6Al-4Valloy as triple layer at D 7 cm for t_D 10 hours

4.2.6 RAMAN Analysis

Fig.(4.23 a and b) shows the intensities of Raman signal corresponding to the HAp triple layer coated cpTi and Ti-6Al-4V alloy. The bonds at   582, 960 and 1055 cm^{-1} for cpTi alloy and 584, and 959 cm^{-1} for Ti-6Al-4V alloy are due to stretching vibrations of the P-O bond. Resolved peaks at 432 cm^{-1} and 430 cm^{-1} for cpTi alloy and Ti-6Al-4V alloy respectively are attributed to the Ca OP bond vibrations in HA and this in good agreement with the work done by groups Jidong Long *et al*[37] . The Raman results are agree with the resoults obtaind by FTIR in Fig.(4.22).

(a)   (b)
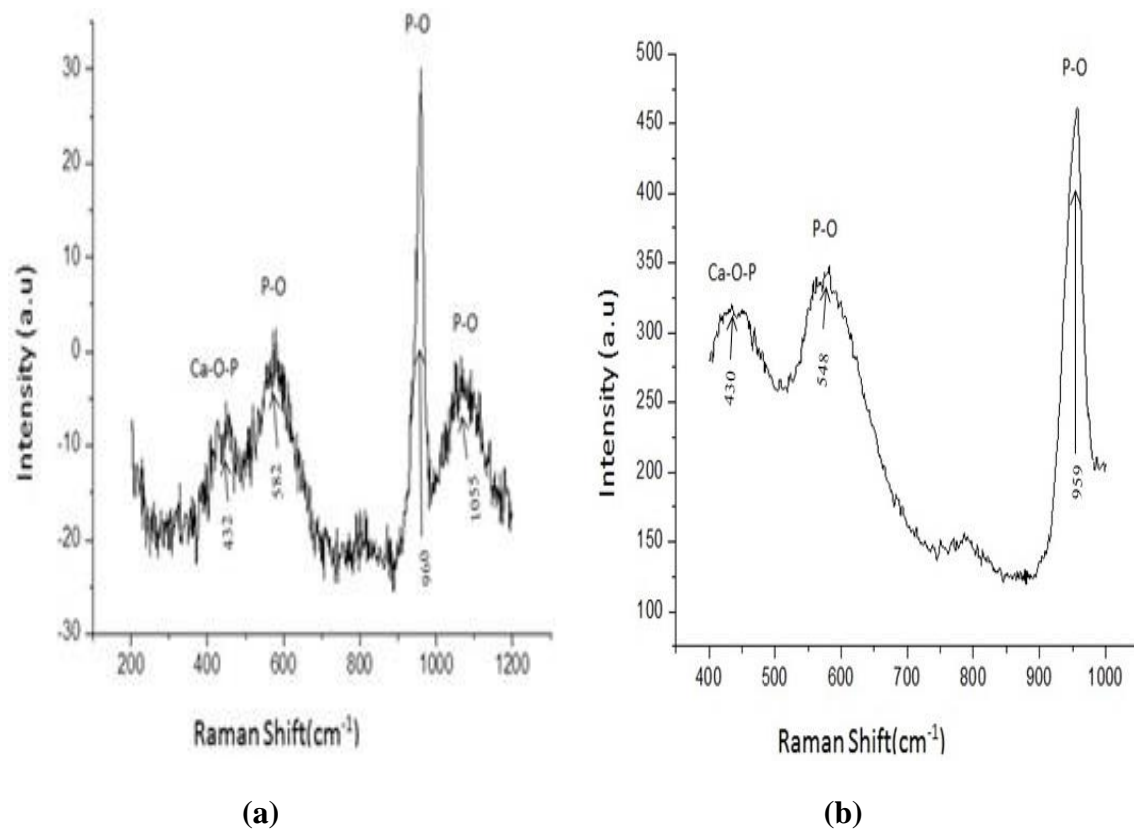
Figure 4.23:Typical RAMAN spectrum of HAp coated (a) cpTi and (b) Ti-6Al-4Valloy as triple layer at D7 cm for t$_D$ 10 hours.

4.2.7   XPS Analysis as Deposited HAp Single and Triple Layers

The elemental and chemical analysis of surface samples at penetration depth 2-5 nm was performed using XPS analysis. A survey scan XPS spectrum of a samples HAp coated Ti-6Al-4V alloy as single and triple layer at D7 cm for t_D 10 hours.A high resolution XPS spectrum of HAp coated Ti-6Al-4V alloy as single at D7 cm for t_D 10 hours , cpTi and Ti-6Al-4V alloy as triple layer at D7 cm for t_D 7 hours. The C1s peak position is at 283.50 eV, this position is in agreement with calibration measuring the reference peak of C1s BE=284eV from the surface contamination.

4.2.7.1   Wide Survey Scan XPS Spectrum
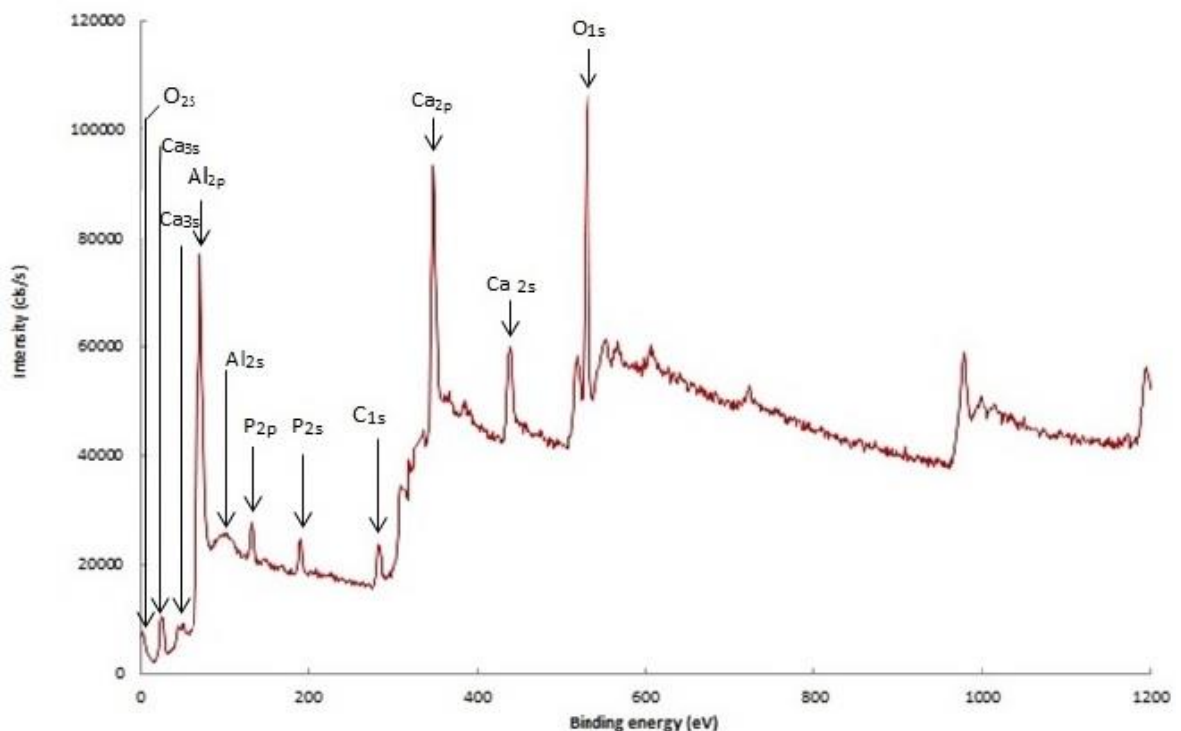
Figure 4.24:XPS spectrum survey scan of thin film HA with precipitated apatite coated on Ti-6Al-4V alloy for single and triple layer at D7 cm for t_D 10and 7 hours respactively.

The major peaks C(1s), O(1s, 2s), Ca(2s, 3s, 2p), and P(2s, 2p) are presented by XPS survey scan in Fig.(4.24) which are similar to these obtained by other authors[109] who worked on HAp deposited from aqueous solutions on hydrophilic silicon substrate.

A series of peaks are observed on a background increases to high binding energy (low kinetic energy). The C1s peak position at 283.50 eV is due to the hydrocarbon(C-H) or carbon(C-C) adsorbed by coating when was exposed to the atmosphere [110].

4.2.7.2   Narrow Scan XPS High Resolution Spectrum

The high resolution XPS spectra around C1s, O1s, Ca 2p 1/2, P 2p of the HAp samples are shown in Fig. (4.25) and the peak positions due to different chemical states are listed in Table (4.11). The spectroscopic nomenclature is directly equal to XRD source that more definitely belongs to the various quantum numbers.   Any change in chemical composites of material give the different shapes in peaks (splitting peaks, single or overlapping peak), splitting peaks belong to spin orbital splitting coupling. Lower in binding energy mean more electronic charge near the atom and moves towards the reduction [111].

 From Fig. (4.25 A1,A2 and A3), it is seen that the deconvolution of C1s spectrum for HAp single   and triple layer coated Ti-6Al-4V alloy and coated cpTi as triple layer respectively consists of three sub peaks for each sample: the first peaks at 284.58 and 284.33 eV are due to the external adventitious hydrocarbon CH, and the sub peak ,284.40 eV is due to C carbon. The second peaks at binding energies of where as 285.48, 285.63 and 285.2 eV are assigned to hydrocarbon$C_{10}H_8$.The third peaks at 282.02 and 282.92 eV are attributed to $(C_6H_5)_2PCH_2P$ $(C_6H_5)_2$ and the last peak at 286.82 is attributed to CP. XPS loss signals have been used as a way to

extract chemical information regarding to the different functional organic groups (C-O, C-H, C-P, etc.).All our findings are found to be in good agreement with the NIST XPS database and the work done by other group[68,109,110]. From Fig. (4.25B1,B2 and B3), it can be seen that the de convolution of O1s spectrum for HAp coated on Ti-6Al-4V alloy as single and triple layers, triple layer coated on cpTi , O1s spectrum consists of three sub peaks for first and second sample and two sub peaks for third sample : the first peaks at 529.20 , 529.50 and 529.14 eV are attributed to phase CaO.

The second peaks at 531.10 and 531.70eV are assigned to same phase CaO. The O atoms come from different functional groups (namely phosphate O and hydroxyl O) ,the third peaks at 532.82 eV is attributed to the hydroxyl group OH⁻ .This finding of the hydroxyle group are already conformed by Raman and FTIR resoult in section (4.10 &4.11) at the binding energy533.04eV is assigned to phosphate group P_2O_5 phase in accordance with the NIST XPS database and other authors findings [110,112,113]. Fig. (4.25 C1,C2 and C3) shows that the deconvolution of Ca2p spectrum for HAp single and triple layers coated Ti-6Al-4V alloy, and triple layer coated cpTi consists of four sub peaks: the first peaks for first and second samples at 346.70, and 346.20 eVare attributed to phase CaP and for third sample at 344.42 eVis attributed to Ca atom. The second peaks at 346.52,347.04 and 347. 67eV are assigned to CaP, where as the third appeard peak at binding energy of 350.25eV for the single layer HAp coated Ti-6Al-4V alloy and energies of 348.10 and 350.90 eV for the triple layers HAp coated cpTi are assigned to CaP. The bnding energies 349.87 and 351.25eV for single layer coated Ti-6Al-4V alloy are belong to CaO group. The Ca 2p3/2 are presented in the XPS pattern at energies of 346,347,348 and 350eV can be attributed to the chemical phosphate material CPM. While peaks at 344,349 and 351 correspond to

chemical space Ca 2p1/2.The existence of different chemical states for the calcium elements within the HAp film shows their various chemical binding states. Many different materials containing Ca can give a similar binding energy for Ca2p because of the oxidation state of Ca in those materials is similar to the (e.g.,$CaCO_3$,$Ca_3(PO_4)_2$, $Ca_10(PO_4)_6(OH)_2$ ..).They are not exactly the same ,but similar because of the oxidation state of Ca in all these compos are +2 Ca (П).From Fig. (4.25 C1) the peaks of Ca is splitted indicating that there is one type of materials, while Fig. (4.25 C2 and C3) the peaks of Ca are close fitting, refering to the existence of mixture between the materials. The presence of calcium carbonates confirmed by $CaCO_3$ is a good result becoause the CO_3^{2-} ion which constitutes 5-8% of apatite in bone. All the findings are found to be in agreement with the NIST XPS database and worked other group [109,110, 69].From Fig. (4.25 D1,D2 and D3), it can be seen that the convolution of P2p spectrum for HAp single and triple layers coated Ti-6Al-4V alloy, and cpTi as triple layer consists of three sub peaks for each sample: the first peaks for HAp single and triple layers coated Ti-6Al-4V alloy for binding energies at 132.24 ,132.00 and for third sample cpTi coated as triple layer at 132.54eV are identified to be for P. For third sample at 130.5eV, if is assigned to $(C_6H_5)_2PCH_2P(C_6H_5)_2$ .The second peaks for first ,second and third samples for binding energies at 133.51 , 133.28 and 133.70eV respectively are attributed $CaHPO_4$. The third peak : for first and second samples at 134.89 and 134. 49eV are assigned to Anhydrous monocalcium phosphate $Ca(H_2PO_4)_2$. All these peaks are attributed the pyrophosphate groups. A P 2p binding energies of 133.4-133.7 eV are accompanied by a 531.0-531.2 eV O1s binding energies was diagnostic of HAp as shown by other group [112, 114,115].
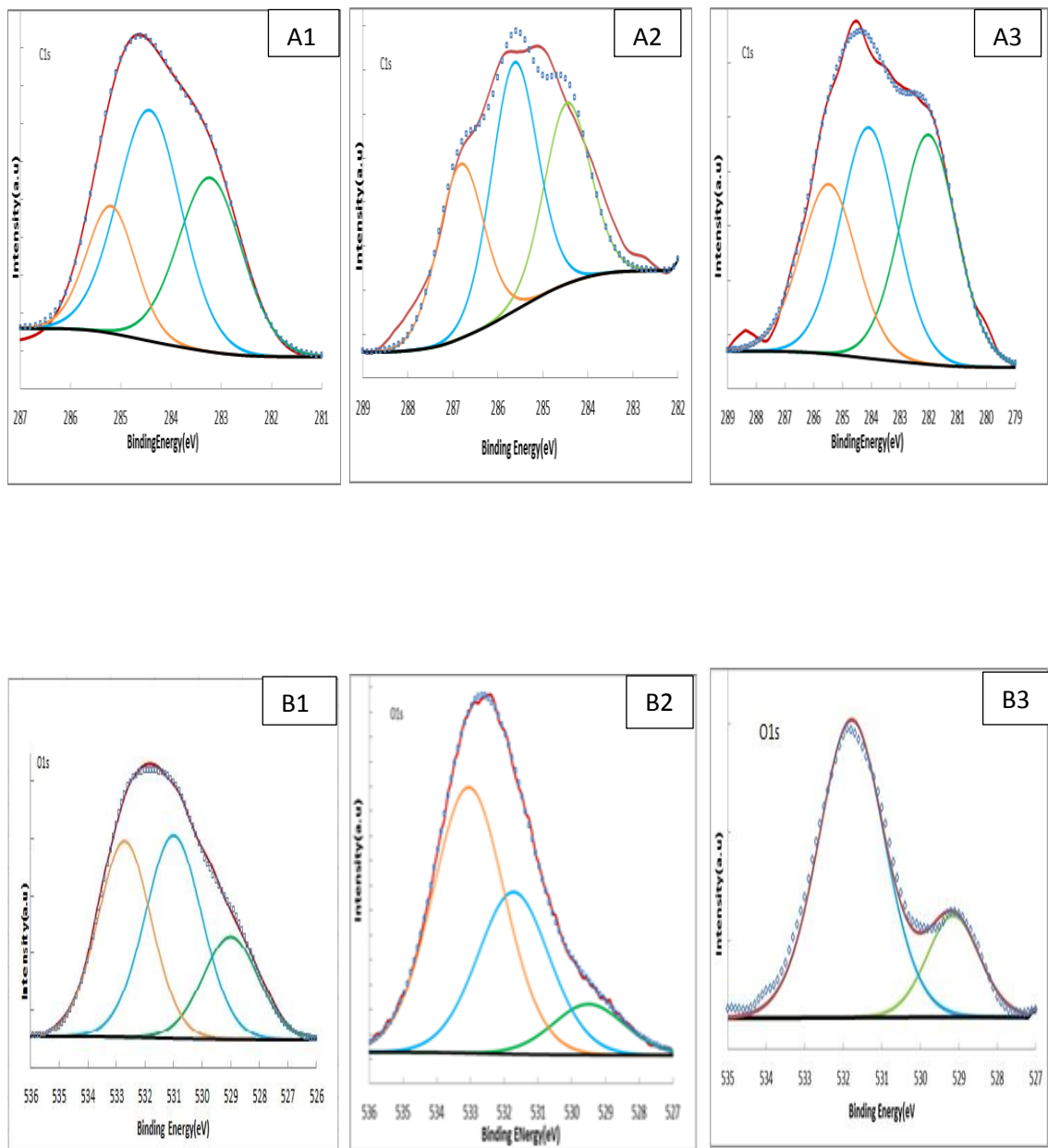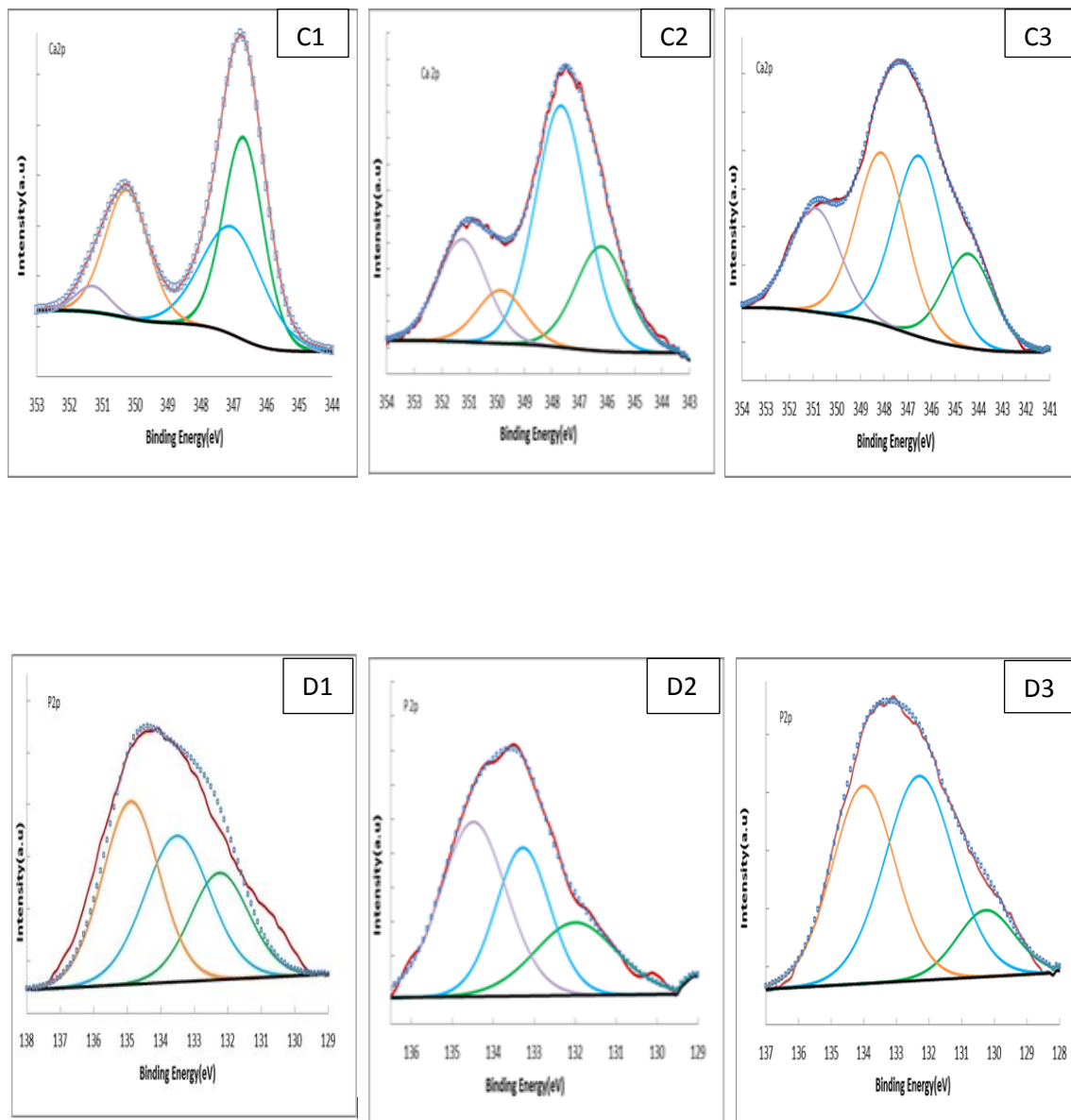
Figure 4.25: XPS spectrum high resolution of C1s, O1s ,Ca2p and P2p thin film HAp with precipitated apatite coated on cpTi and Ti-6Al-4V alloy for single and triple layer at D7 cm for t_D 10 hours.

Table 4.11: XPS spectrum analysis high resolution of C1s, O1s ,Ca2p and P2p of HA film coating cpTi and Ti-6Al-4V alloy as single and triple layers.

Samples	Line	Bonding states	Binding Energy (eV)	FWHM (eV)	Percentages of component (%)
Ti-6Al-4V +HA Single layer	C1s	$(C_6H_5)_2PCH_2P(C_6H_5)_2$	282.92	2.30	36.45
		C	284.40	2.30	36.68
		$C_{10}H_8$	285.48	2.28	26.87
	O 1s	CaO	529.20	2.30	20.71
		CaO	531.10	2.34	41.61
		OH^-	532.82	2.20	37.68
	Ca 2p	CaP	346.70	1.43	38.32
		CaP	347.04	2.20	31.34
		CaP	350.25	1.55	26.13
		$CaCO_3$	351.30	1.22	4.21
	P 2p	P	132.24	2.07	24.01
		$CaHPO_4$	133.51	2.30	36.41
		$Ca(H_2PO_4)_2$	134.89	2.00	39.58
Ti-6Al-4V +HA Triple layer	C 1s	CH	284.58	1.20	29.95
		$C_{10}H_8$	285.63	1.20	41.15
		CP	286.82	2.30	28.98
	O1s	CaO	529.50	2.5	9.07
		CaO	531.73	2.50	26.21
		P_2O_5	533.04	2.50	64.71
	Ca 2p	CaP	346.20	2.22	21.44
		CaP	347.67	2.20	48.92
		CaO	349.87	2.01	9.89
		CaO	351.25	2.09	19.74
	P 2p	P	132.00	2.35	23.37
		$CaHPO_4$	133.28	1.56	31.59
		$Ca(H_2PO_4)_2$	134.49	1.89	45.03
cpTi + HA Triple layer	C 1s	$(C_6H_5)_2PCH_2P(C_6H_5)_2$	282.00	2.32	36.49
		CH	284.33	1.500	45.95
		$C_{10}H_8$	285.20	1.149	19.41
	O1s	CaO	529.14	1.60	21.46
		CaO	531.78	2.00	78.54
	Ca 2p	Ca	344.42	2.44	16.81
		CaP	346.52	2.50	33.06
		CaP	348.10	2.48	31.13
		CaP	350.90	2.50	18.99
	P 2p	$(C_6H_5)_2PCH_2P(C_6H_5)_2$	130.50	1.04	8.90
		P	132.54	2.36	38.06
		$CaHPO_4$	133.70	2.36	53.04

4.2.8 Biomemitic Immersion Test

The biocompatibility experiments were performed by immersed Ti-6Al-4V alloy samples coated by HAp single layer (at D 7 cm for t_D 10 hours) and tripe layer (at D7 cm for t_D 7 hours) for one month in SBF with the compositions shown in Table (3.3). Fig. (4.26) shows the retrired samples after one month immersion with prominent HAp layer formed biomimetically on the surface and this resoults are in good aggrement with author Edwin van der Wal[101].
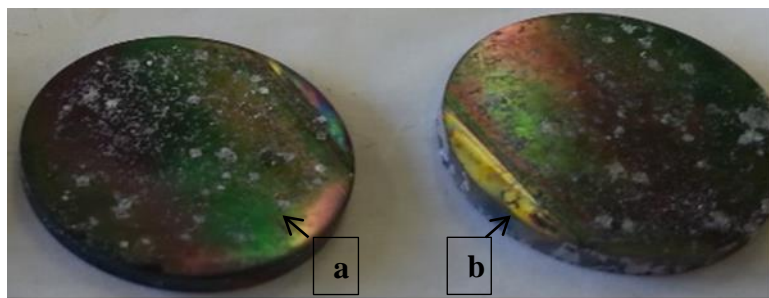
Figure 4.26: Ti-6Al-4V alloy immersion in Simulated Body Fluid after coated with :(a) HAp as single layer and (b)three layer (TiO$_2$+Al$_2$O$_3$+HAp)

4.2.8.1 EDS Analysis of HAp Triple Layer After Immersion

The Fig. (14.27 a and b) shows EDS composition analysis for Ti-6Al-4V alloy coated with single and triple layer HAp respectively,the concentration of the elements are listed in Table (4.12). EDS patterns show that the deposition of Ca and P in single and triple layer samples and the energy transitions elements Ca Kα and Ca Kβ are 3.69KeV and 4.01 KeV respectively ,onther energy transition for P Kα at energy of 2.01 KeV. Also other peaks (C,O,Na,Mg,Cl,K), the components of SBF-incubated sample. The energy transitions elements O Kα is 0.5KeV, energy transition for Na Kα and Na Kβ are 1.041KeV and 1.067 KeV respectively,energy transitions 1.253KeV and 1.259KeV which belong to MgKα and MgKβ respectively ,energy transition for Cl Kα and Cl Kβ are 2.61KeV and 2.81 KeV respectively, the peaks at energy of 3.31KeV represent in the KKα,

and 4.508KeV and 4.93KeV which are belongs to TiKα and   TiKβ respectively and AlKα appears at energy of 1.48 KeV .The present   high intensity Ti and Al in three layer analysis Table(4.11) belong to first TiO_2 and second Al_2O_3 coated layers respectively. It can be concluded from the EDS patterns in Table(4.12) that Ca and P concentration on the film triple layer on Ti-6Al-4V alloy more than that single layer. The initial HAp surface on the sample was found to have suitable an inter grain to growth the apatite   in a solution SBF.

(a)   (b)
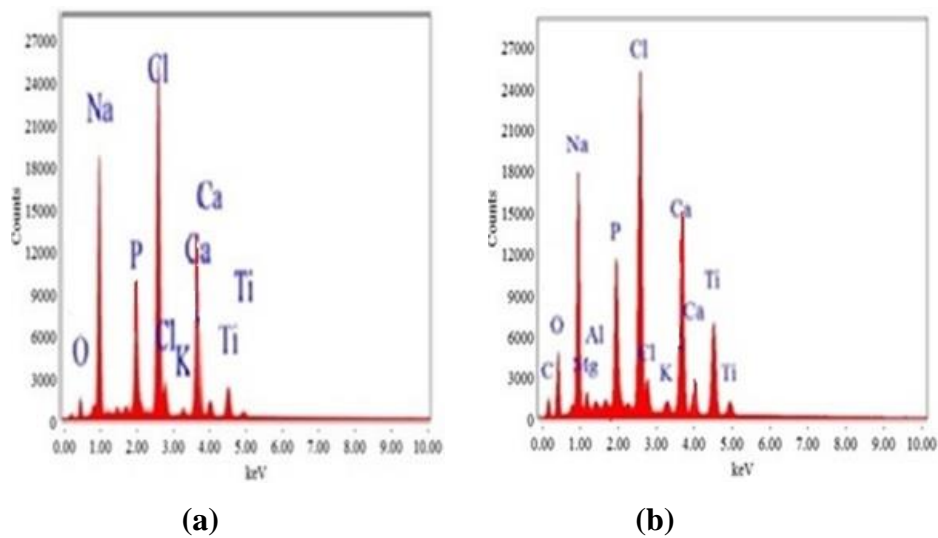
Figure 14 .27: EDS results of immersion Ti-6Al-4V alloy coated with HAp t_D 10 hours as (a) single and (b) triple layer in SBF.

Table 4.12: EDS data   results of immersion Ti-6Al-4V alloy coated with HAp for t_D 10 hours as single and triple layer in SBF.

Ti6Al4V alloy coated with HAp		C	O	Na	Mg	Al	P	Cl	K	Ca	Ti
Single layer	Wt%	14.82	6.95	22.29	1.14	----	5.82	33.61	2.78	12.60	----
	At%	29.34	10.32	23.05	1.11	----	4.47	22.54	1.69	7.47	----
Triple layer	Wt%	22.95	11.00	14.40	1.18	0.39	6.94	16.38	0.80	14.07	11.89
	At%	41.60	14.79	13.63	1.06	0.31	4.88	10.06	0.44	7.64	5.40

4.2.8.2   XRD Analysis of HAp for Single and Triple Layer After Immersion

Fig. (4.28 a & b) show the XRD patterns of Ti-6Al-4V alloy HAp coated with single and triple layers immersed in SBF for one month. Compairing these patterns with patterns presented in Figs. (4.14 &4.16) for the sample befor immersion ,the 2θ reflection of CaP phases located between 25° and 30° shows the degradation of the most of the Calcium Phosphorous coumpond phase along with enhancement of the HAp (211) phase.

(a)

(b)
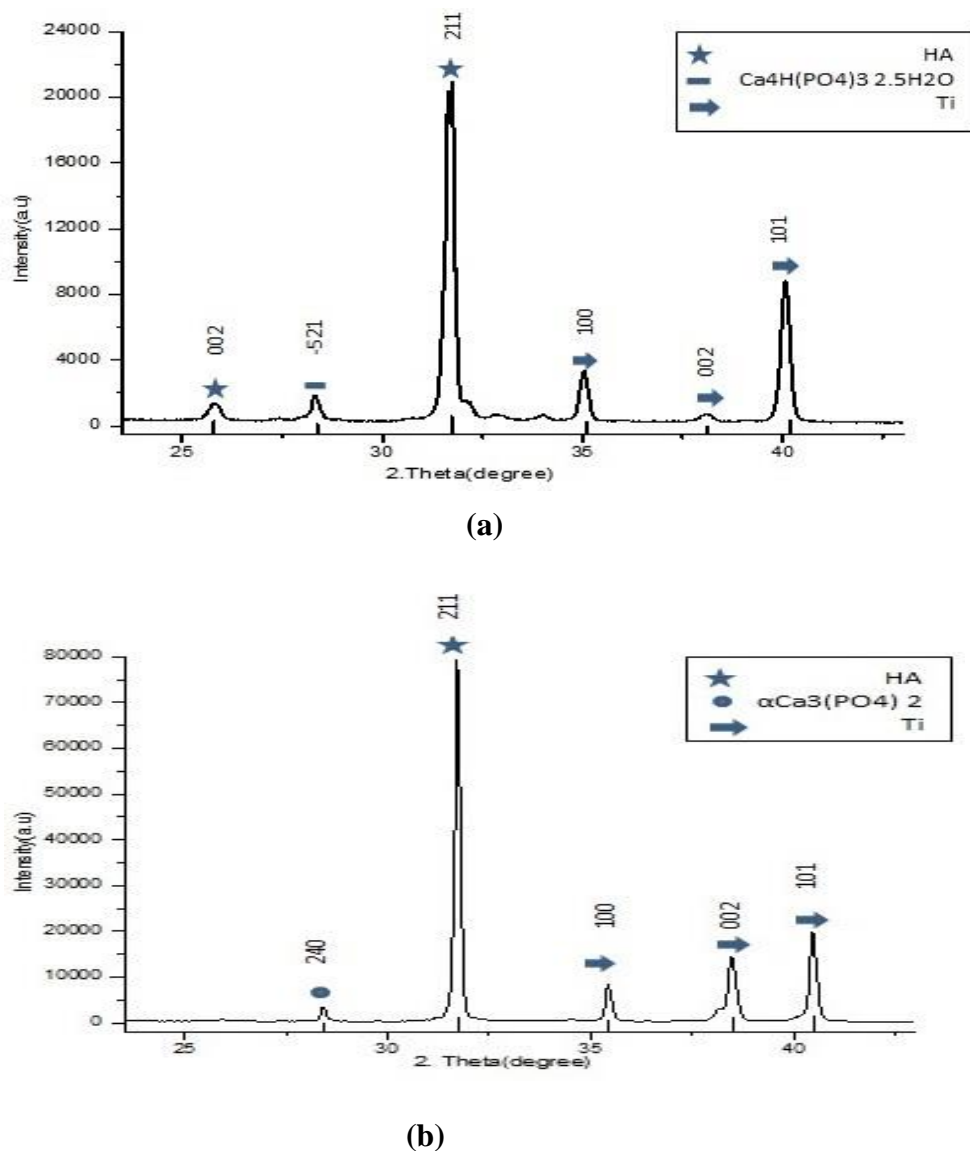
Figure 4.28: XRD patterns of Ti-6Al-4V alloy coated with HAp for t_D 10 hours as (a) single layer and (b) tribe layer after immersion in SBF for one month.

This indicats the increasing of the thickness of the HAp layer due to the biomemitic process during the immersion in SBF accompany with the dissolution of othere CaP compound phases(OCP,CP and TCP). The patterns show peak in(211) at 2θ (31.7)preferred orientation with high crystallinty , wich was increased in intensity for triple layer and remined the same intensity for the single layer of HAp coating compared to the intensity of the same peaks before immersion in Figs. (4.14&4.16). Titanium substrate peaks, (10 0), (0 0 2) and (101) at 2θ (35,38 and 40.7) are presented with lower intensities.

The purpose from immersing the samples in SBF are to attract the apatite species (Ca &P) spectra from solution .This result is in agood agreement with finding of Yong Liu *et al*[43].

4.2.8.3 SEM Analysis of HAp Triple Layer After Immersion

The SEM images in Figs. (4.29 a & b) and (4.30 a & b)presents the surface of Ti-6Al-4V alloy coated with single and triple layer of HAp after immersion in SBF for one month compare with Figs. (4.18 d) and (4.20 b) befor immersed respectively .The SEM morphology shows a variation in the dendrite morphology for single and triple layer coatings immersed in SBF.
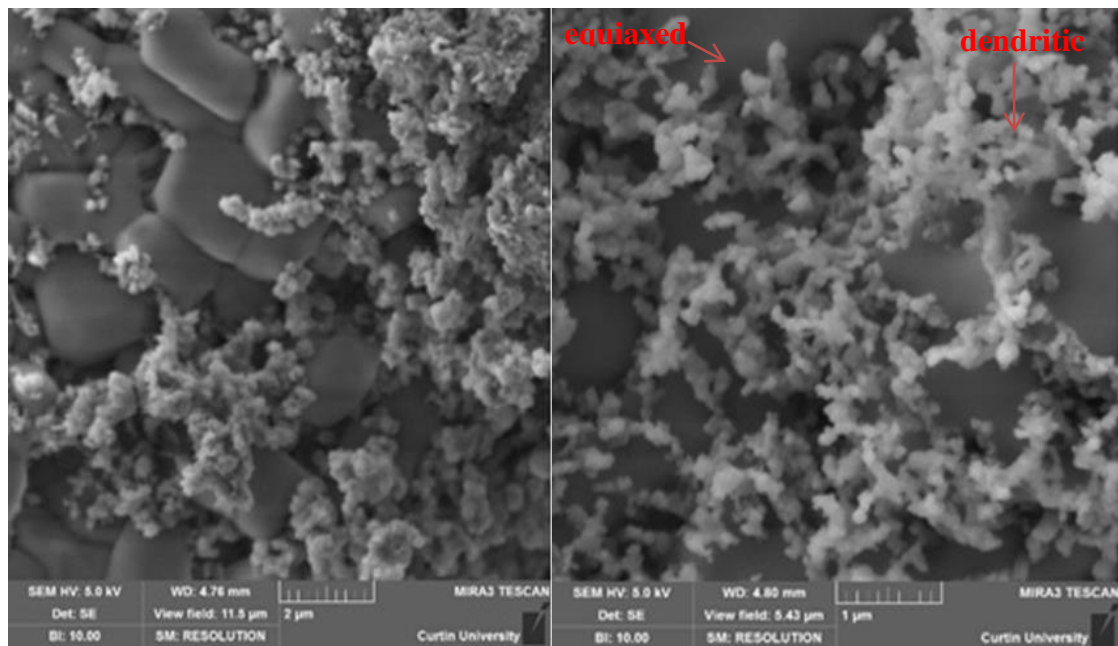
(a)   **(b)**

Figure 4.29: (a) and(b) top-view SEM image of immersion Ti-6Al-4Valloy coated by film HAp as single layer after immersion in SBF for one month.

The components of apatite (Ca &P)in SBF could penetrate in the coated surface through the porosities, leading to the growth of new layer with series of spherical shaped apatite linked togther and well bonded to the components of the coated layer. this is in agreement with Maria Helena Santos *et al*[116]. Fig. (4.29 a & b) show the formation of corse-dendritic hydroxapatait deposited from SBFsolution covering partially the equiaxed grains of the orginal HAp single layer that deposited by RFsputtring.

Whereas the dendritic HAp morphology depositedon the triple layer sample was find and uniform layer covring fully the original HAp layer as can be seen from Fig. (4.30 a &b).
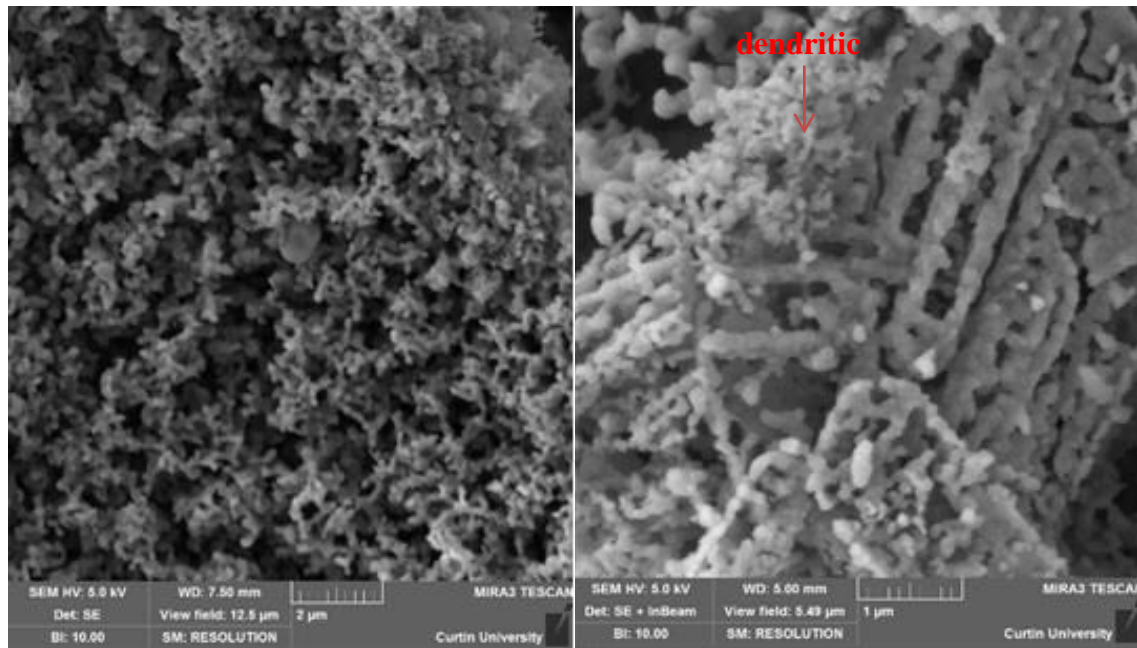
(a)   (b)

Figure 4.30: (a) and(b)top-view SEM image of immersion Ti-6Al-4Valloy coated by film HAp as triple layer after immersion in SBF for one month .

One of the two aimes of surface modification of medical alloys is to protect the surface aginst corrosion which need a porosity free surface to reduce the active ion attachment to the base metal and the secound aim is to create a rough and porous surface to enhance the tissue-implant bonding.

The morphology present in this section is one of the best solutions for tissus reaction.The reason are tissue growth and anckoring needs and very rough and porous surface which have been seen in the single and triple layers HAp coated samples after immersion in SBF.From electrochemical point of view, (corrosion) covering the base metal by the first layer of TiO_2 and following by the second layer of Al_2O_3 leads to the formation of the bonding layer Fig.(4.17 c&d) that blocks the pathway of active ions to attack the substrate .The final HAp single and triple layers prepared by RFsputtering and biomatic proceses are to increasing the biocompatibility

where as the first and second layers(TiO_2 and Al_2O_3) are to enhance the corrosion behaviour of the base metal.

4.2.8.4 XPS Analysis of HAp Triple Layer After Bimmersion

The elemental and chemical analysis of the samples surface were done using XPS analysis. The XPS techniques used were survey and high resolution scan XPS spectrum of a sample HAp coated Ti-6Al-4Valloy as triple layer at D7 cm for t_D 7 hours after immersion in SBF for one month. The instrument was calibrated by the C1s peak position at 283.50eV.

A) Wide Survey Scan XPS Spectrum
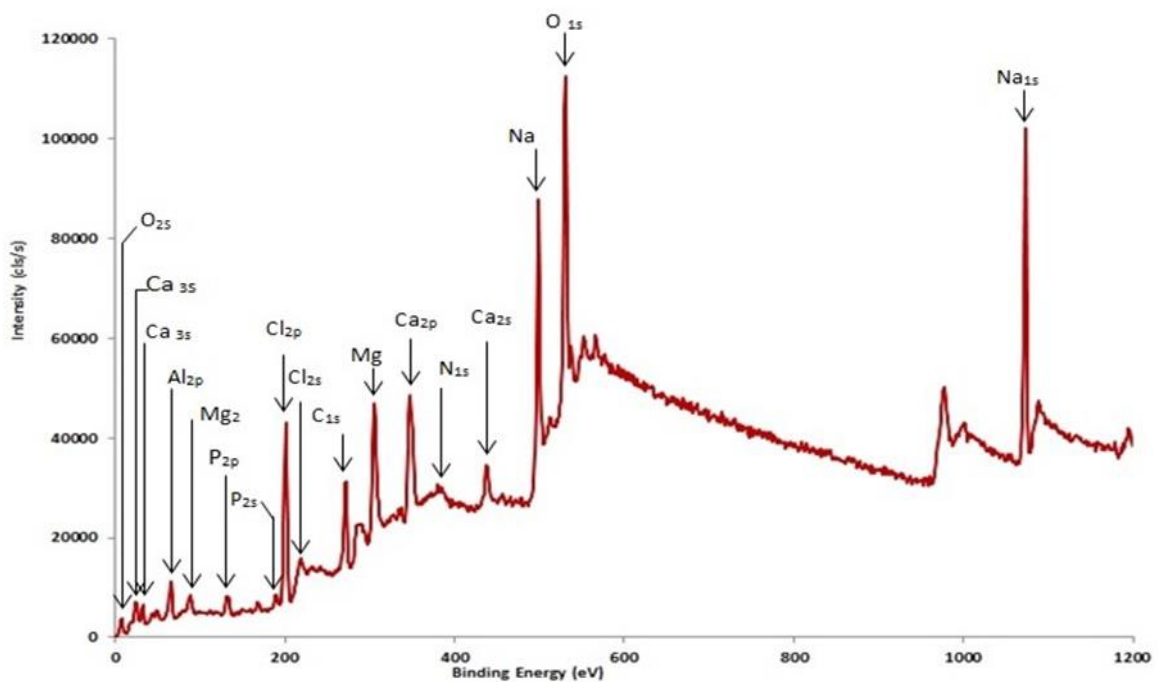
Figure 4.31: XPS spectrum survey scan of immersion Ti-6Al-4V alloy coated by thin film HAp as triple layer at D7 cm and t_D 10 hours.

The major peaks of C(1s), O(1s, 2s), Ca(2s, 3s, 2p), and P(2s, 2p) with

 small peaks of Mg, Cl and Na contaminant from SBF reagents are confirmed by XPS survey scan in Fig.(4.31). These results are in aggrement with finding of Jennifer Vandiver1 *et al* [116].

B) Narrow Scan XPS High Resolution Spectrum

The high resolution XPS spectra around C1s, O1s, Ca 2p 1/2, P 2p of the HAp triple layer deposited samples are shown in Fig. (4.32) and the peak positions of the different chemical states are listed in Table (4.13).

Fig.(4.32 A) and Table (4.13), the C 1s characterize the chemical states of carbon which has main peaks deconvoluted into three sub peaks at 283.38 and 284.91 eV due to the external adventitious of carbon atoms and 288.02 eV assigned to $NaC_2H_3O_2$,and this Na are reagents contaminant in SBF .Our findings are found to be in good accordance with the NIST XPS database and the work done by other authors Ren-Jei Chung *et al* and Jennifer Vandiver *et al* [109,116]. Comparison between the peaks in Figs.(4.25 A2) and (4.32 A) and data in Tables (4.13)and(4.11) after immersion shows that the peaks width are increased due to appearance of the peak 288.02 eV which may assigned to the $NaC_2H_3O_2$ and increas in the carbon atoms concentration which may be come from SBF and atmosphere.

In Fig.(4.32 B) the O 1s spectrum contains three sub peaks at binding energy of 529.77eV and 531.65eV which are attributed to CaO and the peaks at 533.28eV are attributed to P_2O_5 as considered in the NIST XPS database and workdone by other group Gerard Eddy *et al*[108]. Figs. (4.25 B2) and (4.32 B), data Tables (4.11) and (4.13) show that the O spectrums are approximately have the same peaks positions after and befor immersion.
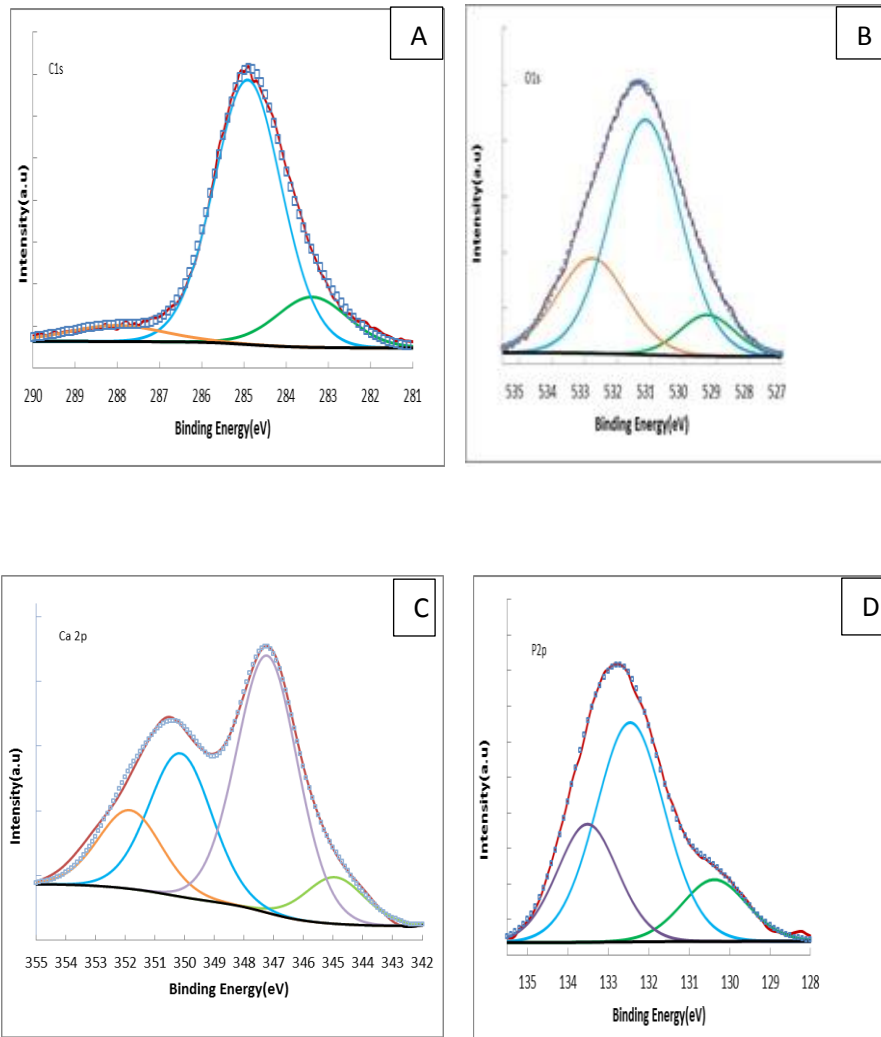
Figure 4.32: High XPS spectrum analysis resolution of C1s, O1s ,Ca2p and P2p coated Ti-6Al-4V alloy with triple layer of HAp immersed in SBF for one month .

Table 4.13: High XPS spectrum analysis resolution of C1s, O1s ,Ca2p and P2p coated Ti-6Al-4V alloy with triple layer of HAp immersed in SBF for one month .

Samples	Line	Bonding states	Binding Energy(eV)	FWHM(eV)	Percentages of component (%)
immersion Ti6Al4V +HAp Triple layer	C1s	C	283.38	2.00	19.42
		C	284.91	1.88	42.36
		$NaC_2H_3O_2$	288.02	2.68	38.22
	O 1s	CaO	529.77	1.99	9.07
		CaO	531.65	2.50	26.21
		P_2O_5	533.28	2.50	64.71
	Ca 2p	Ca	344.93	2.35	8.51
		CaP	350.14	2.50	27.78
		CaP	351.84	2.50	15.23
		CaP	347.22	2.43	48.48
	P2p	$(C_6H_5)_2PCH_2P(C_6H_5)_2$	130.37	1.90	15.37
		p	132.45	2.00	57.37
		$Ca(H_2PO_4)_2$	133.51	1.76	27.26

The 2p1/2 signal in Figure (4.32 C) at binding energies 344.39, eV is corresponding to the Ca element. The peaks at 347.22, 350.14 eV and 351.48 are assigned to the Calcium phosphate group CaP reported byRen-Jei Chung *et al* [109]. The binding energy at 344.93 eV which was indexed according to the NIST XPS database was assigned to Ca atom. From Figs. (4.25 C2&4.32 C), data tables (4.13) and (4.11) the peaks width of Ca spectrums was increased and more signals belong to the Calcium phosphate group were detected after immersion. This was conformed by the SEM observation, Fig.(30 a&b) the triple layer sample coverd by a new HAp layer was formed due to the biomomitic process after immersion.

The main peaks P 2p in Figure(4.32 D) are divided into three sub peaks at 130.37eV and 133.51 eV which can be attributed to the pyrophosphate groups.The two subpeaks signal at binding energies 130.37 and 133.51 eV are assigned to the phosphate group $(C_6H_5)_2 PCH_2P (C_6H_5)_2$ and $Ca(H_2PO_4)_2$ respactively, whereas the energy at 132.45 eV belongs to the phosphorons

atom (P) with maximum intensiy. Figures (4.25 D2&4.32D),and data Tables (4.13&4.11) the P spectrums approximately have same position beaks after and before immersion. The NIST XPS database asimed the above mensiond binding energy to the anhydrous monocalcium phosphate $Ca(H_2PO_4)_2$,our results also conformed by Donglu Shi[114].

4.2.9   *In vitro* Corrosion Investigation (electro chemical study)

The uncoated and coated cpTi and Ti-6Al-4V alloys with single layer coating HAp for t_D 10 hours and three layers $(TiO_2+Al_2O_3+HAP)$ with t_D 7 hours deposited HAp at D7 cm were used to investigate the passive behaviour in SBF. The n corrosion test techniques includ OCP, LSV and EIS were used to evaluat corrosion parameters for different specimens with different surface coatings.

4.2.9.1   Open Circuit Potential (OCP)

 Consists are in a period during which no current can flow and no potential can be applied to the working electrode. Figs. (4.33) and (4.34) show the techniques (OCP) for cpTi and Ti-6Al-4V alloy were to show coated with single layer HAp and three layers. All samples were found to show quasi-steady state value of potcnteal. For the potential of coated samples shifted towards the noble direction for both coating condtions single and three layers specimens. The OCP potential recorded was -270 and +270 mVfor the single and three layer coating respectively comparing to the uncoated cpecimen -650mV. Such a positive potential for three layers coated specimen indicates that the passivation layer was increased by coating and the shift was mor noticible to the three layer specimen more than that for the single layer one.

The same OCP behavior was accorded for the Ti-6Al-4V alloy coated with single layer and three layers.The OCP of the single layer and the three layer were -220mV and 100mV respectively compared with uncoated specimen –650mV.The three layer coating deposited on cpTi specimen show better OCP +270mV than that for Ti-6Al-4V alloy -100mV.

Figure 4.33:The steady-state OCP for cpTi coated with HAp single and three layers in comparsion to uncoated in simulated body fluid.

Figure 4.34: The steady-state OCP for Ti-6Al-4V alloy coated with HAp single and three layers in comparsion to uncoated in simulated body fluid.

4.2.9. Linear Sweep Voltammetry(LSV)

The measurements in hydrodynamic steady-state conditions in Figs. (4.35) and (4.36) show (LSV) for cpTi and Ti-6Al-4V alloy uncoated and coated with single HAp and three layers in comperision with uncoated . The values of corrosion potential (E_{corr})moved towards the nobil region which has similler behaviour seen in values in Figs. (4.33) and (4.34). Depending on (ASTM and NACE), the E_{corr} value are undepend if the surface type are different or not simeliar. Fig. (4.36) for cpTi the uncoated ,coated with single layer and three layer the passive regain were observed approximately started at 0.24,0.5 and 0.15V respectively, also from Fig. (4.36) for Ti-6Al-4V alloy the uncoated ,coated with single layer and three layer started at 0.25,0.4 and 0.2V respectively due to formation oxide layer. For both : uncoated cpTi and Ti-6Al-4V alloy the formation of passive region started approximately from same region as showed by outhor Mustafa Shakir [78], the corrosion progressed in the passive regain for the specimen coated with single layer more than uncoated one while the specimen coated with three layers was quite effective against further corrosion due to the formation of stable oxide layer. From Table (4.14), the I_{corr} value for cpTi and Ti-6Al-4V alloy coated with single layer are much lower than that the un coated and for the three layer coated specimen the I_{corr} are more less than that for the single layer coated specimen. The shift I_{corr} towards the negative direction means improvement in the passivation layer after coating leads to reduce the I_{corr} value. Table(4.14) also shows that the passivation current density (Ipass) at 500mV for the cpTi and Ti-6AL-4V specimens coated with single and triple layer are much less than that for uncoated one and the specimens were passive over long range of positive applied voltage as can be seen from Figs. (4.34&4.36).
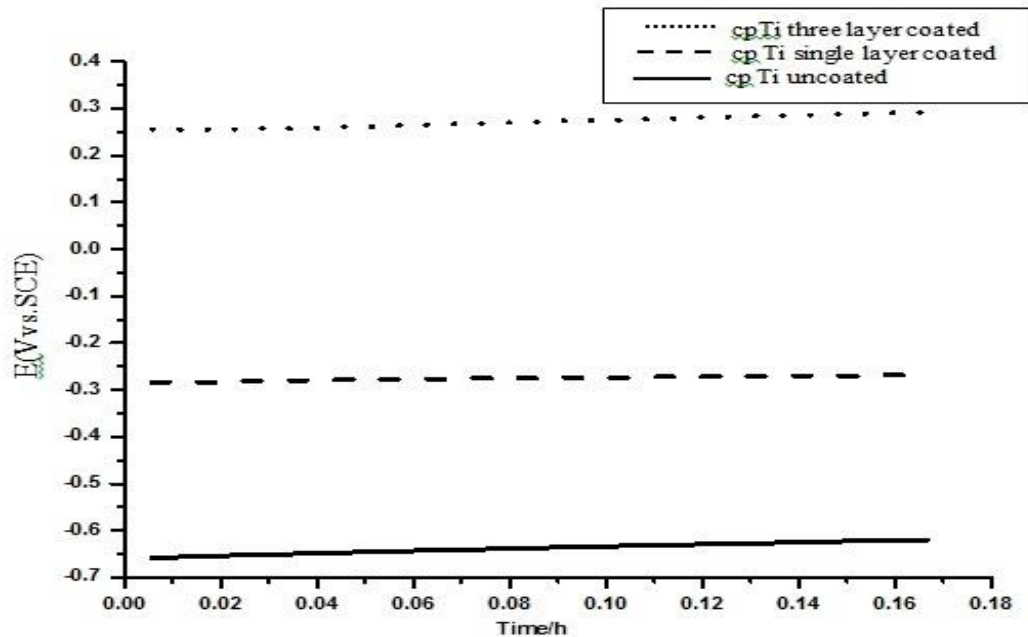
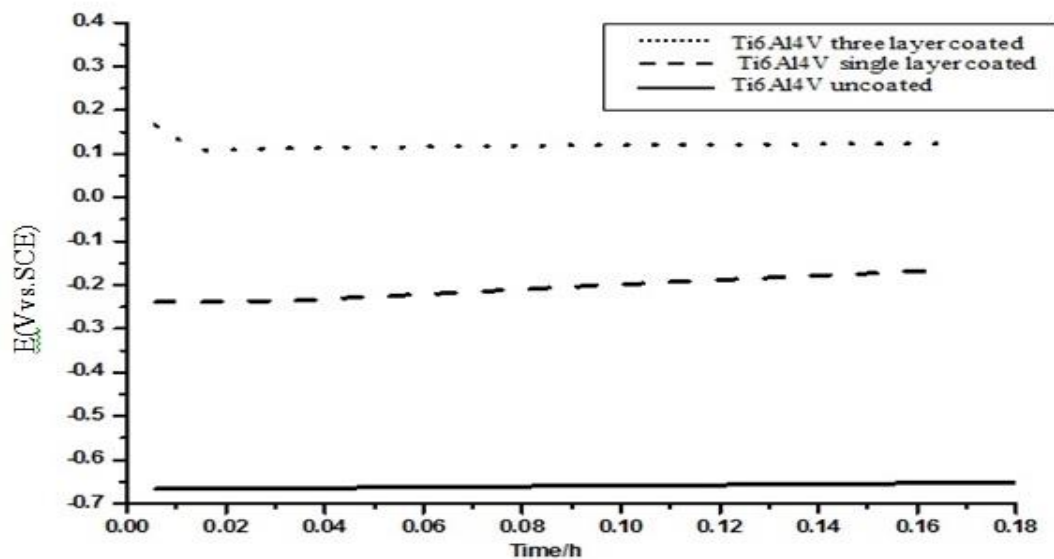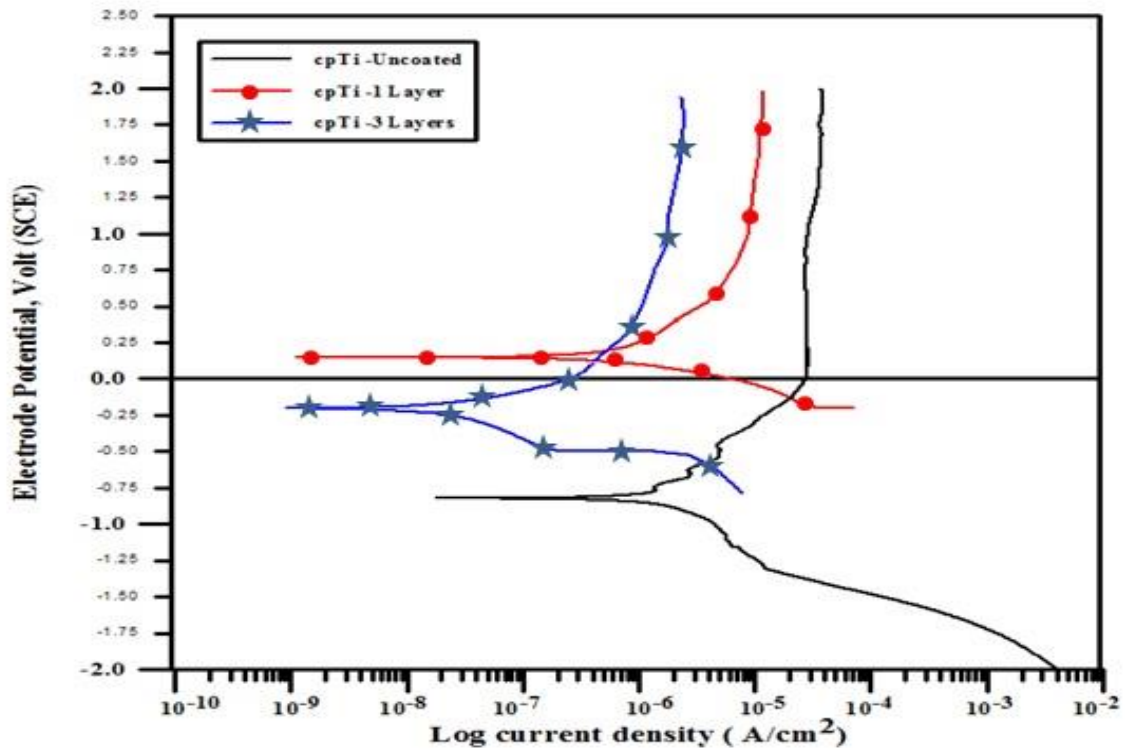**Figure 4.35: LSV diagrams for cpTi coated with HAp single and three layers in comparsion to uncoated in simulated body fluid.**
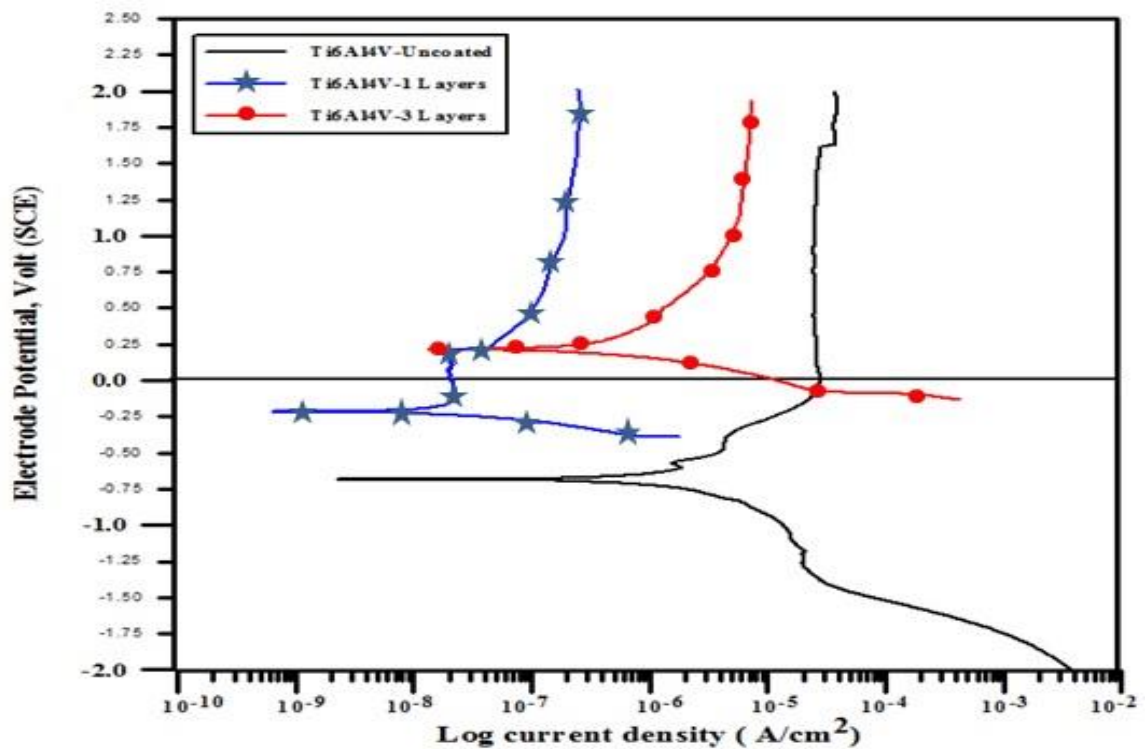
Figure 4.36: LSV diagrams for Ti-6Al-4V alloy coated with HAp single and three layers in comparsion to uncoated in simulated body fluid.

Corrosion characteristics of coatings are affected by (crystallinity, purity, brittle fractures, porosity and ion penetration the coating into substitution) ,it is clear from SEM image for cpTi and Ti-6Al-4V alloy coated with HAp single layer Figs. (4.18 c and d) there are brittle fractures possibility which can affect on the formation of passive region but this did not prevent the improvement in I_{corr} .

Table 4.14: Corrosion parameters for cpTi and Ti-6Al-4V alloy uncoated and coated with HAp as single and triple layers.

Samples	Log I_{corr} (A/cm^2)	I_{corr} (A/cm^2)	E_{corr} (mV)	βa (mV/Dec)	βc (mV/Dec)	β (V/Dec)	Rp (Ohm.cm^2)	Corrosion Rate C_R(mmpy)	Ipass (A/cm^2)
CpTi uncoated	4 $\times 10^{-6}$	-5.39	-780	220.8	223.5	48.228 $\times 10^{-3}$	12.057 $\times 10^3$	3.479 $\times 10^{-5}$	2.5 $\times 10^{-5}$
CpTi single layer coated	8 $\times 10^{-7}$	-6.09	180	260.9	62.9	22.866 $\times 10^{-3}$	2.858 $\times 10^4$	6.958 $\times 10^{-6}$	2 $\times 10^{-6}$
CpTi three layer coated	6 $\times 10^{-8}$	-7.22	-200	204.7	77.9	15.772 $\times 10^{-3}$	2.62×10^5	4.349 $\times 10^{-7}$	2 $\times 10^{-7}$
Ti6Al4V uncoated	5 $\times 10^{-6}$	-5.30	-800	287.6	363.0	69.676 $\times 10^{-3}$	13.935 $\times 10^3$	4.447 $\times 10^{-5}$	2 $\times 10^{-5}$
Ti6Al4V single layer coated	7 $\times 10^{-7}$	-6.15	210	183.1	236.4	34.610 $\times 10^{-3}$	4.94×10^4	6.088 $\times 10^{-6}$	1 $\times 10^{-6}$
Ti6Al4V three layer coated	8 $\times 10^{-8}$	-7.09	-220	392.8	100	44.803 $\times 10^{-3}$	5.600 $\times 10^5$	6.958 $\times 10^{-7}$	1 $\times 10^{-7}$

The RF plasma sputtering HAp coatings had a better corrosion resistant ability with an increased polarization resistance value in comparsion with

other samples HAp as single layer coated Ti-6Al-4V alloy by sprayed plasma method [35]. Improved corrosion resistance was due to a coating surface modification with higher crystallinity and less dissoluble.The improvement in corrosion parameters includes also polarization reistance and corrostion ratio especially for the specimens coated with three layer. This type of behaviour in corrosion resistance for the three layer specimen

are due to the coverage of the substrate surface fully without any micro cracks .

Also, it is found that the welding region has more effect on increasing the resistance corrosionas shows in Figs.(4.16 c and d) . Coated samples showed good corrosion resistance compared to the uncoated one, as can be shown in Table (4.14) that all corrosion parameters are improved using RF sputteringcoating.

4.2.9.3 Electrochemical Impedance Statestical Measurements(EIS)

An equivalent electronic circuit model (Randle's circuit) for the electrochemical system was suggested and the impedance data were obtained by fitting the experimental data to an appropriate proposed circuit model open circuit stability of the passive film in SBF solutions. Equivalent circuit depicts the corrosion model.

The compromises of the Polarization resistance (R2) in parallel with the capacitance of coated layer (C2), in series with the resistance of solution (R1), were used for the EIS model. R1 is the uncompensated resistance of the electrolyte between the working and the reference electrode; R2 is the polarization resistance or the charge transfer resistance at the working electrode/electrolyte interface, related to the rate of corrosion reactions at the passive domain;(C2) is the specific double-layer capacitance at the working electrode/electrolyte interface.

Figure (4.37) show the Nyquist plots for the uncoated cpTi and Ti-6Al-4V alloy in comparison to the single layer coated specimens. The plots show nearly same capacitive behaviour for the uncoated cpTi and Ti-6Al-4V alloy and the capacitance cpTi are less than Ti-6Al-4V alloy as can be show from Table (4.15) (impedance value are the reciprocal of capacitance). It can be seen from Nyquist presented in Fig.(4.37) that the

coated specimens   with HAp in single layer immersed in SBF solution
exhibits capacitive behaviours which is similar to the passive system
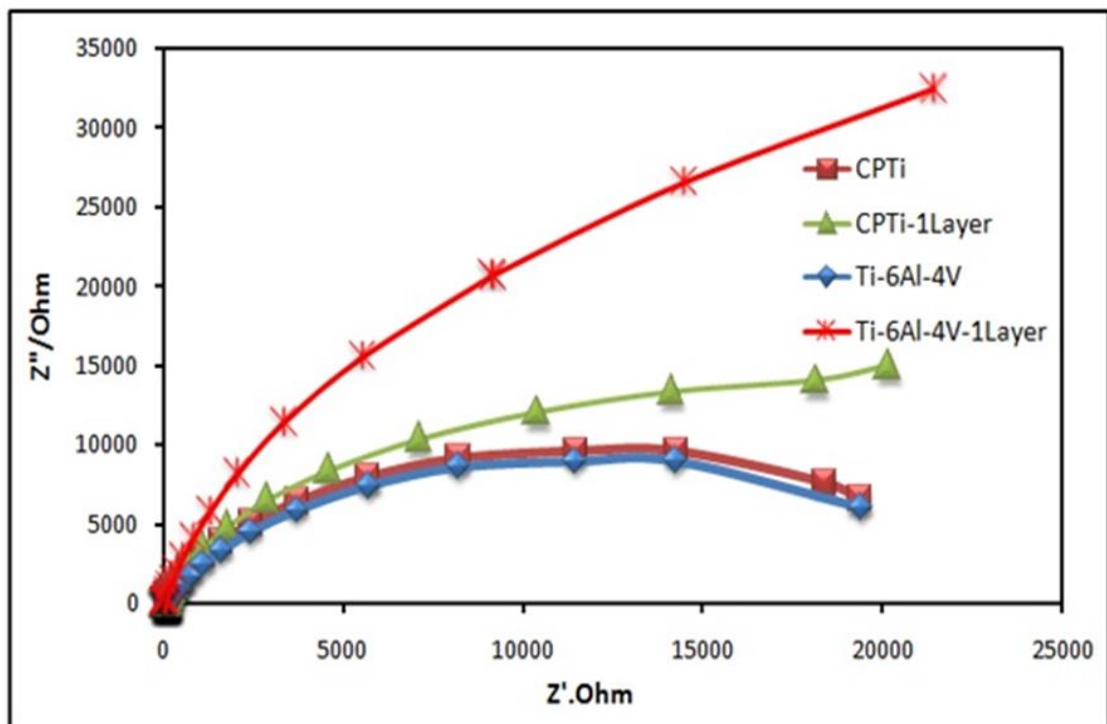
**Figure 4.37 : Nyquist plots of the uncoated and single layer HAp coated cpTi and
Ti-6Al-4V alloy.**

(a)   (b)
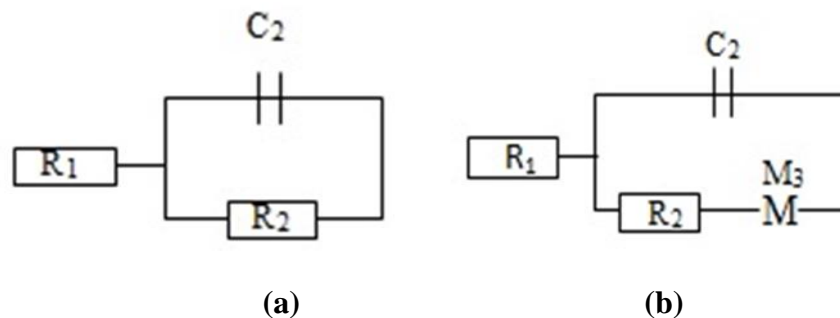
Figure 4.38: Randle circuit for(a) uncoated cpTi and Ti-6Al-4Valloy

(b) HAp single layer coated cpTi and Ti-6Al-4Valloy

Figs.(4.38 a and b)the equivalent circuit (Randle's circuit)for cpTi and Ti-
6Al-4V alloy uncoated and coated with HAp single layer   respectively .
Figure (3.38) covered the porosity in the natural oxide layer of the uncoated

cpTi and Ti-6Al-4V alloy after coating with HAp single layer for that an internal impedance was add to the equivalent circuit represented by (M).
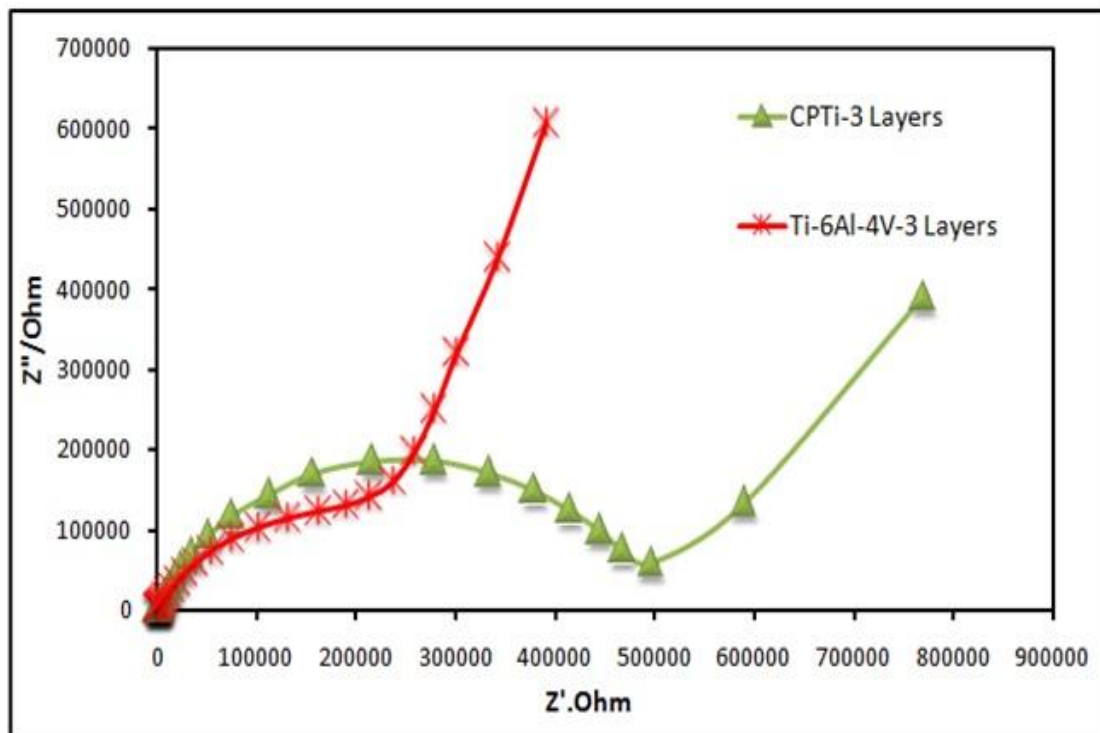
Figure 4.39:Nyquist plots of the triple layer coated cpTi and Ti-6Al-4V alloy
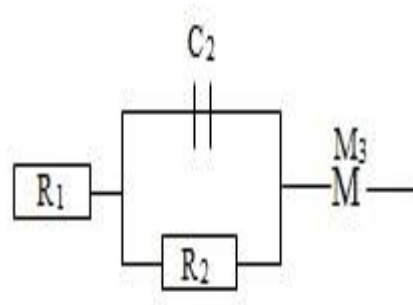
Figure 4.40 : Randle circuit forHAp tripl layer coated cpTi and Ti-6Al-4Valloy

In the triple layer as show in Fig. (4.39) for cpTi and Ti-6Al-4V alloy coated with triple layer HAp and Figures(4.40) show the equivalent circuit (Randle's circuit)for cpTi and Ti-6Al-4V alloy an external impedance was add to the equivalent circuit represented by (M).

 Coating the substrate surface cpTi and Ti-6Al-4V alloy are well covered by the coats sub layers ($TiO_2+Al_2O_3$) which blocks all the natural oxide

porosities and resit the active ions like Cl$^-$ and O$^+$ to transfer from the solution to the substrate, so that the treible layer coating shows very low capacitance and leads to high impedance ,Table (4.15).

Table 4.15: The equivalent circuit parameters for cpTi and Ti-6Al-4V alloy uncoated and coated with HAp as single and triple layers

Samples	R1 (Ohm)	R2 (Ohm)	C (Farad)	M (Ohm)
CpTi uncoated	1070	22800	1.246×10^{-6}	---------
CpTi single layer coated	80.68	34865	4.568×10^{-7}	9492
CpTi three layer coated	60.57	508276	1.251×10^{-10}	66252
Ti6Al4V uncoated	4023	26300	1.574×10^{-6}	--------
Ti6Al4V single layer coated	32.7	94551	1.645×10^{-7}	10615
Ti6Al4V three layer coated	60.57	402325	1.33×10^{-10}	449366

In Nyquist plots when the line is produced on the Complex-Plane graph with 45 degree a capacitance CPE is placed in parallel to a resistor, a Cole-Element (depressed semi-circle) is produced. It's very clear from Fig. 4.37 that the cpTi and Ti-6Al-4V specimens coated with single layer, the complex-plane graphs produced a 45 degree lines. For the triple layer coated cpTi and Ti-6Al-4V specimens , the usual interpretation of the impedance diagrams in Fig. 4.39 is the following: the high-frequency (HF) part is related to the last layer coating while the low frequency (LF) part corresponds to the reactions occurring on the metal through defects and pores in the first and second layer coatings (TiO_2&Al_2O_3). The diagrams in Fig. 4.39 are also characterized by two time constants. However, the second time constant is not well defined and in fact, a linear part appeared in the HF range, which suggests that diffusion processes occur through the coating.

Chapter Five

Conclusions and Suggestions

5.1 Conclusions

The deposition of single layer of (TiO_2 and HAp) and triple layer (TiO_2+ Al_2O_3+HAp) on medical alloy cpTi and Ti-6Al-4V alloy .are succefuly cared out using RF sputtering .

It may be concluded that:

1- Structural and elemental phase on the surface of the final layer complaining to the other CaP compound phases. Also the investigation using XPS shows the different function group and mainly the CaP groups.

2- Immersion test of the single and triple layers coated samples in the Simulated Body Fluid (SBF) for one month shows the thickening of the hydroxyapatite layer through the biomimetic process by increasing the Ca and P concentration on the surface which are confirmed by the structural and elemental analysis (XPS, XRD, EDS, SEM).The apatite layer thickness increment can enhance the biocompatibility of the samples by providing like structure bone on the surface.

3- Electrochemical parameters provided from electrochemical investigation done on the HAp single and triple layers show improvement in the corrosion resistance where decreasing the corrosion potential E_{corr} and current I_{corr} along with very high impedance resistance can be attributed to the formed bonding layer in the interface between TiO_2 and Al_2O_3 layers which blocks the path way for the active ions to attack the substrate.

4- The investigations reviled that the HAp coated Ti and titanium alloys are very good solution to enhance the biocompatibility for surgical implant application.

5.2 Suggestions

1- *In vivo* test for demo fid surface by implant ion (animals studies).

2- Syto toxic city studies and the final deposited layers.

3- Preparation and characterization of composite layer (e.g.TiO_2+HAp , Al_2O_3+HAp..ect).

4-Choos different biomaterial such as Zr_2O_3 instead of Al_2O_3.

5-Increasing the biomimetic test time (immersion) more than one month to study the effect of time on growth of apatite layer on the sample.

6-Use different types of SBF to camper the effect of SBF on corrosion test.

References

1. Mark Long and H.J.Rack; *"Titanium alloys in total joint replacement materials science perspective Biomaterials"*; Journal of Biomaterials. Vol 19, P.1621- 1639(1998).

2. M.E. Engelbrecht, N.F Treurnicht, G. Akdogan. and N .Sacks; *"Functional performance and machinability of titanium alloys for medical implants: a review"*;SAIIE 25 Proceedings Stellenbosch, South Africa. (11th of July 2013).

3. Yaarob Mohammed Salman;*"A study of electrophoretic deposition of alumina and hydroxyapatite on tapered Ti-6Al-7Nb dental implants: mechanical and histological evaluation"* ;Ph.D thesis, University of Baghdad (2011).

4. Z. Paszenda, W. Walke and S. Jadacka;*" Electrochemical investigations of Ti6Al4V and Ti6Al7Nb alloys used on implants in bone surgery"* ;Journal of Achievement in materials and manufacturing engineering Vol.38. Issue 1(2010).

5. G lutjernig and J.C williams;*"Titanium"* ; 2nd edition (Springer 2007).

6. Joyce Y.Wong and Bronzino Joseph D;*"Biomaterials"* ; Taylor and Francis Group LLC(2007).

7. Thair L.Al- Zubaydi;*" Studies on thermo mechanically processed and nitrogen ion implanted Ti-6Al-7Nb Biomedical alloy"*; Ph.D thesis, University of Anna (2002).

8. Thair LAl- Zubaydi, U. Kamachi, S. Rajagopalan and R. Asokamani, Baldev Raj; *"Surface characterization of passive film formed on nitrogen ion implanted Ti-6Al-4V and Ti-6Al-7Nb alloys using SIMS"*;Journal of Corrosion Science Vol.45, P.1951- 1967(2003).

References

9. Jeffrey Robert Piascik;*"Evaluation of structure and material properties of RF Magnetron sputter-deposited yttria stabilized Zirconia thin films"*; Ph.D. thesis, University of North Carolina (2007).

10. W.P.S.L.Wijesinghe; *"Overview to hydroxyapatite nanoparticles and their applications"*; Journal of Biomaterials Vol.1(2014).

11. Young Jung No, Seyed-iman Roohani-Esfahani and Hala Zreiqat; *"Nanomaerials: the next step in injectable bone cements"*;Journal of NanomaerialsVol.9, No. 11, P.1745-1764(2010).

12. Mohammad Abdullah; *"Enhancement of properties of zirconia-based ceramic composites by controlling the characteristics of reinforcement Species"*;Ph.D. thesis University of Nilore, Islamabad, Pakistan (2012).

13. A.Daka,J.Lafait ,M.Abd-Lefdil and C.Sella;*"Optical study of titanium dioxide thin films prepared by RF sputtering"*; Journal of Condensed MatterVol.2, No.1 (1999).

14. L. Pawlowski;*"Thick Laser coatings: a review"*; Journal of BiomaterialsVol.5, No.8,P. 279-295(1999).

15. H.C.Yao,W.T.Wa,M.C.Chiu and F.S.Shieu; *" Characterization and microstructure of titanium dioxide prepared by radio frequency magnetron sputtering"*; Journal of Electrochemical Society Active Member Vol.123, No.66(2000).

16. Wenjie Zhang, Ying Li and Fuhui Wang; *"Properties of TiO_2 thin films prepared by magnetron sputtering. Journal of Mater"*; Sc.TechnolVol.18, No.2(2002).

17. Lei Miao, Ping Jin, Kenji Kaneko and Sakae Tanemurea,; *"Sputter deposition of polycrystalline and epitaxial TiO_2 films with anatase and rutile structures"*; 8th International Conference on Electronic Materials (14th of June 2002).

18.   Janos Takacs and Ozsvath peter; *"Surface modification of metal implants with plasma sprayed layers"*; Journal of Biomaterials Vol.5, P.54-59(2005).

19.   Xiaobing Zhao, Xuanyong Liu, Ch uanxian Ding and Paul Chu; *" In vitro bioactivity of plasma-sprayed TiO₂ coating after sodium hydroxide treatment"*;Journal of Surface and Coating TechnologyVol.200, P.5487-5492(2006).

20.   Maria C. Advincula, Firoz G. Rahemtulla, Rigoberto C, Earl T. Ada, Jack E. Lemons and Susan L Bellis; *" Osteoblast adhesion and matrix mineralization on sol-gel-derived titanium oxide"*;Journal of BiomaterialsVol.27, P.2201-2212(2006).

21.   Tuli Dey, Poulomi Roy, Ben Fabry and Patrik Schmuki; *" Anodic mesoporous TiO₂ layer on Ti for enhanced formation of biomimetic hydroxyapatite"*; Journal of Acta Biomaterialia Elsevier (2011).

22.   Ching-Hua Wei and Ching-Min Chang; *"Polycrystalline TiO₂ thin film with different thicknesses deposited on unheated substrates using RF magnetron sputtering"*; Journal of Materials Transactions Vol.52, No. 3, P.554-559(2011).

23.   Krishna, Dangeti Siva Rama; Sun, Yong and Chen, Zhong; *"Magnetron sputtered TiO₂ films on stainless steel substrate"*; Elsevier Vol.19,No.15,P.4860–4864 (2011).

24.   V. Khalili, J. Khalil-Allafi and H. Maleki Ghalen; *"Titanium oxide coating on NiTi shape memory substrate using electrophoretic deposition process"*; International Journal of EngineeringVol.26, Vol.7, P.707-712(2013).

25. Christopher Jeremy Tredwin; *" Sol-Gel Derived Hydroxyapatite, Fluorhydroxyapatite and Fluorapatite Coatings for Titanium Implants"*;Ph.D. thesis University of College London (2009).

26. Jeffrey Robert Piascik;*"Evaluation of Structure and Material Properties of RF Magnetron Sputter-Deposited Yttria-Stabilized Zirconia Thin Films"* ; Ph.D. thesis University of North Carolina at Chapel Hill (2007).

27. Jaffe, William L. and Scott and David F; *"Current Concepts Review - Total Hip Arthroplasty with Hydroxyapatite-Coated Prostheses"*; Bone Joint Surg Am Vol.78, P.1918-34(1996).

28. Hyun-Min K., Fumiaki Miyaji, Tadashi Kokubo and Takashi Nakamura; *" Preparation of bioactive Ti and its alloys via simple chemical surface treatment"*; Journal of Biomedical Materials ResearchVol.32, Issue3, P.409–417(1996).

29. Gross, Karlis A., Volfgangs Gross, and Berndt,Christopher C; *"Thermal Analysis of Amorphous Phases in Hydroxyapatite Coatings"*; Journal of Am. Ceram. SocVol.81, pp.106-12(1998).

30. Wolke J.G.C, Groot K.DE, and Jansen J.A; *"Dissolution and adhesion behavior of radio-frequency magnetron sputtered Ca-P coatings"*; Journal of material ScienceVol.33, P.3371-3376(1998).

31. Masayuki K., Hirakata Luciana M., Youji Miyamoto, Fumiaki K. and Kenzo A.;*"Surface-layer Modification of Hydroxyapatite Ceramic with Acid and Heat Treatments"*; Journal of Dental MaterialsVol.21, No.2,P. 170-180(2002).

32. Takayoshi Nakano., Kaibara K., Umakoshi Y., Imazato S, Ogata K., Ehara A., Ebisu S. and Okazaki M; *"Change in Microstructure and solubility Improvement of HAp Ceramics by Heat-treatment in a vacuum"*; Journal of Materials TransactionsVol.43, No.12, P.3105-3111(2002).

33. Ricardo M. Souto, Lazb Marıa M. and Reis Rui L; *"Degradation characteristics of hydroxyapatite coatings on orthopaedic TiAlV in simulated physiological media investigated by electrochemical impedance spectroscopy"*, Journal of BiomaterialsVol.24, P.4213–4221(2003).

34. Shuyan Xu, J. D. Long, L. Sim, C. H. Diong and K. Ostrikov; *"RF Plasma Sputtering Deposition of Hydroxyapatite Bioceramics: Synthesis, Performance, and Biocompatibility"*; Journal of Plasma Process. PolymVol.2,P. 373–390(2005).

35. Chun-Cheng Chen and Shinn-Jyh Ding; *"Effect of Heat Treatment on Characteristics of Plasma Sprayed Hydroxyapatite Coatings"*;Materials TransactionsVol. 47, No. 3, P.935-940(2006).

36. V.F. Pichugin, S.I. Tverdokhlebov, R.A. Surmenev, E.V. Shesterikov, M.A. Riabtseva A.A. Kozelskaya and I.A. Shulepov; *"Surface Morphology and Properties of Calcium Phosphate Thin Films Formed by Plasma of RF-Magnetron Discharge"*; Physical basic of radiation-related technologies Vol. 47, No. 5, P. 35-40(2008).

37. Jidong Long, Lina Sim, Shuyan Xu, and Kostya Ostrikov, Reactive;*"Plasma-Aided RF Sputtering Deposition of Hydroxyapatite Bio-implant Coatings"*; Chem. Vap. Deposition13, P.299–306(2007).

38. Paulo G. Coelho, Se´rgio Luiz de Assis, Isolda Costa and Van P. Thompson; *"Corrosion resistance evaluation of a Ca- and P-based bio ceramic thin coating in Ti-6Al-4V"*;Journal of Mater Sci: Mater Med Vol.20, P.215–222(2009).

39. V.A. Mamaeva , A.I. Mamaev and V.N. Borikov; *"Pulsed High Power Action and Technology of Nanostructural Bioceramic Coatings"*;Journal of Mater Sci: Mater Med No. 5, P.38–43(2009).

40. Jayachandran Venkatesan and Se Kwon Kim; *"Effect of Temperature on Isolation and Characterization of Hydroxyapatite from Tuna (Thunnus obesus) Bone"*; Journal of Materials(2010), Vol.3, P.4761-4772.

41. Carl Lindahl;*"Biomimetic Deposition of Hydroxyapatite on Titanium Implant Materials"*;Carl Lindahl, Uppsala University(212).

42. Rajan Anand; *" Electrophoretic Deposition of Hydroxyapatite on Ti6Al4V"*; B.Sc. thesis, National Institute of Technology, Rourkela (2012).

43. Yong Liu, Balyun Huang., Jianmin Ruand. and Yuehui HE; *"Behaviour of composition Ca/P bioceramics in simulated body fluid"*; Journal of Mater Sci. TechnolVol.14(1994).

44. Shinn-Jyh Ding; *" Properties and immersion behavior of magnetron-sputtered multi-layered hydroxyapatite/titanium composite coatings"*; Journal of BiomaterialsVol.24, P.4233–4238(2003).

45. Yu-PengLu, Mu-Sen Li, Shi-TongLi, Zhi-GangWang and Rui-Fu Zhu; *"Plasma-sprayed hydroxyapatite + titania composite bond coat for hydroxyapatite coating on titanium substrate"*;Journal of BiomaterialsVol.25, P.4393–4403(2004).

46. R Tomaszek ,L Pawlowski ,J Zdanowski ;*"Microstructural transformations of TiO_2,Al_2O_3+$13TiO_2$ and Al_2O_3+$13TiO_2$ at plasma spraying and laser engraving"*;Journal surface and coating Technology 185,P.137-149(2004).

47. Zuqiang Qi;*"Processing microstructure and mechanical behavior of nanocomposite multilayers"*;Ph.D. Thesis, University of Science and Technology Beijing, China, (2004).

48. Hae-Won Kim, Young-Hag Koh, Long-Hao Li, Sook Lee and Hyoun-Ee Kim; *" Hydroxyapatite coating on titanium substrate with titania buffer layer processed by sol–gel method"*; Journal of Biomaterials Vol.25, P.2533–2538 (2004).

49. Chun-Cheng Chen, Tsui-Hsien Huang, Chia-Tze Kao and Shinn-Jyh Ding;*"Characterization of Functionally Graded Hydroxyapatite/ Titanium Composite Coatings Plasma-Sprayed on Ti Alloys"*; Journal of Biomedical Materials Research Part B: Applied Biomaterials Wiley Periodicals, Inc. (2005).

50. Zhou-Cheng Wang, Yong-Jin Ni and Jin-Cong Huang; *" Fabrication and characterization of HAp /Al$_2$O$_3$ composite coating on titanium substrate"*; Journal of Biomedical Science and Engineering, Vol.1,P.190-194(2008).

51. Wisanu Boonrawd and Mohd. Hamdi Abd. Shukor ;*"Radio Frequency Magnetron Sputtering HA/Ti Coatings Deposited Using Double-Layered Target: Phase Composition and Film Adherence of Heat-Treated Coatings"*;The 11th Asia Pacific Industrial Engineering and Management Systems Conference, Melaka, 7 – 10 (2010).

52. I. Mercioniu, G. E. Stan, R. Bercia, S. Ciuca and N. Popescu-Pogrion; *"Obtaining and characterization of HA/Y$_2$O$_3$:αAl$_2$O$_3$ system for bio applications"*; Journal of Nanomaterials and Biostructures Vol. 7, No. 3, P.917 – 932(2012).

53. L. Mohan, D. Durgalakshmi, M. Geetha, T.S.N. Sankara Narayanan and R. Asokamani; *"Electrophoretic deposition of nanocomposite (HAp+TiO$_2$) on titanium alloy for biomedical applications"*; Ceramics International Vol38 ,P.3435–3443(2012).

54. Wanhill R, Barter S; *"Fatigue of beta processed and beta heat-treated titanium alloys"*; book Copyright by Springer(2012) .

55. J R Scully; *"Polarization resistance method for determination of instantaneous corrosion rates"*; Journal Since &Engineering Vol.56,No.2 ,P.199-218(2000).

56. Xuanyong Liua,b, Paul K. Chub and Chuanxian Din; *"Surface modification of titanium, titanium alloys,and related materials for biomedical applications"*; Materials Science and Engineering Vol .47 , P.49–121(2004).

57. Joyce Y.Wong, Joseph D.Bvonzino; *"Biomaterials"*; book Tailar & and France group(2007).

58. Satenra Kumar,T.S.N.Sankara Narayanan and S.Ganesh Sundara Raman;*"Thermal oxidation of Ti6Al4V alloy :Microstructural and electrochemical characterization"*; Material Chemistry and Physics Vol. 119, P.337-346(2010).

59. Reza Fazel;*"Biomedical Engineering –Form Theory to Applications"*; book Copyright by INTECH EUROPE(2011) .

60. Luana Marotta Reis de Vasconcellos and Yasmin Rodarte Carvalho;*"Biomedical Engineering – Technical Applications in Medicine"* ; book   Copyright by INTECH EUROPE(2012).

61. Jung Won Cho; *"Pulsed DC reactive magnetron sputtering of aluminum nitride thin"*; Ph.D. thesis University of North Carolina State, (2002).

62. R.Wendt , K.Ellmer and K.Wiesemann ; *" Thermal power at substrate during ZnO :Al thin film deposition in a planar magnetron sputtering system"*; Journal Apply PhysicsVol.82, No. 5, P.2115-2122(1997).

63. Haj Ibrahim; *"Dépôt de couches minces à saut et gradient d'indice par plasma en résonance cyclotron"*; Ph.D. thesis The deposition of multilayer and gradient index thin films by MDECR-PECVD University of ROSTAING , (2007).

64. Tolga Tavsanoglu; *"Deposition and characterization and characterization of single and multilayered boron carbide and boron carbonitride thin films by different sputtering configurations"*;Ph.D. thesis University   of Technique Istanbul, (2009).

65. Yoshimura and Suda; *"Ceramic implant materials"*; book Copyright by Chemical Rubber(1994).

66. Ian Mc Carthy; *"The physiology of bone blood flow: a review"*; Journal bone joint surgery Vol.88,P.4-9(2006).

67. Caeiro JR, González P and Guede D; *"Biomechanics and bone (& II):Trials in different hierarchical levels of bone and alternative tools for the determination of bone strength"*;Rev Osteoporos Metab Miner Vol.5 ,No 2,P. 99-108(2013).

68. Aoki H; *"Apatite—amazing.biological material"*;Tokyo. Ishiyaku Pub, Inc. Japan(1999).

69. Jallot E; *"Nanoscale physico-chemical reactions at bioceramics-bone tissues interface"*;Ph.D. thesis University Blaise Pascal, France (2003).

70. Elliott J C; *"Studies in inorganic chemistry: Structure and chemistry of the apatites and other calcium orthophosphates"*;Amsterdam: Elsevier(1994).

71. Dong J, Kojima H, Uemura T, Kikuchi M, Tateishi T and Tanaka J; *"In vivo evaluation of a novel poroushy droxyapatite to sustain osteogenesis of transplanted bone marrow-derived osteoblastic cells"*; J Biomed Mater Vol.(57),No.2, P.208-216(2001).

72. Karin Eufinger; *"Effect of deposition conditions and doping on the structure, optical properties and photocatalytic activity of d.c. magnetron sputtered TiO_2 thin films"*; Ph.D. thesis University of Wetenschappen: Natuurkunde, (2007).

73. Azza Amin El-Hamshary; *" Influence of reactive sputtering process parameters on the structure and properties of TiO_2 thin films"*;M.Sc thesis University of aus Kairo: Ägypten(2011).

74. Ioana Luciu; *" RF plasma synthesis and characterization of thin films for transparent conductors"*; Ph.D. Thesis University of TRENTO: Italy(2012) .

75. Karen Davis; *" Material Review: Alumina (Al_2O_3) "*; Ph.D. Thesis University of EU (2010).

76. Takashi Shirai, Hideo Watanabe, Masayoshi Fuji and Minoru Takahashi; *"Structural Properties and Surface Characteristics on Aluminum Oxide Powders"*;Ceramics Research Laboratory, Nagoya Institute of Technology Vol. 9, P.23-31(2009).

77. J.R. Davis Davis and Associates;*"Surface engineering for corrosion and wear resistance"*; book Copyright by ASM International(2001).

78. Mustafa Shakir Hashim Al-Hif; *"Surface modification of titanium alloys by coating with Iraqi fishbone to enhance ocsseointegration and improve corrosion resistance In vitro and In vivo a study"*;Ph.D. thesis college of science University Al-Mustansiriya (2014).

79. U.R uperto Antonio; *" Investigation of saabilizing Agents in thin Sol-Gel Zirconium Oxide Anti-corrosion Coating on Iron Materials"*;Ph.D. thesis Technician University Darmstadt(2010).

80. G. Ping and J.J. Beaudoin; *"National Research"*; 1206-1220Council of CanadaP.1206-1220(1998).

81. N.G. Thompson and J.H. Payer; *"Corrosion Testing Made Easy: DC Electrochemical Test Methods";*TX: NACE International (1998).

82. W. S. Tait; *"An introduction to Electrochemical Corrosion Testing for Practicing Engineers & Scientists";*USA:Pair O Docs Pubns, (1994).

83. J. M. Gustavsson*Corrosion Protection Using Conductive Polymers"*;Ph.D. thesis .University of Wollongong, (2007).

84. P. Zarras, N. Anderson, C. Webber, D. J. Irvin and J. A. Irvin, A. Guenthner and J. D, Stenger-Smith;*"Radiation Physics and Chemistry"*; Vol 68,P. 387-394(2003).

85. - M. Eliziane Pires de Souz, E. Ariza, M. Ballester, I. Valéria Pagotto Yoshida, L. Augusto Rochab, and C. Marina de Alvarenga Freire; *"Materials Research"*; Vol. 9, No. 1, P.59-64(2006).

86. Lemons J.E, Venugopalan R. and Lucas Linda C; *"Corrosion and Biodegradation"*;Handbook of Biomaterials Evaluation, Scientific, Technicaland clinical testing of implant materials, (Eds) Andreas F. von Recume, Second Edition, Edwards Brothers, Ann Arbor, MI ,USA, P. 155-167(1999) .

87. T.Melih; *"Microstructural and electrochemical characterization of Ti-6Al-4V ELI alloy"*; MSc .thesis Middle east technical university,(2006).

88. D.William and Materials; *" Materials Science and Engineering An Introduction"*; John Wiley and Sons ,Inc(2007) .

89. J.R .Davis; *"Corrosion:Understanding the basic"*; ASM International,(2000).

90. R.Pierre Roberge.(2000). Handbook of;*"Corrosion Engineering "*;McGraw-Hill.

91. J.Hayder; *"Improvement of mechanical and corrosion properties of dentail amalgam alloy"*; PhD thesis ,University of technology ,Iraq(2007).

92. T.David; *"Corrosion science and technology"*;CRC press(1998)`.

93. D.A.Jones; *"Principles and prevention of corrosion 2nd"* ;Upper Saddle River, prentice Hall (1996).

94. L.L.Shreir ,R.A*;" Metal Environment Reactions"*;Butterworth – Heinemann(2000).

95. A. Juliawati Binti; *"Biotribocorrosion Perforrmance of titanium alloy Ti-6Al-4V and stainless steel 316L under simulated body fluid environment"*; M.Sc. Thesis .University Technology Malaysia (2008).

96. Rawaa abbas mohammed; *"An investigation into the Electropolymerization and Corrosion Protection Properties of Nanostructured Polypyrrole on some metals and alloy";* M.Sc. Thesis. College of Science -University of Baghdad (2014).

97. Craig Bruce D. Handbook of; *"Corrosion Data"*;ASM Metals ParkOhio, USA, P. 53-61(1989).

98. Thomas Edward W; *" The Physics of Ion Implantation. Ion Plating and Implantation Application to Materials, Proceeding of a Conference on the Application of Ion Plating and Implantation to Materials"*; ASM MetalsPark Ohio, USA, P. 7-14(1986).

99. Robert T.Kiepura,Bonnie R.Sanders ;*"Metallograph and Microstructures";* Hand book ninth edition Vol.9 America Society for Metals (1985).

100. D.D. Deligianni, N. Katsala, S. Ladas, D. Sotiropoulou and J. Amedee, Y.F. Missirlis ; *"Effect of surface roughness of the titanium alloy Ti-6Al-4V on human bone marrow cell response and on protein adsorption";*Biomaterials Vol.22 ,P. 1241-1251(2001).

101. Edwin van der Wal; *"Bioactivity and Surface Reactivity of RF-sputtered Calcium Phosphate Thin Films";*PhD thesis Technology Foundation STW, University Utrecht (2003).

102. Roman A. Surmenev , Maria A. Surmeneva, Kirill E. Evdokimov and Vladimir F. Pichugin; *"The influence of the deposition parameters on the properties of an RF-magnetron-deposited nanostructured calcium phosphate coating and a possible growth mechanism";*Surface & Coatings Technology Vol.205 ,P. 3600–3606(2011).

103. Nidhi Kantharia, Sonali Naik, Sanjay Apte, Mohit Kheur, Supriya Kheur and Bharat Kale; *" Nano‑hydroxyapatite and its contemporary applications"*; Journal of Dental Research and Scientific Development Vol. 1,Issue 1(2014).

104. Gérard Eddy Poinern, Ravi Krishna Brundavanam, Nicholas Mondinos and Zhong-Tao Jiang; *"Synthesis and characterisation of nanohydroxyapatite using an ultrasound assisted method"*; Ultrasonics Sonochemistry Vol.16 ,P. 469–474 (2009) .

105. Jennifer Vandiver1, Nelesh Patel, William Bonfield, and Christine Ortiz; *"Nanoscale Morphology of Apatite Precipitated onto Synthetic Hydroxyapatite from Simulated Body Fluid"*; Biomaterials Vol.81,No.7 , P.1705(2003).

106. Thekra Ismael Hammed; *"Histological and Mechanical Evaluation of Electrophoretic Bioceramic Deposition on Ti-6Al-7Nb Dental Implants"*; PhD thesis   College of Dentistry University of Baghdad(2007).

107. Ravi Krishna Brundavanam, Zhong-Tao Jiang , Peter Chapman, Xuan-Thi Le, Nicholas Mondinos ,Derek Fawcett a and Gérrard Eddy Jai Poinern; *"Effect of dilute gelatine on the ultrasonic thermally assisted synthesis of Nano hydroxyapatite"*; Ultrasonics Sonochemistry Vol.18 ,P. 697–703(2011).

108. Gérard Eddy Poinern, Ravi Krishna Brundavanam, Nicholas Mondinos and Zhong-Tao Jiang; *"Synthesis and characterisation of Nano hydroxyapatite using an ultrasound assisted method"* ;Ultrasonics SonochemistryVol.16, P. 469–474(2009) .

109. Ren-Jei Chung, Ming-Fa Hsieh, Rabi Narayan Panda and Tsung-Shune Chin;*" Hydroxyapatite layers deposited from aqueous solutions on hydrophilic silicon substrate"*; Surface and Coatings Technology Vol.165 ,P. 194–200(2003).

110. Hyun-Young Shin, Jae-Young Jung, Sung-Wook Kim, and Woo-Kul Lee; *"XPS Analysis on Chemical Properties of Calcium Phosphate Thin Films and Osteoblastic HOS Cell Responses "*;Journal Ind.Eng.Chem Vol.12, No.3, P.476-483(2006).

111. D.Briggs and M.P.Seah; *"Practical surface analysis by auger and X-ray photoelectron spectroscopy"*; book John Wiley &Sons, Ltd(1983).

112. Charles C. Chusuei and D. Wayne Goodman; *"Calcium Phosphate Phase Identification Using XPS and Time-of-Flight Cluster SIMS"*; Anal. Chem Vol.71, P.149-153(1999).

113. S. Kaciulis, G. Mattogno , L. Pandolfi, M. Cavalli, G. Gnappi, and A. Montenero; *" XPS study of apatite-based coatings prepared by sol–gel technique"*; Applied Surface Science Vol.15,P. 1–5(1999).

114. Donglu Shi; *" Introduction to Biomaterials";* book copy whrit by Tsinghua University Press(2006).

115. Wei Xia, Carl Lindahl, Jukka Lausmaa and Håkan Engqvist; *" Biomimetic Hydroxyapatite Deposition on Titanium Oxide Surfaces for Biomedical Application"*; book   copy whrit by InTech Europe(2011).

116. Maria Helena Santos, Marise de Oliveira, Luciana Palhares de Freitas Souza,Herman Sander Mansur and Wander Luiz Vasconcelos; *"Synthesis Control and Characterization of HydroxyapatitePrepared by Wet Precipitation Process";* Materials Research Vol.4 ,No.7,P.625-630(2004).

Appendix A

cp Ti Certificate

BAOJI JINSHENG METAL MATERIAL CO., LTD

MILL TEST CERTIFICATES NO: BJJSMLF130810

EN10204 3.1 DATE: 10, Aug.2013

Commodity: GR2 TITANIUM BAR					Finish: ANNEALED	
Specification: ASTM F67						

Size[mm]	Heat No.	Quantity[kg]	Net Weight[kg]	Lot No.
Dia 20×700	JS1210430	1	1	JS120316

Chemical Composition (WT. %)

	Ti	Fe	C	N	O	H	Residual element	
							Each	Total
Requirement	Remainder	≤ 0.30	≤ 0.08	≤ 0.03	≤ 0.25	≤ 0.015	≤0.10	≤0.40
Result	Remainder	0.12	0.02	0.02	0.16	0.001	≤0.10	≤0.40

Physical Property

	Tensile Strength [Mpa]	Yield Strength [Mpa]	Elongation [%]	Reduce of area [%]
Requirement MIN	345 MIN	275 MIN	20 MIN	30 MIN
Result	615	550	23	54

Other Test

Visual Inspection	Dimensional Inspection	DPI Test
Acceptable	Acceptable	Acceptable
Micro Structure	Surface Contamination Test	Ultrasonic Test
Acceptable	Acceptable	Acceptable

Hereby certify this product conforms to ALL specifically listed technical requirements, and other requirements for these specifications. furthermore, I certify the above stated quantitative result were derived from testing and analysis and are accordance with the reference specification(s) requirements

Note:
1:Hydrogen-----product analysis

VICE-MANAGER OF QUALITY DEPARTMENT
BAOJI JINSHENG METAL MATERIAL CO.,LTD

Appendix B

Ti 6Al 4V Alloy Certificate

BAOJI   JINSHENG   METAL   MATERIAL   CO.,LTD

**MILL TEST CERTIFICATES**   NO: 20130806

EN10204 3.1   DATE: August 23, 2013

Commodity: TITANIUM BAR								Finish: ANNEALED	
Specification: ASTM F136									
Size [mm]		Grade		Quantity [pc]		Net Weight [kg]		Lot No.	
Dia20×700mm		Ti6Al4V ELI		1pc		1.0kgs		JS20130510-114	

Chemical Composition (WT. %)

Requirement	Ti	Al	V	Fe	C	N	H	O	Residual element	
									Each	Total
	Remainder	5.5-6.5	3.5-4.5	≤ 0.40	≤ 0.1	≤ 0.05	≤ 0.0125	≤ 0.20	≤0.10	≤0.40
Result	Remainder	6.3	4.0	0.18	0.01	0.01	0.003	0.11	≤0.10	≤0.40

Physical   Property

Requirement MIN	Tensile Strength [Mpa]	Yield Strength [Mpa]	Elongation [%]	Reduction of area [%]
	895 MIN	825 MIN	10MIN	25 MIN
Result	965	850	13	30

Other Test

Visual Inspection	Dimensional Inspection	DPI Test
Acceptable	Acceptable	Acceptable
Micro Structure	Surface Contamination Test	Ultrasonic Test
Acceptable	Acceptable	Acceptable

Hereby certify this product conforms to ALL specifically listed technical requirements, and other requirements for these specifications. furthermore, I certify the above stated quantitative result were derived from testing and analysis and are accordance with the reference specification(s) requirements

Note:
1:Hydrogen-----product analysis

VICE-MANAGER OF QUALITY DEPARTMENT
BAOJI JINSHENG METAL MATERIAL CO.,LTD

Appendix C

TOBAS Program Final Report of XRD Lab.
for Apatite Concentration
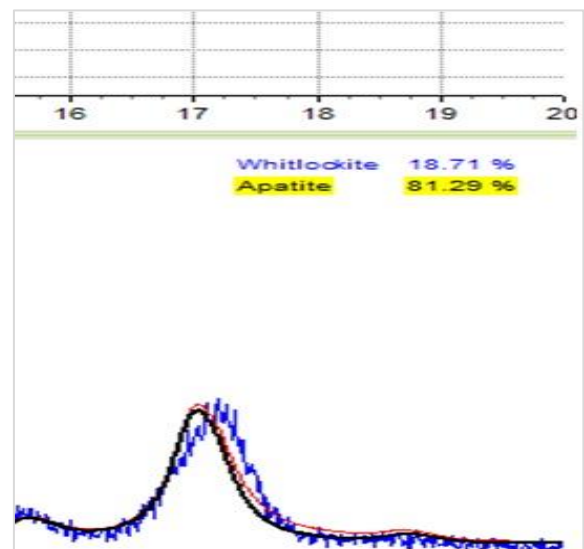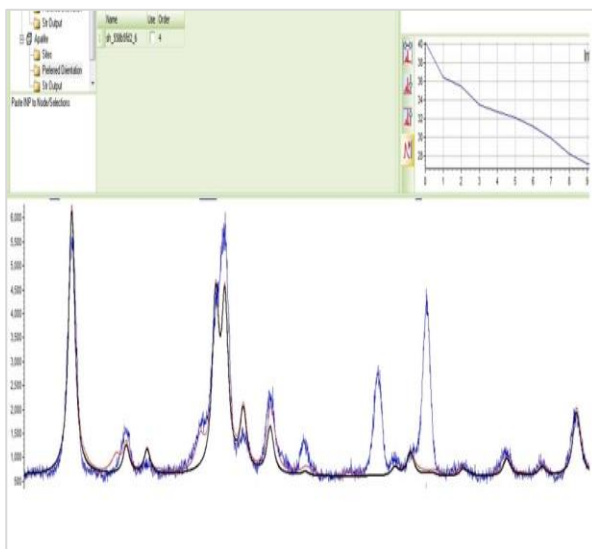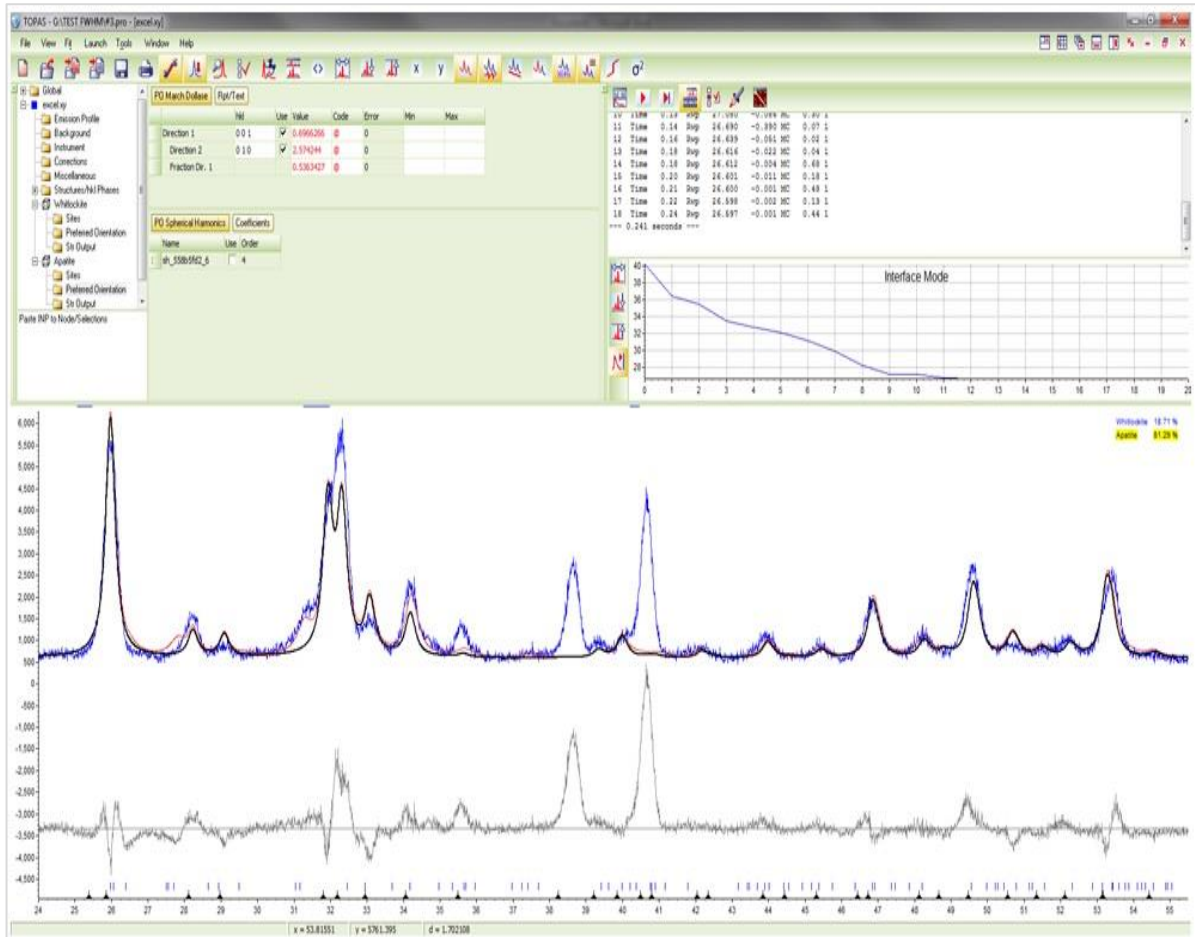
تعديل سطوح التيتانيوم وسبيكــة التيتانيــوم باستخدام المواد الاحيائية السيراميكية بواسطة الرشرشة بالتـرددات الراديويـــة

أطروحة

مقدمة الى كلية العلوم / جامعة النهرين

وهي جزء من متطلبات نيل درجة الدكتوراه فلسفه في الفيزياء

من قبل

دنيا عبد الصاحب هاشم حمدي

بكالوريوس علوم فيزياء- كلية العلوم / جامعة النهرين (1997)

ماجستيـــر علوم فيزياء- كلية العلوم / جامعة النهرين (2003)

اشراف

د. ثائر لطيف مزعل   د. ثامر عبد الجبار جمعة

باحث علمي اقدم   أستاذ مساعد

جمادي الاخرة 1437 هـ   اذار 2016 م

الخلاصة

تضمن العمل في هذه الاطروحه عمليات الترسيب لطبقه احاديه وثلاثيه من مادة هايدروكسيد اباتايت (HAp)على اساسات من التيتانيوم النقي تجاريا (cpTi) وسبيكة تيتانيوم المنيوم فناديوم (Ti-6Al-4V).وايضا في هذا العمل تمت فحوصات الكهروكيميائيه خارج الجسم بتكوين بتكوين الهيدروكسيد اباتايت بعمليات المحاكات الاحيائيه على الطبقات المطليه بتغطيس في محلول مشابه لمحلول الجسم (SBF) بداله حامضيه 7.4 ودرجة حرارة الغرفه. ان شروط الترذيذ بالامواج الراديويه مثل ظغط الفراغ ،درجة حرارة الاساسات ،القدره المسلطه،نوع ومعدل تدفق الغاز وزمن الترسيب قد تم تثبيتها فيما تم تغير المسافه بين الاساسات والهدف حيث كانت(7 و9 سم) .

لقد تم اجراء التحاليل التركيبيه للطبقات الاحاديه والثلاثية المرسبه باستخدام تقانات حيود الاشعه السينيه XRD،المجهر الالكتروني الماسح SEM،وتقانة انتقالات فورير للاشعه فوق الحمراءFTIR ،مطيافية رامان RAMAN ومطيافية الاشعه السينيه الفوتو الكترونيه XPS.فيما اجريت التحاليل العناصريه باستخدام مطيافية كف الطاقه EDS لغرظ التحقق من التوافق الاحيائي للطلائات فان الطبقات التي تكونت تم تغطيسها في محلول SBFلمدة شهر .بعد شهر واحد من التغطيس اجريت التحاليل التركيبيه بنفس التقانات التحليله التي استخدمت قبل التغطيس .

لقد اجريت تحاليل كهرو كيميائيه على الطبقات المرسبه باستخدام فحص جهد الدائره المفتوحه (OCP) ،فولتية المسح الخطي (LSV) ومطيافية الممانعه الكيميائيه(EIS) في محلول (SBF) .لقد اظهرة نتائج حيود الاشعه السينيه بان الطبقه المرسبه يسيطر على تركيبها (HAp) لكلا الطبقتين الاحاديه والثلاثيه كما اظهرت التحاليل وجود اطوار لمركبات كالسيوم- فسفورمثل مركبات الكالسيوم فسفور احاديه (CP)والثلاثيه(TCP) والثمانيه(OCP) مع ظهور بعض اطوار التيتانيوم للاساسات .لقد اظهرة دراسات حيود الاشعه السينيه لطبه الاحاديه المرسبه للتيتانيا (TiO$_2$) ان الطور السائد الذي يغطي سطح الاساسات هو طور الروتايل للاوكسيد التيتانيوم.

لقد وجد من تحليل العناصر باستخدام مطيافية الطاقه المتشتته (EDS) لطبقات الاحاديه والثلاثيه المرسبه على (cpTi) وسبيكة (Ti-6Al-4V) باستخدام مطيافةتشتت الطاقه ان انتقالات

الطاقه هيه طبقا للعناصر المسيطره وهي كالسيوم Ca وفسفورp والتي تسود طبقة الهايدروكسيدابتايت HAp وهي نفس النتائج التي اظهرتها تقانة حيود الاشعه السينيه XRD.

لقد بينت تحاليل مطيافية الاشعه السينيه الفوتو الكترونيه (XPS) للنماذج التي غطست في محلول (SBF) لمدة شهر بان نوع الاواصر والمركبات التي تشكلت.لقد كانت نتائج (XPS) تتطابق مع مشاهداتنا باستخدام (SEM) ونتائج(FTIR) و(RAMAN).لقد وجد من تحليل (XPS) ان معظم المركبات التي تغطي السطح هي مركبات Ca-P بالمقارنه مع مجاميع الكاربوكسيل(C-O,C-H) وهذا يؤكد عمليات التحقق التي اجريت باستخدام حيود الاشعه السينيه والتي اظهرت ان طور(HAp) يزداد تركيزه على السطح من خلال الشده العاليه التي ظهرة في حيود الاشعه عند زاوية الحيود (31.7=2θ) بالاتجاة الافظل (211) لكلا الطبقتين الاحاديه والثلاثيه المرسبه كذلك اظهرت نتائج حيود الشعه السينيه اختفاء مركبات Ca-P الاخرى عدا (HAp) بعد التغطيس في SBF لمدة شهر واحد مثل(OCP,TCP) .ان زيادة تركيز (HAp) بعد التغطيس يؤشر الى حدوث عملية فيزياكيمياويه (عملية المحاكات الاحيائيه) والتي ادت الى زياده ترسيب P- و Ca+ من المحلول المشابه للجسم وان هذين الجذرين ارتبطا معا لتكوين (HAp) اظافي رافعا تركيز (HAp) المرسب اساسا .

لقد اكدت المعاملات الكهروكيميائيه المستنبطه من جهد الدائره المفتوحه والمسح الخطي لطبقات الابتايت المرسب بالشكل الاحادي والثلاثي تحسن في مقاومة التآكل لكلا الاساسات (cpTi) وسبيكة (Ti-6Al-4V) من خلال انحراف جهد الدائره المفتوحه باتجاه المنطقة النبيله Ecorr ونقصان تيار التآكل Icorr ومعدل التاكل السنوي CR بالمقارنه مع الاساسات غير المطليه .

لقد اكدت قياسات مطيافية الممانعه الكهروكيميائيه هذا التحسن بمعاملات التاكل الناتجه من فحوصات جهد الدائره المفتوحه (OCP) وفولتية المسح الخطي (LSV) من خلال السعه الواطئه جدا المسجله النماذج المطليه بالمقارنه مع النماذج غير المطليه والتي تعني بان عمليات الطلاء للطبقات الاحاديه والثلاثيه ادت الى حماية الاسطح بزيادة ممانعة الدائره المكافئه والذي ادى الى غلق مسار الايونات الفعاله -O و Cl+ من ان تهاجم المعدن الاساس.